DETECTION OF COHERENT ENERGY TRANSFER PATHWAYS IN PHOTOSYNTHESIS WITH TWO-DIMENSIONAL ELECTRONIC SPECTROSCOPY

By

Jerome Daniel Roscioli

A DISSERTATION

Submitted to
Michigan State University
in partial fulfillment of the requirements
for the degree of

Chemistry – Doctor of Philosophy

2018

ABSTRACT

DETECTION OF COHERENT ENERGY TRANSFER PATHWAYS IN PHOTOSYNTHESIS WITH TWO-DIMENSIONAL ELECTRONIC SPECTROSCOPY

By

Jerome Daniel Roscioli

Light harvesting proteins in photosynthetic organisms contain highly ordered arrays of chromophores responsible for the collection of energy from solar photons. The organization of the chromophores may lead to collective excitations (excitons) that are delocalized over many molecules in the array. The delocalized excitations allow for coherent, or wavelike, energy transfer between the chromophores, rather than a particle-like, incoherent, energy transfer process. It has been proposed that these collective excitations may direct the flow of energy along the most efficient pathway to enhance the fitness of photosynthetic organisms. Photosynthetic organisms may also favor closely packed chromophore arrays because the structure is compact whilst optimizing large optical cross sections for absorption. Control of the coupling between chromophores may lead to a photoregulatory mechanism, which could control the energy transfer rate as a function of ambient light intensity fluctuations. Broad-band two-dimensional electronic spectroscopy (2DES) can be used to elucidate donor–acceptor pathways and mechanisms for both coherent and incoherent excitation energy transfer (EET) in photosynthetic light-harvesting proteins. In this dissertation, 2DES is applied to determine how quantum coherent energy transfer occurs between carotenoids and chlorophylls (Chls) in the peridinin-chlorophyll protein (PCP), a mid-visible peripheral light-harvesting protein in marine dinoflagellates that delivers excitation energy to photosystem II. PCP is unique in that it uses a

carotenoid, peridinin, as the main light harvesting chromophore and that it can be reconstituted with different chlorophylls to change the energy landscape without causing structural changes. Through 2DES experiments on native PCP with Chl *a*, we show that although the collective excitations of chromophores are very short lived, they lead to an enhanced quantum yield compared to that for conventional, incoherent energy transfer mechanisms. Replacing the native Chl *a* acceptor chromophores with Chl *b* slows energy transfer from peridinin to Chl despite narrowing the donor–acceptor energy gap. The formyl substituent on the Chl *b* macrocycle hastens decoherence by sensing the surrounding electrostatic noise, leading to lower EET efficiencies. This work is significant because it improves our understanding of the role of coherent energy transfer in photosynthetic light harvesting. This information may prove useful when designing materials featuring strongly interacting electronic chromophores for the collection of solar energy for the generation of fuels or for use in photocatalysis.

To The Love of My Life
Krista

ACKNOWLEDGEMENTS

I would like to thank my advisor Professor Warren Beck for his guidance and support through my time at Michigan State University. His teaching methods were completely selfless, always taking advantage of every opportunity to teach me how to become a better person and scientist. Thank you for being patient with me, always allowing me to find my own path, and constantly looking out for my best interest. I am extremely grateful to have had you as my advisor and mentor.

Soumen Ghosh, thank you for being the best colleague anyone could ask for. You are the most honest, kind person I have ever met. Thank you for your support through all the years we worked together in the Beck Lab. Thank you to Michael Bishop, who was always patient with me while I was trying to learn the complex ideas of 2DES. I appreciate your always being available for me whenever I have questions, without obligation. Ryan and Jason, best of luck in finishing your time at Michigan State University. I suspect you will both continue great work in the Beck Lab and in your future endeavors. Finally, I would like to thank my committee members, Professor Marcos Dantus, John McCracken, and James McCusker, for always challenging me.

This work was supported by the Photosynthetic Systems program of the Chemical Sciences, Geosciences and Biosciences Division, Office of Basic Energy Sciences, Office of Science, U.S. Department of Energy under Award Number DE-SC0010847. Professor Roger Hiller (Macquarie University) prepared samples of wild-type PCP and of the peridinin and the expression construct for PCP that were required for the Chl *b* reconstitution procedure.

TABLE OF CONTENTS

LIST OF TABLES

LIST OF FIGURES

KEY TO ABBREVIATIONS

2DES, two-dimensional electronic spectroscopy

Ala, alanine

Asn, asparagine

ATP, adenosine triphosphate

CCD, charge-coupled device

Chl, chlorophyll

DEAE, diethylaminoethyl

DO, diffractive optic

EET, excitation energy transfer

ESA, excite state absorpted

FID, free induction decaY

FMO, Fenna–Matthews–Olson complex

FWHM, full-width half maximum

GSB, ground state bleach

ICT, intramolecular charge transfer

LH1, light harvesting complex I

LH1-RC, light harvesting complex I-reaction center super complex

LH2, light harvesting complex II

LO, local oscillator

LPSVD, linear prediction singular value decomposition

Lys, lysine

MIIPS, multi-photon intrapulse interferometric phase scanning

NADPH, nicotinamide adenine dinucleotide phosphate

NMR, nuclear magnetic resonance

ND, neutral density

NOPA, noncollinear optical parametric amplifier

OD, optical density

PCP, peridinin–chlorophyll protein

PDB, protein data bank

Per, peridinin

PSII, Photosystem II

RC, reaction center

rPCP–Chl *a*, reconstituted peridinin–chlorophyll *a* protein

rPCP–Chl *b*, reconstituted peridinin–chlorophyll *b* protein

SE, stimulated emission

Ser, serine

SM, spherical mirror

TA, transient absoprtion

THG, third harmonic light

Trp, tryptophan

Tyr, tyrosine

WMEL, wave mixing energy level diagram

WL, white light continuum

WP, wedge pairs

wtPCP–Chl *a*, wild-type peridinin–chlorophyll *a* protein

SUMMARY

The purpose of the work in this dissertation was to address how quantum coherence is involved in excitation energy transfer pathways (EET) in the peridinin–chlorophyll protein (PCP). We perform two-dimensional electronic spectroscopy (2DES) experiments on two forms of PCP with different chlorophyll pigments in order to better understand the coherent (wavelike) EET within the protein. As will be discussed later, 2DES is an extremely powerful technique for determining EET mechanisms between donor and acceptor chromophores. Large amplitude oscillations and doubly excited (exciton) features in the 2DES spectra allows for the direct detection of coherent EET pathways between donors and acceptors. By analyzing the temporal characteristics of these observed features, we were able to address each of the following specific aims:

1) Does coherence mediate the EET process within PCP?
2) How does vibrational coupling between peridinin and chlorophyll play a role in EET?
3) How does the system-bath coupling play a role in the decoherence process in PCP?

The content of the dissertation is organized as follows:

Chapter 1 discusses what is currently known about the mechanisms of energy transfer in light harvesting proteins. The literature survey includes prior studies of structure and function of light harvesting complexes and emphasizes studies on PCP. It covers both the nonradiative decay pathway of carotenoids and the electronic interactions between chromophores and their impact on the function of light harvesting. Several outstanding questions that are treated specifically in the following chapters on the experimental work we conducted are presented. This chapter

concludes with a brief discussion of 2DES and why it was employed to address these questions.

Chapter 2 reviews the experimental method used in the following studies. The theory behind nonlinear spectroscopy is discussed and the experimental setup of the 2DES spectrometer we built for these studies is described in detail. The methods of data collection and analysis are also reported.

Chapter 3 presents the results of broadband 2DES experiments that determine the excitation energy transfer mechanisms between peridinin and chlorophyll *a* in PCP. The results provide the first definitive observations of quantum coherence between carotenoid and chlorophylls in a light-harvesting protein. In PCP, this coherent, <20 fs energy transfer channel accounts for the majority of the quantum yield of excitation energy transfer from peridinin to chlorophyll *a*. The excitation energy transfer mechanism is proposed.

Chapter 4 addresses the role of quantum coherence in excitation energy transfer in light-harvesting proteins, the matching of exciton (electronic) levels with vibrational levels of the component chromophores. This study employed preparations of PCP in which chlorophyll *a* was replaced with chlorophyll *b*. A complete structural analysis is performed and the mechanism of excitation energy transfer in light harvesting is discussed as a whole.

Chapter 5 discusses the overall significance of the work and suggests some extensions that can be used as the basis for future work.

Chapter 1: Photosynthetic Light Harvesting

Light harvesting proteins in photosynthetic organisms contain highly ordered arrays of chromophores. The structural arrangement of the chromophores allow for electronic interactions that lead to delocalization of electrons over many molecules. This chapter covers the structure of light harvesting proteins found in photosynthetic organisms and then reviews how the chromophores within such proteins interact with each other. After that brief overview, the focus shifts to peridinin–chlorophyll protein (PCP). A literature review of previous work on PCP is presented and followed up with our hypothesis and approach to further the understanding of coherent (wavelike) energy transfer in PCP.

1.1 The Function of Light Harvesting Proteins

Photosynthesis is the membrane-based biological process of converting energy from solar photons into free energy capable of supporting life. In the early stages of photosynthesis, light-harvesting proteins capture solar energy and transfer that energy to the reaction center through excitation energy transfer (EET) processes involving the coupling of electronic chromophores. The excitation gets spatially and energetically funneled to a dimer in the membrane-bound reaction center that, upon excitation, initiates the electron transfer process. An electron is transferred to a lower energy acceptor, where a cascade of downhill electron transfer reactions occur to separate the charges across the membrane. The final stages of photosynthesis stabilize the separated charges through the formation of chemical bonds in molecules like adenosine triphosphate (ATP) and nicotinamide adenine dinucleotide phosphate (NADPH). These

molecules then reduce carbon dioxide into stable sugars that are exported throughout the organisms to fuel many cellular processes.[1]

Because environmental surroundings differ significantly across the planet, plants and algae have evolved to contain many different light-harvesting complexes in order to account for their individual circumstances. The chromophore clusters in the light-harvesting proteins contain a variety of pigments that are suitable for the type of light that is abundant for certain species. Within this dissertation, we focus mainly on light-harvesting complexes that contain chlorophylls and carotenoids as the primary absorbers. Regardless of the exact chromophores, most light harvesting complex organize the pigments within the protein in a highly specific fashion, as if to arrange the chromophores' orientations to optimize interchromophore coupling for enhanced light harvesting capabilities.[2]

1.2 Structures

Over the last 30 years nearly all of the different types of photosynthetic light harvesting proteins have been crystallized and their high resolution X-ray crystal structures have been obtained. The structures of light harvesting complexes can be used along side ultrafast spectroscopic techniques to determine the EET mechanism in light harvesting complexes. Commonly studied light harvesting complexes are the Fenna-Matthews-Olson complex (FMO),[3–7] the light harvesting complex II (LH2),[8–12] and the peridinin–chlorophyll protein (PCP).[13–16] The general structure of a light harvesting antenna system consists of three main groups: the harvester, the mediator, and the reaction center. The light harvester is usually the most prevalent to increase the total number of photons that are absorbed so that there are more opportunities for energy to be transferred to the reaction center. The mediator assists EET

between the harvester and the reaction center because harvesters are often peripheral proteins (outside of the membrane). The mediator aids in transferring energy from the peripheral complexes to integral light harvesting proteins or reaction centers. Lastly, as described above, the reaction center then converts this energy into an electrochemical potential gradient. Reaction centers can absorb a photon directly and initiate the electron transfer process, but the presence of harvesters and mediators acts to enhance the number of excitations that reach the reaction center. The layering of these antenna systems provides an energetic and spatial arrangement of chromophores to ensure efficient EET to the reaction center.

1.2.1 Fenna–Matthews–Olson Complex

The first pigment-protein complex to have it's structure revealed through X-ray crystallography was the water soluble Fenna-Matthews-Olson complex (FMO) from the green sulfur bacteria *Prosthecochloris aestuarii* (3EOJ.pdb) and *Chlorobaculum tepidum* (3ENI.pdb).[17] Green sulfur bacteria are found in low-light environments such as underwater depths of approximately 100 meters. Since photons are at a much lower concentration at these depths, these bacteria employ very large light harvesters called chlorosomes that contain an extremely large amount of chromophores including as many as 250,000 chlorophyll molecules.[18] FMO then mediates EET between these peripheral chlorosomes to the membrane-bound reaction centers. FMO exists as a trimer, with each subunit containing a cluster of seven bacteriochlorophyll *a* chromophores. The crystal structure (Figure 1.1) shows that the protein scaffold binds the chromophores through ligation of its amino acids to the metal center on the chlorophylls. The FMO complex has been of considerable interest because of the small amount of pigments within the protein pocket, making it a nice model system for studying interchromophore coupling. The

proximity and arrangement of the chlorophylls provide a framework of delocalized wavefunctions that energetically and spatially funnel excitation energy toward the lowest energy exciton and reaction center (Figure 1.2).[6]

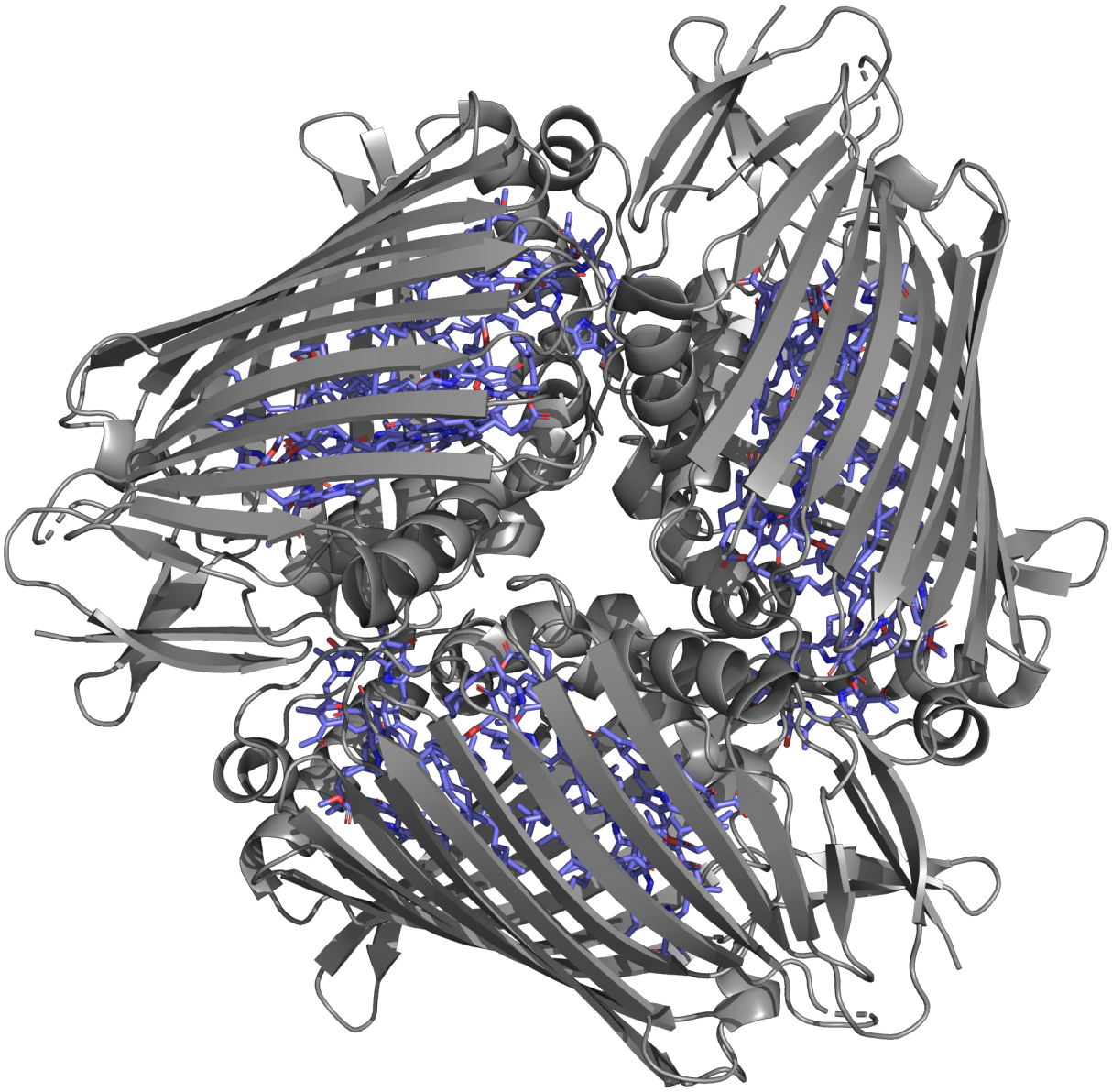

Figure 1.1. X-ray crystal structure of the Fenna-Matthews-Olson Protein from *Chlorobaculum tepidum* (3ENI.pdb)[17]. The protein acts as a mediator of energy transfer between chlorosomes and the reaction center. Each monomer contains seven chlorophyll (blue sticks) molecules encapsulated in a β-sheet shell (gray ribbons).

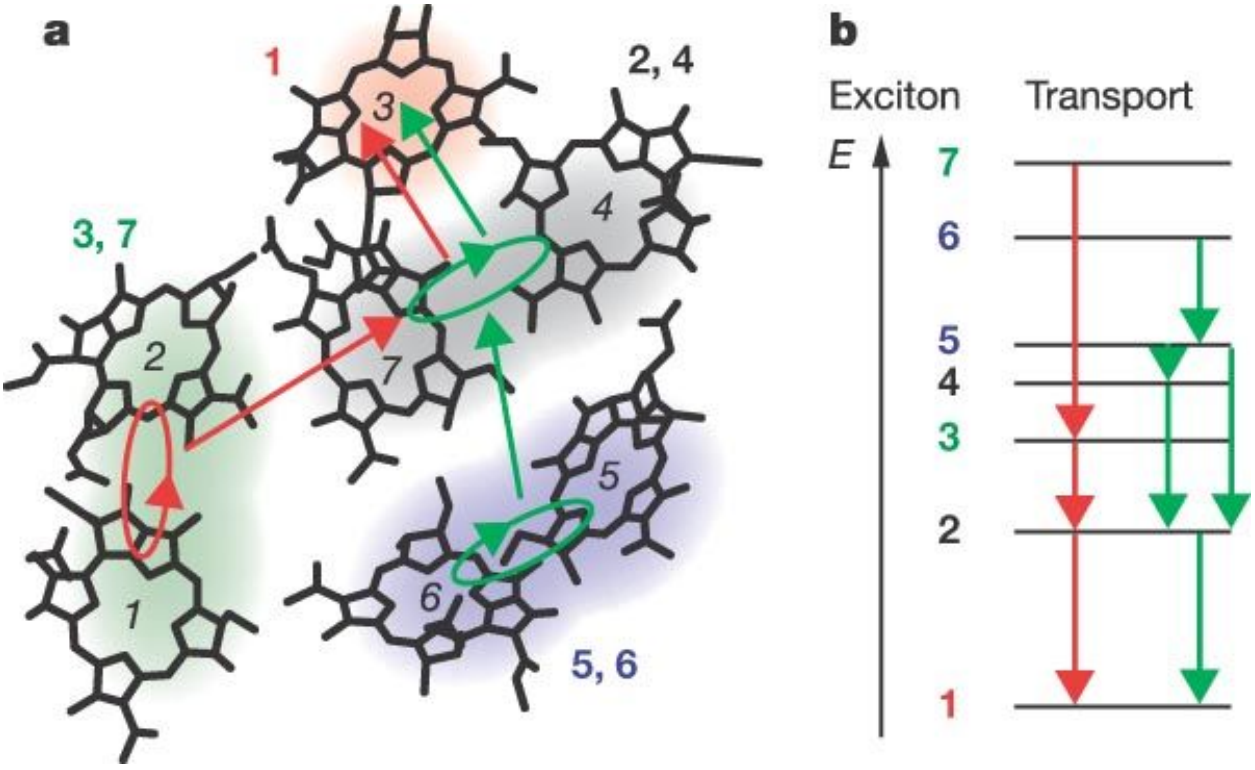

Figure 1.2. Structural arrangement and wavefunction delocalization of the bacteriochlorophylls within a FMO complex monomer. From reference 6. Copyright (2005) SpringerNature, used with permissions. (a) The shaded areas and ringed arrows represent delocalization between two chromophores. The straight arrows show the direction of EET between delocalized pairs of chlorophylls. (b) Energy level diagram corresponding to (a). Energy relaxation within the manifold of delocalized states hops over multiple states due to different structural orientations and distances of surrounding chlorophylls.

1.2.2 Light Harvesting Complex II

The photosynthetic light harvesting system found in purple bacteria exhibits similar electronic wavefunction delocalization and excitation energy funneling. Purple bacteria are found in anaerobic aquatic environments like mud and stagnant water. The light harvesting complex in purple bacteria is the light harvesting complex II (LH2). LH2 transfers its energy to the mediating complex light harvesting complex I (LH1), which is closely associated with the reaction center (RC). It has been shown that LH1 forms two concentric rings around two reaction centers forming the two-fold symmetric LH1-RC complex (Figure 1.3) and ten LH2 proteins surround the LH1-RC complex.[19] Figure 1.4 shows the crystal structure of LH2 from *Rhodopseudomonas acidophila* (1NKZ.pdb).[20] As shown, the protein is made up of nine subunits that form a ring-like structure. Within each subunit are three bacteriochlorophylls and a single carotenoid enclosed by two alpha helices. The protein scaffold stacks the bacteriochlorophylls into two rings. One ring consists of nine B800 bacteriochlorophylls and the other consists of 18 B850 bacteriochlorophylls. In LH1-RC, LH1 contains 28 subunits, each containing 2 bacteriochlorophyll B880 molecules. The structures of these proteins and their chromophores is thought to geometrically align the chlorophyll dipole moments to enhance interchromophore coupling between the pigments to increase efficiency.[8] Notice that the chromophores become lower energy species as the distance between them and the reaction center decrease, which enforces directionality of energy transfer in the system.

The carotenoids in LH2 are in close proximity to both B800 and B850 (~3.5 Å) and act as a light harvester by amplifying the absorption of blue-green photons in LH2. Subsequently, the excitation energy is initially transferred to B800 and B850, and ultimately relaxes to the lowest

energy chromophore, B850.[9,21] Nevertheless, it is likely the carotenoids in this complex are more useful as photoprotection agents than as light harvesters, simply due to the fact that they are vastly outnumbered by chlorophylls.

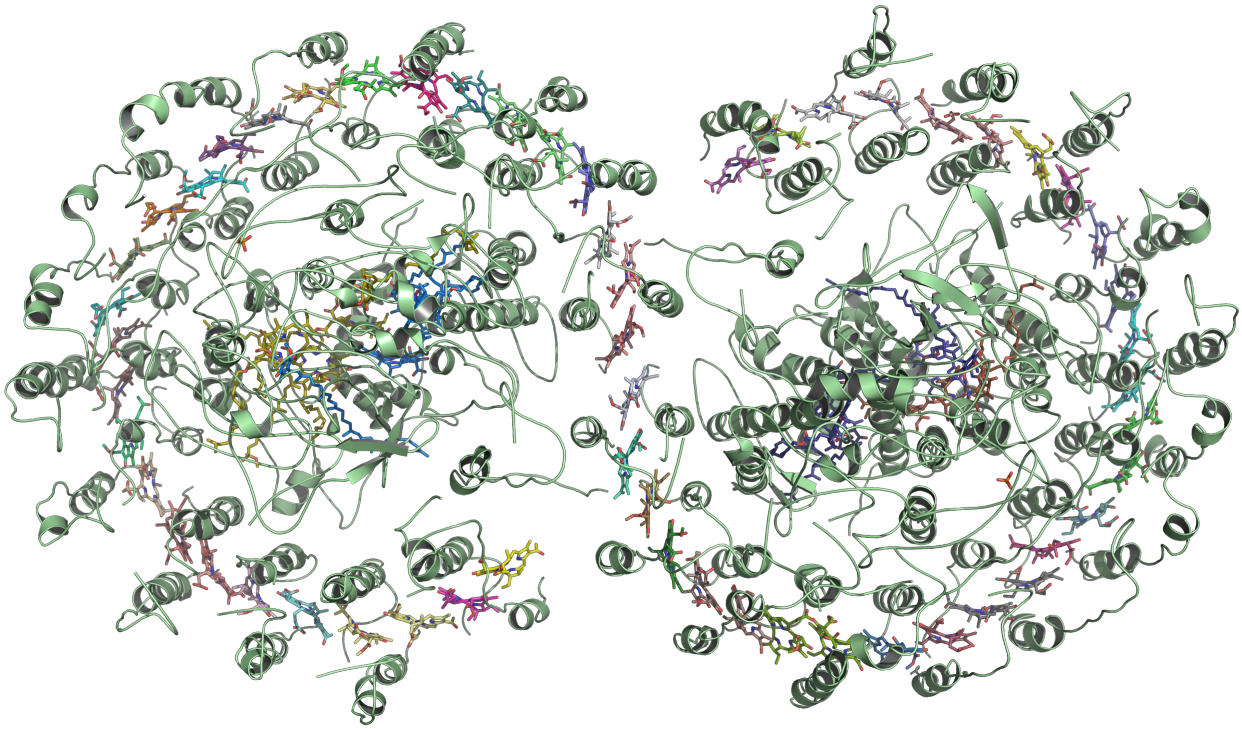

Figure 1.3. X-ray crystal structure of the LH1-RC complex from *Rhodobacter sphaeroides* (4V9G.pdb).[22] The complex contains the LH1 mediating complex that wraps around two individual reaction centers. LH1 contains 56 bacteriochlorophyll pigments that are responsible for collecting energy from surrounding LH2 complexes and passing that energy to the reaction centers.

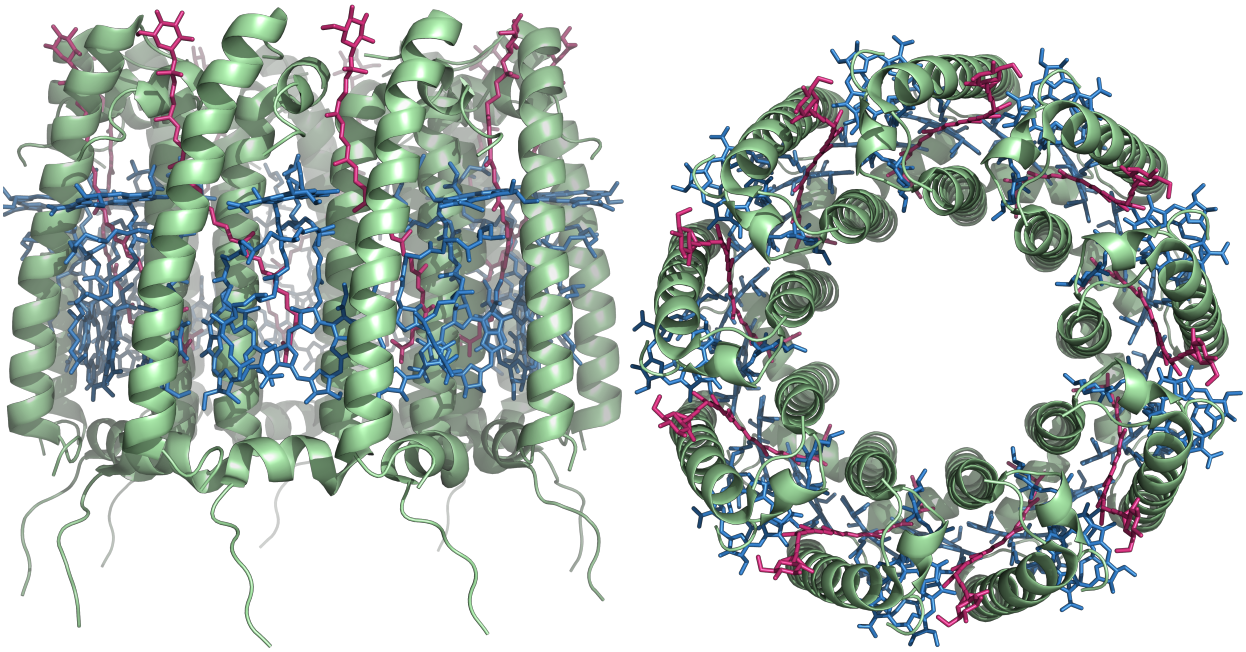

Figure 1.4. X-ray crystal structure of the LH2 complex from *Rhodopseudomonas acidophila* (1NKZ.pdb).[20] The side view (left) shows the two bands of B800 (top) and B850 (bottom) bacterichlorophyll (blue sticks) within the protein as well as the associated carotenoid (red sticks). The top view (right) shows the ring geometry of the complex. LH2 is the primary light harvesting protein in purple bacteria and is responsible for collecting solar energy and transferring that energy to LH1 within the LH1-RC complex.

1.2.3 Peridinin–Chlorophyll Protein

Unlike most light harvesting complexes, a water-soluble, peripheral light-harvesting complex found in marine dinoflagellates, peridinin–chlorophyll protein (PCP), has more carotenoids than chlorophylls. Dinoflagellates are commonly found on the sedimentary surface or subsurface of shallow bodies of water. The additional peridinins greatly increase the absorption of solar photons in a region where chlorophyll does not absorb. The x-ray crystal structure of PCP from *Amphidinium carterae* (1PPR.pdb) shows that the complex exists as a trimer with each unit containing eight peridinin, two chlorophylls, and two lipids.[23] Each monomer has an approximate $C_{2,h}$ symmetry with two clusters of four peridinins all in near van der Waals contact with a chlorophyll (Figure 1.5). In this case, the peridinins act as the primary light harvester and transfer the excitation energy to the chlorophylls at extremely efficient yields.[24] The mechanism of EET in this heterochromophoric cluster is still being investigated, and is the main focus of this thesis. Nonetheless, it is evident, again, that the structure of PCP exhibits a highly ordered crystal-like structure of its chromophores, likely to enhance its EET function.

The mechanism of energy transfer seems to require the chromophores to be arranged in a particular fashion to have proper pigment-pigment interactions for successful energy transfer. It is likely these complexes evolved to have a protein scaffold that optimize the chromophore arrangement to enhance EET. An efficient EET process is vital to the survival of photosynthetic organisms, especially in low light environments, as they act as an amplification system to the reaction center. Light harvesting complexes act to increase the efficiency by increasing the total spectral range and magnitude of absorption for a photosynthetic apparatus.

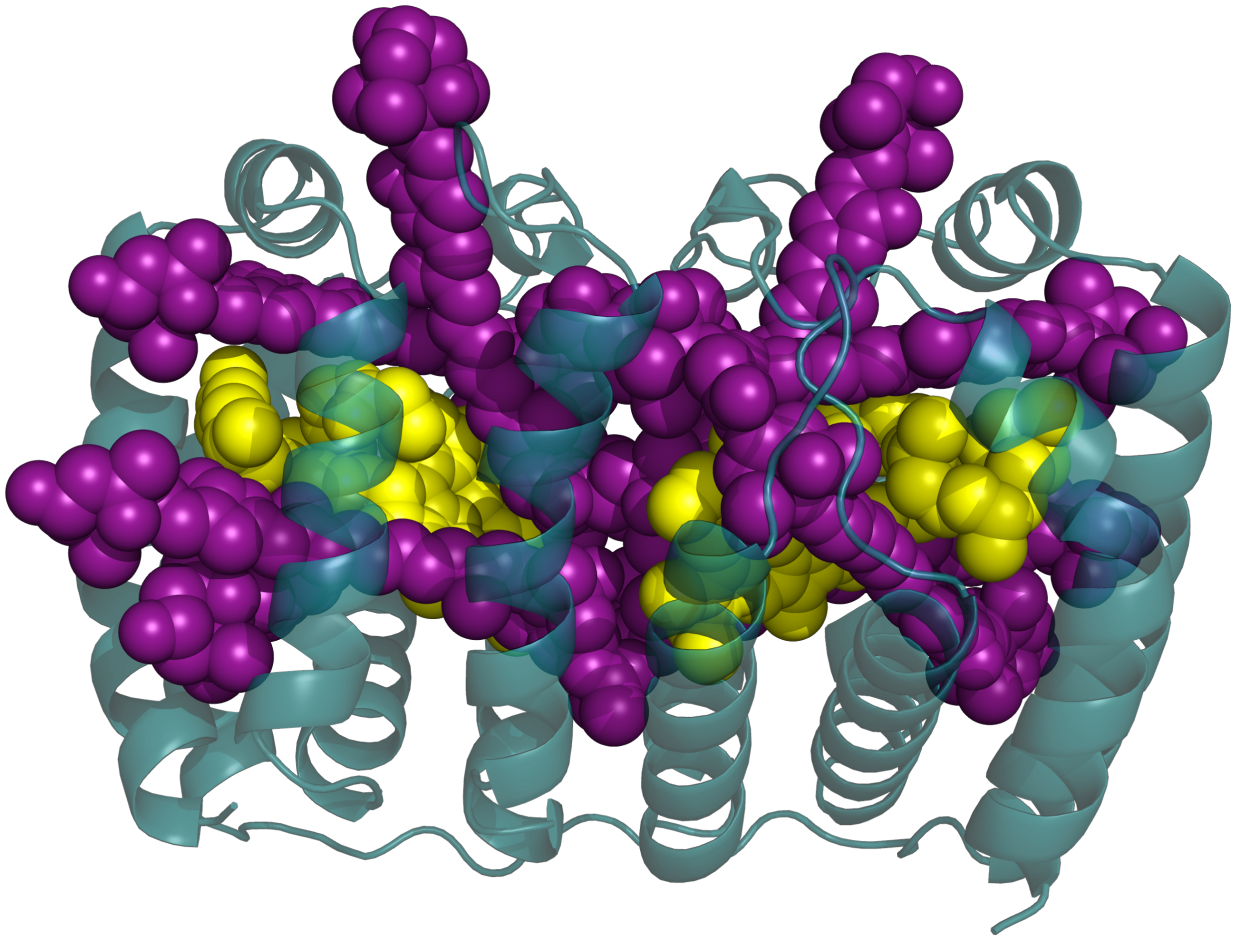

Figure 1.5. X-ray crystal structure of PCP from *Amphidinium carterae* (1PPR.pdb).[23] The complex contains eight peridinin (purple spheres), two chlorophylls (yellow spheres), and two lipids (not shown) inside a basket of α-helices (green ribbons).

1.3 Energy Transfer Mechanisms

The mechanism of energy transfer in light harvesting proteins has been of considerable interest over the last couple of decades. The efficiency of the EET process in LH2 is 70%[25] and in PCP is 90%[26,27]. If the mechanism behind these processes was fully understood, the knowledge could be applied to new materials to convert solar energy to electricity or fuels at much higher efficiencies than is currently available.

The strength of interaction between chromophores plays a significant role in determining the type of energy transfer that a system undergoes. The orientation and distance between the electric dipoles on the two chromophores determine the strength of the interaction. Depending on the strength of the chromophore-chromophore coupling and the strength of the chromophore-environment coupling, the excitation energy transfer could hop between chromophores in an incoherent manner or be wavelike, delocalized excitations over multiple chromophores (coherence). The rate of incoherent EET between the chromophores can be describe with Fermi's golden rule

$$k_{DA} = \frac{1}{\hbar^2 c} |V_{DA}|^2 J_{DA} \tag{1.1}$$

where k_{DA} is the rate between the donor and acceptor, V_{DA} is the electronic coupling strength between the chromophores, and J_{DA} is the spectral overlap integral.

If chromophores are in the weakly coupled regime (the chromophores interact with the solvent more than they interact with each other) then incoherent energy transfer occurs. One can determine if the chromophores are weakly coupled by comparing the absorption spectrum of the two chromophores in solution against the two chromophores in the coupled complex. If the two

spectra are identical, it is likely that the wavefunctions or electron densities are localized on the two chromophores independently. The Förster energy transfer mechanism[28] describes an incoherent hopping of excitation from one chromophore to another. It requires the emission spectrum of the donor to be resonant with the absorption spectrum of the acceptor. The donor nonradiatively transfers its energy to the acceptor through transition dipole-transition dipole interactions. The rate at which the hopping occurs is expressed as

$$k_{DA} \propto \frac{\kappa^2}{\tau_D R^6} \int \mathrm{d}\nu \frac{f_D(\nu)\epsilon_A(\nu)}{\nu^4} \tag{1.2}$$

where κ is the orientation factor of the dipole moments, τ_D is the lifetime of the donor, and R is the distance between the dipole moments. As stated before, the rate also depends on the transition dipole strength overlap integral between the emission of the donor, $f_D(\nu)$, and absorption of the acceptor, $\epsilon_A(\nu)$.

If the chromophores are in the intermediate to strongly coupled regime (the chromophores interact with each other more than they interact with the solvent) then their wavefunctions can mix to form delocalized wavefunctions over both pigments. Strong interactions would cause a splitting of the energy states for the two chromophores that could manifest itself as a shift in the absorptions spectrum. Electronic splitting was detected in a mutated LH2 complex where the B800 chlorophylls were removed from the complex, yet circular dichroism spectra reveal a strong feature around 800 nm.[29] That feature is due to an exciton, collective excitation, that results from the strongly coupled B850 chlorophylls. A review of strong coupling in photosynthesis is conducted in the next section.

It could be argued that there is no need for fast, coherent energy transfer in light harvesting systems. The lifetime of chlorophyll is on the order of nanoseconds, which is more than enough time for the incoherent hopping mechanism to be efficient, considering it occurs on the picosecond timescale. Further, these rates are faster than the electron transfer process, so random diffusion of energy transfer could be sufficient to provide enough excitations to the reaction center for the photosynthetic reaction to occur. An incoherent mechanism would only require a large quantity of chromophores in a random arrangement. Yet, the crystal structures of these proteins reveal highly ordered chromophore arrangements, which suggest a more coherent process, where the chromophores are strongly interacting. Whether coherent processes contribute to the fitness of photosynthetic organisms has been of considerable interest and is addressed in subsequent chapters.

The incoherent EET mechanism could be plausible for some systems based on the rate argument presented above, but if we consider the heterochromophoric interactions between chlorophylls and carotenoids in PCP, incoherent energy transfer processes would not be favorable as the nonradiative lifetime of carotenoids is significantly shorter than chlorophylls. The diffusive energy transfer process would be in competition with nonradiative decay of the carotenoid itself, which would likely decrease the efficiency of the complex significantly. In this case, strong chromophore interaction and fast coherent energy transfer processes could enhance the efficiency of the EET process.

1.4 Strong Coupling in Energy Transfer

A brief description of a dimer of chromophores will aid in understanding how chromophores could interact to lead to quantum coherence in more complex light harvesting

systems. The following is adapted from Cantor and Schimmel.[30] First, consider a simple noninteracting system with two identical monomers that only have two states each, the ground state, *a*, and the excited state, *b*. In the ground state of the dimer, both monomers are in their ground state. The first excited state of the dimer would be one monomer in its excited state and the other in the ground state. No matter which monomer gets excited, the absorption spectrum of the dimer is at the same energy gap of the monomer. Such a case can be treated with separation of variables, where the dimer Hamiltonian is simply a sum of the individual monomer Hamiltonians (Equation 1.3) and the dimer wavefunctions are the product of the monomer wavefunctions:

$$\hat{H} = \hat{H}_1 + \hat{H}_2 \tag{1.3}$$

$$\Psi_{1a,1a} = \phi_{1a}\phi_{2a} \tag{1.4}$$

$$\Psi_{1b,2a} = \phi_{1b}\phi_{2a} \tag{1.5}$$

$$\Psi_{1a,2b} = \phi_{1a}\phi_{2b} \tag{1.6}$$

where Equation 1.4 is for the ground state, Equation 1.5 is the first excited state where chromophore 1 gets excited, and Equation 1.7 is the first excited state with the excitation on chromophore 2. Consider a similar scenario, except now allow the two monomers to electronically interact but the electrons remain localized on each monomer (weak coupling). In this case, the electric fields of each molecule perturb the other molecule. An interaction like this changes the dimer Hamiltonian to include a new term, the dipole-dipole interaction operator $\hat{V}_{12}$ (Equation 1.7). Because the interaction is only a perturbation, the wavefunctions are considered to be the same as the noninteracting molecules. However, upon excitation the excited state electric field of the first monomer is felt by the other monomer, which could cause a transfer of excitation to the second monomer. The excitation can rapidly transfer between the two

chromophores. Then, a more realistic set of dimer wavefunctions for this scenario includes an unaffected ground state, but a set of wavefunctions Ψ_{B+} and Ψ_{B-} that are linear combinations of the monomer excited state wavefunctions, rather than independent monomer wavefunctions (Equations 1.8 and 1.9).

$$\hat{H} = \hat{H}_1 + \hat{H}_2 + \hat{V}_{12} \tag{1.7}$$

$$\Psi_{B+} = 1/\sqrt{2}\left(\Psi_{1b} + \Psi_{2b}\right) \tag{1.8}$$

$$\Psi_{B-} = 1/\sqrt{2}\left(\Psi_{1b} - \Psi_{2b}\right) \tag{1.9}$$

Solving the Schrödinger equation using the dimer Hamiltonian and wavefunctions for both excited states yields two excited states separated by $2V_{12}$. The perturbation $\hat{V}_{12}$ has split the excited state of the dimer into two states, also known as exciton splitting.[30]

All of the above theory requires the system's states to be stationary, with no fluctuation of energy. So the previous work up is only true for two molecules in vacuum. In the case of photosynthetic organisms, the chromophores are in a condensed phase, where not only do they interact with other chromophores, but they also interact with the surroundings, or bath. The molecules simultaneously couple with the energy of the surrounding system and surrounding chromophores simultaneously. Both the ground state and excited state of a chromophore are generally stabilized upon solvation, but the excited state is usually stabilized more, as excited states have larger dipoles and polarizabilities. If the chromophore is polar and is placed into a polar surrounding, permanent dipole effects control system-bath coupling, otherwise it is usually induced dipole moment effects that control system-bath coupling.[31]

The interplay between chromophore to chromophore coupling and chromophore to solvent coupling controls what type of interactions occur in the whole system. In order for a

dimer of chromophores to mix quantum mechanically in a condensed phase, their interaction strength must be stronger than their interaction with the surroundings. It then makes sense that photosynthetic organisms employ chromophore clusters that are bound by protein, to increase the chromophore to chromophore interaction, increasing EET efficiencies. If the chromophores interacted more strongly with the surrounding solvent, energy would be lost to the surrounding instead of reaching its biologically intended destination.

Investigations regarding the nature of carotenoid and chlorophyll interactions in light harvesting systems failed to form a single conclusion as to how and if strong coupling is involves in the EET mechanism. It has been suggested by Fleming et al.[7,32] that efficient EET of light harvesting requires long lived electronic coherences. Other studies of light harvesting complexes in green plants[33–35] suggests that charge-transfer reactions between carotenoids and chlorophylls contribute to the regulation of EET to Photosystem II (PSII). Nonetheless, these and other results[36–39] suggest that EET and nonradiative decay channels must be delicately balanced for efficiency to be enhanced. The protein environment then must properly orient the chromophores to not only interact with each other to optimize electronic interactions, but to also control system-bath coupling to ensure the fitness of the light harvesting species.

1.5 Background of Peridinin–Chlorophyll Protein

PCP is an ideal candidate to further investigate carotenoid and chlorophyll interactions within light harvesting systems. PCP is unique because the main light harvesting species is a carotenoid, which, as alluded to previously, suggests that the fitness of PCP may by reliant upon quantum coherence for efficient EET. PCP absorbs mid-visible photons and transfers the excitation energy to Chl in membrane-bound light-harvesting proteins via the Förster resonant

energy transfer mechanism.[40] It can be reconstituted with different chlorophyll chromophores[41], allowing the energy gap between the donor peridinin and acceptor chlorophyll to be tunable. Being able to tune the energy gap, without significantly perturbing a pigment-protein structure, makes PCP an ideal candidate to study how coherence is involved in energy transfer between donor and acceptor chromophores. We will be able to adjust the energy landscape of the chromophore cluster without changing the electrostatic environment. The energy level diagram for PCP is represented in Figure 1.6.[42–47]

The strong peridinin absorption band in the PCP complex arises from the strongly allowed S_0 to S_2 transition.[44,48–52] The S_2 state is depleted very rapidly (<100 fs) through nonradiative relaxation to the S_1 state.[52–61] Because the S_2 state decays so rapidly, it is reasonable to suggest that most of the EET in PCP must come through the S_1 state. The S_1 state then decays to the S_0 state. However, the S_0 to S_1 transition is symmetry forbidden, rendering the S_1 state a 'dark' state.[62] Further, carotenoids exhibit very weak fluorescence from the S_1 state, so the dipole strength of the S_1 state is very small, but nonzero.[48,49,59,63–73] Because the dipole strength of S_1 is very small, it is likely that any energy transfer from the S_1 state to Chl Q_y would be of poor efficiency as the dipole strength overlap integral would be small. Regardless, it has been shown that carotenoids, particularly peridinin due to its carbonyl substituent, exhibit intramolecular charge transfer (ICT) character.[61,74–85] Many studies have tried to incorporate ICT character into the EET mechanism of PCP to console the fact that S_1 has poor dipole strength. The first hypothesis suggests that the S_1 state propagates along an ICT coordinate linking diabatic S_1 and ICT states,[74,75,81,86] and a second hypothesis suggests that S_1 and the ICT state are mixed quantum mechanically.[78,87] Both of these hypothesis simply increase the dipole strength of S_1

through increased ICT character so as to increase the EET to Chl. One final hypothesis suggests that the S_1 state and the ICT state are the same state and the ICT character is derived from quantum mechanical mixing of the S_1 and S_2 state.[88] No matter the case, if the main EET pathway is through the S_1 state, the mechanism requires an increase in dipole strength of the S_1 state.

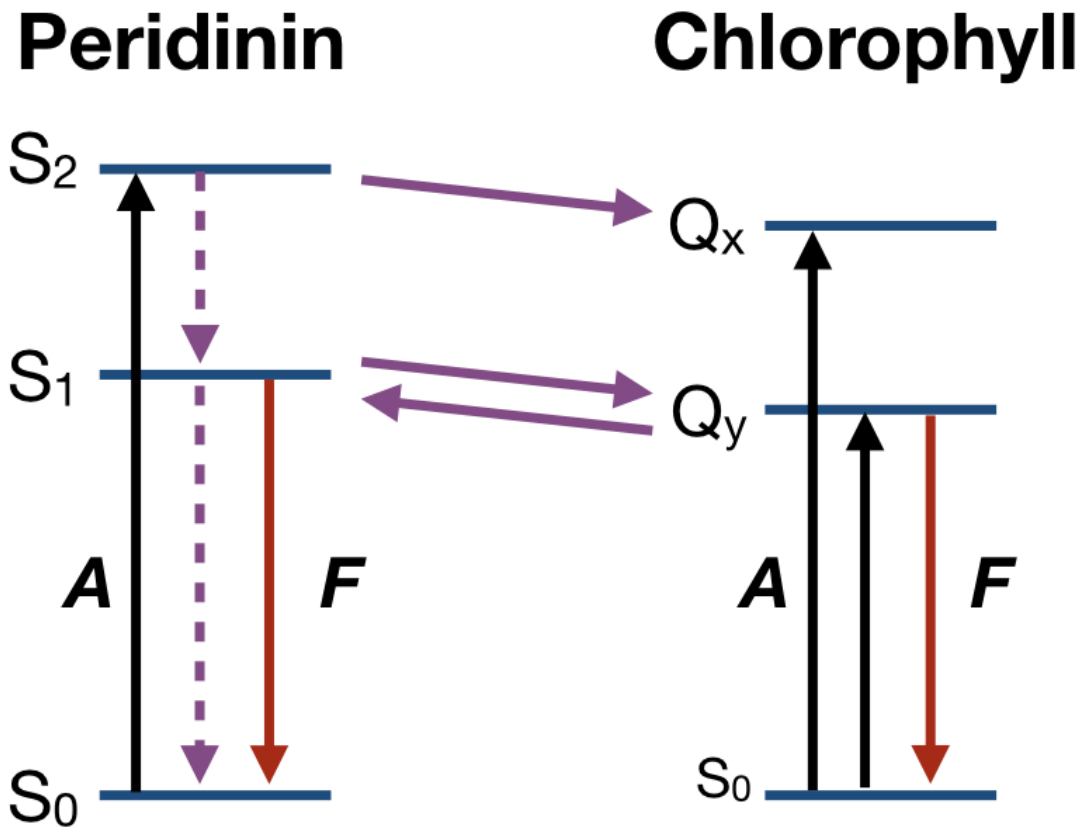

Figure 1.6. Energy level diagram showing the relative positions of states for carotenoids and Chls. Also depicted are the various pathways for intramolecular and intermolecular energy conversions. Black arrows represent the absorption of light. Dashed arrows represent intramolecular nonradiative decay pathways and horizontal arrows depict energy transfer pathways.

More recent work in our group,[89–92] however, has been able to refine the model using heterodyne transient grating spectroscopy with 40 fs pulses in place of transient absorption spectroscopy with ~100 fs pulses. Not only did these studies have increased time resolution, but they also employed global models and numerical simulations to support the model. The main result of this collection of work was the inclusion of an intermediate excited state for peridinin between S_2 and S_1 termed S_x, which has been previously discussed in the literature.[93,94] Many of the previous studies accounted for the S_x state as a vibrationally excited S_1 state, but numerical simulations by Ghosh[90] determined that S_x is indeed an independent electronic state. The formation of S_x is also accompanied by the formation of ICT character, determined by the S_x lifetime dependence on average polar solvation time and viscosity for a series of solvents.[91] A logical conclusion then is that S_x is the best assignment for the donor state for the ps energy transfer process, not the dark S_1 state as previously suggested. If S_x is indeed the primary donor for the ps timescale, we avoid the contradiction that S_1 has poor dipole strength, yet still acts as the primary EET donor. However, this model requires the EET to happen very fast (<5 ps), reaching the lower limit of acceptable rates for that of Förster energy transfer. That is why we believe that collective excitations and coherence plays a major role in light harvesting EET efficiencies.

1.6 Hypothesis and Approach

The conclusion that EET in PCP occurs mainly through the S_2 and S_x channel[92] has led us to the hypothesis that efficient EET in PCP requires more than simple incoherent EET mechanism. The inclusion of coherent EET may be able to account for the efficient and remarkable rates at which EET occurs in PCP. However, the role of delocalized energy states in

energy transfer in PCP has, up to this point, not yet been determined. If there is any presence of exciton coupling in PCP, two-dimensional electronic spectroscopy (2DES) has the ability to detect it through observation of off-diagonal cross peaks between donor and acceptor states.[95,96]

To help us understand the exact mechanism of coherent and incoherent processes in PCP, we employed 2DES with ultrashort broad-band laser spectra allowing us to observe direct EET pathways between the chromophores in PCP. By replacing the Chl *a* in wild-type PCP with Chl *b*, we were able to adjust the energy gaps between the donor and acceptor species to test any effects that may have on the EET mechanism. The main questions addressed in this dissertation are:

1) Does electronic delocalization mediate EET process within PCP?
2) How does the vibrational coupling between peridinin and chlorophyll play a role in EET?
3) How does the system-bath coupling play a role in the decoherence process in PCP?

2DES is an extremely powerful technique for studying these energy transfer processes. Previous studies investigating EET in PCP[26,77,97,98] were done using ultrafast (~100 fs pulses) transient absorption spectroscopy (TA). Here, 2DES experiments have two main advantages over these TA studies. First, our broad-band pulses were processed using an adaptive pulse shaper that compressed the pulse duration to 8 fs. Pulses that short are a significant increase in time resolution relative to the previous experiments, allowing use to resolve ultrafast dynamics. Second, and arguably even more importantly, 2DES has a second axis of frequency resolution that TA simply cannot provide. TA studies are performed by collected pump induced changes in the absorption spectrum as a function of waiting time between the pump and probe pulse, T. Any overlapping features in the spectrum are difficult to resolve from each other as there is only a

single wavelength axis. In 2DES spectroscopy, the pump pulse is split into two pulses and the time delay between the pump pulses (coherence time, τ) is scanned with a fixed waiting time T between the second pump pulse and the probe pulse. Fourier transformation of the τ axis provides the second axis of the spectra, termed the excitation axis. These spectra are to be interpreted as correlation spectra that allow one to connect an excitation event with a detected event after some waiting time, T. For instance, in PCP, after peridinin is excited, it transfers its energy to Chl, so an off-diagonal cross peak feature in the spectra would appear at an excitation wavelength that corresponds to peridinin and a detection wavelength that corresponds to Chl, completely resolved from purely peridinin and purely Chl features. Therefore, studying the position and kinetics of the 2DES features can be the most powerful way of detecting EET and determining its mechanism. A full description of 2DES is presented in the following chapter.

REFERENCES

REFERENCES

(1) Blankenship, R. E. *Molecular Mechanisms of Photosynthesis*; John Wiley & Sons, 2014.

(2) Mirkovic, T.; Ostroumov, E. E.; Anna, J. M.; van Grondelle, R.; Govindjee; Scholes, G. D. Light Absorption and Energy Transfer in the Antenna Complexes of Photosynthetic Organisms. *Chem. Rev.* 2017, *117* (2), 249–293.

(3) Fransted, K. A.; Caram, J. R.; Hayes, D.; Engel, G. S. Two-Dimensional Electronic Spectroscopy of Bacteriochlorophyll *a* in Solution: Elucidating the Coherence Dynamics of the Fenna-Matthews-Olson Complex Using Its Chromophore as a Control. *J. Chem. Phys.* 2012, *137*, 125101.

(4) Hayes, D.; Engel, G. S. Extracting the Excitonic Hamiltonian of the Fenna-Matthews-Olson Complex Using Three-Dimensional Third-Order Electronic Spectroscopy. *Biophys. J.* 2011, *100* (8), 2043–2052.

(5) Engel, G. S.; Calhoun, T. R.; Read, E. L.; Ahn, T. K.; Mančal, T.; Cheng, Y. C.; Blankenship, R. E.; Fleming, G. R. Evidence for Wavelike Energy Transfer through Quantum Coherence in Photosynthetic Systems. *Nature* 2007, *446*, 782–786.

(6) Brixner, T.; Stenger, J.; Vaswani, H. M.; Cho, M.; Blankenship, R. E.; Fleming, G. R. Two-Dimensional Spectroscopy of Electronic Couplings in Photosynthesis. *Nature* 2005, *434* (7033), 625–628.

(7) Cheng, Y.-C.; Fleming, G. R. Dynamics of Light Harvesting in Photosynthesis. *Annu. Rev. Phys. Chem.* 2009, *60*, 241–262.

(8) Papiz, M. Z.; Prince, S. M.; Hawthornthwaite-Lawless, A. M.; McDermott, G.; Freer, A. A.; Isaacs, N. W.; Cogdell, R. J. A Model for the Photosynthetic Apparatus of Purple Bacteria. *Trends Plant Sci.* 1996, *1* (6), 198–206.

(9) Ostroumov, E. E.; Mulvaney, R. M.; Anna, J. M.; Cogdell, R. J.; Scholes, G. D. Energy Transfer Pathways in Light-Harvesting Complexes of Purple Bacteria as Revealed by Global Kinetic Analysis of Two-Dimensional Transient Spectra. *J. Phys. Chem. B* 2013, *117* (38), 11349–11362.

(10) Wormit, M.; Harbach, P. H. P.; Mewes, J. M.; Amarie, S.; Wachtveitl, J.; Dreuw, A. Excitation Energy Transfer and Carotenoid Radical Cation Formation in Light Harvesting Complexes - a Theoretical Perspective. *Biochim. Biophys. Acta* 2009, *1787* (6), 738–746.

(11) Krueger, B. P.; Scholes, G. D.; Fleming, G. R. Calculation of Couplings and Energy-Transfer Pathways between the Pigments of LH2 by the Ab Initio Transition Density Cube Method. *J. Phys. Chem. B* 1998, *102* (27), 5378–5386.

(12) Polli, D.; Cerullo, G.; Lanzani, G.; De Silvestri, S.; Hashimoto, H.; Cogdell, R. J. Carotenoid-Bacteriochlorophyll Energy Transfer in LH2 Complexes Studied with 10-Fs Time Resolution. *Biophys. J.* 2006, *90* (7), 2486–2497.

(13) Kleima, F. J.; Hofmann, E.; Gobets, B.; van Stokkum, I. H.; van Grondelle, R.; Diederichs, K.; van Amerongen, H. Förster Excitation Energy Transfer in Peridinin-Chlorophyll-a-Protein. *Biophys. J.* 2000, *78* (1), 344–353.

(14) Damjanović, A.; Ritz, T.; Schulten, K. Excitation Transfer in the Peridinin-Chlorophyll-Protein of *Amphidinium Carterae*. *Biophys. J.* 2000, *79* (4), 1695–1705.

(15) Niedzwiedzki, D. M.; Jiang, J.; Lo, C. S.; Blankenship, R. E. Low-Temperature Spectroscopic Properties of the Peridinin–chlorophyll *a*–protein (PCP) Complex from the Coral Symbiotic Dinoflagellate *Symbiodinium*. *J. Phys. Chem. B* 2013, 11091–11099.

(16) Lampoura, S. S.; Krueger, B. P.; Van Stokkum, I. H. M.; Salverda, J. M.; Gradinaru, C. C.; Rutkauskas, D.; Hiller, R. G.; Van Grondelle, R. Energy Transfer in the Peridinin Chlorophyll *a* Protein of *Amphidinium carterae* Studied by Polarized Absorption Measurements. *Int. J. Mod. Phys. B* **2001**, *15* (28n30), 3849–3852.

(17) Tronrud, D. E.; Wen, J.; Gay, L.; Blankenship, R. E. The Structural Basis for the Difference in Absorbance Spectra for the FMO Antenna Protein from Various Green Sulfur Bacteria. *Photosynth. Res.* 2009, *100*, 79–87.

(18) Oostergetel, G. T.; van Amerongen, H.; Boekema, E. J. The Chlorosome: A Prototype for Efficient Light Harvesting in Photosynthesis. *Photosynth. Res.* 2010, *104* (2-3), 245–255.

(19) Baghbanzadeh, S.; Kassal, I. Distinguishing the Roles of Energy Funnelling and Delocalization in Photosynthetic Light Harvesting. *Phys. Chem. Chem. Phys.* 2016, *18* (10), 7459–7467.

(20) Papiz, M. Z.; Prince, S. M.; Howard, T.; Cogdell, R. J.; Isaacs, N. W. The Structure and Thermal Motion of the B800-850 LH2 Complex from *Rps. Acidophila* at 2.0 Å Resolution and 100 K: New Structural Features and Functionally Relevant Motions. *J. Mol. Biol.* 2003, *326* (5), 1523–1538.

(21) Scholes, G. D.; Fleming, G. R. On the Mechanism of Light Harvesting in Photosynthetic Purple Bacteria: B800 to B850 Energy Transfer. *J. Phys. Chem. B* 2000, *104*, 1854–1868.

(22) Qian, P.; Papiz, M. Z.; Jackson, P. J.; Brindley, A. A.; Ng, I. W.; Olsen, J. D.; Dickman, M. J.; Bullough, P. A.; Hunter, C. N. Three-Dimensional Structure of the Rhodobacter Sphaeroides RC-LH1-PufX Complex: Dimerization and Quinone Channels Promoted by PufX. *Biochemistry* 2013, *52* (43), 7575–7585.

(23) Hofmann, E.; Wrench, P. M.; Sharples, F. P.; Hiller, R. G.; Welte, W.; Diederichs, K. Structural Basis of Light Harvesting by Carotenoids: Peridinin-Chlorophyll-Protein from *Amphidinium Carterae*. *Science* 1996, *272* (5269), 1788–1791.

(24) Polívka, T.; Pascher, T.; Sundström, V.; Hiller, R. G. Tuning Energy Transfer in the Peridinin-Chlorophyll Complex by Reconstitution with Different Chlorophylls. *Photosynth. Res.* 2005, *86*, 217–227.

(25) Krueger, B. P.; Scholes, G. D.; Gould, I. R.; Fleming, G. R. Carotenoid-Mediated B800-B850 Coupling in LH2. *Phys. Chem. Comm.* 1999, *2*, 34–40.

(26) Bautista, J. A.; Hiller, R. G.; Sharples, F. P.; Gosztola, D.; Wasielewski, M.; Frank, H. A. Singlet and Triplet Energy Transfer in the Peridinin-Chlorophyll *a*-Protein from *Amphidinium Carterae*. *J. Phys. Chem. A* 1999, *103* (14), 2267–2273.

(27) Damjanović, A.; Ritz, T.; Schulten, K. Energy Transfer between Carotenoids and Bacteriochlorophylls in Light-Harvesting Complex II of Purple Bacteria. *Phys. Rev. E* 1999, *59*, 3293–3311.

(28) Förster, T. Zwischenmolekulare Energiewanderung Und Fluoreszenz. *Annu. Physik* 1948, *2*, 55–75.

(29) Koolhaas, M. H. C.; Frese, R. N.; Fowler, G. J. S.; Bibby, T. S.; Georgakopoulou, S.; van der Zwan, G.; Hunter, C. N.; van Grondelle, R. Identification of the Upper Exciton Component of the B850 Bacteriochlorophylls of the LH2 Antenna Complex, Using a B800-Free Mutant of *Rhodobacter Sphaeroides*. *Biochemistry* 1998, *37*, 4693–4698.

(30) Cantor, C. R.; Schimmel, P. R. *Biophysical Chemistry. Part II: Techniques for the Study of Biological Structure and Function*; W. H. Freeman and Company: San Francisco, 1980.

(31) Kelley, A. M. *Condensed-Phase Molecular Spectroscopy and Photophysics*; John Wiley & Sons: Hoboken, New Jersey, 2013.

(32) Fleming, G. R.; Scholes, G. D. Physical Chemistry - Quantum Mechanics for Plants. *Nature* 2004, *431*, 256–257.

(33) Holt, N. E.; Zigmantas, D.; Valkunas, L.; Li, X.-P.; Niyogi, K. K.; Fleming, G. R. Carotenoid Cation Formation and the Regulation of Photosynthetic Light Harvesting. *Science* 2005, *307* (5708), 433–436.

(34) Avenson, T. J.; Ahn, T. K.; Zigmantas, D.; Niyogi, K. K.; Li, Z.; Ballottari, M.; Bassi, R.; Fleming, G. R. Zeaxanthin Radical Cation Formation in Minor Light-Harvesting Complexes of Higher Plant Antenna. *J. Biol. Chem.* 2008, *283* (6), 3550–3558.

(35) Ahn, T. K.; Avenson, T. J.; Ballottari, M.; Cheng, Y.-C.; Niyogi, K. K.; Bassi, R.; Fleming, G. R. Architecture of a Charge-Transfer State Regulating Light Harvesting in a Plant Antenna Protein. *Science* 2008, *320* (5877), 794–797.

(36) Pascal, A. A.; Liu, Z.; Broess, K.; van Oort, B.; van Amerongen, H.; Wang, C.; Horton, P.; Robert, B.; Chang, W.; Ruban, A. Molecular Basis of Photoprotection and Control of Photosynthetic Light-Harvesting. *Nature* 2005, *436* (7047), 134–137.

(37) Ruban, A. V.; Berera, R.; Ilioaia, C.; van Stokkum, I. H. M.; Kennis, J. T. M.; Pascal, A. A.; van Amerongen, H.; Robert, B.; Horton, P.; van Grondelle, R. Identification of a Mechanism of Photoprotective Energy Dissipation in Higher Plants. *Nature* 2007, *450* (7169), 575–578.

(38) Bode, S.; Quentmeier, C. C.; Liao, P.-N.; Hafi, N.; Barros, T.; Wilk, L.; Bittner, F.; Walla, P. J. On the Regulation of Photosynthesis by Excitonic Interactions between Carotenoids and Chlorophylls. *Proc. Natl. Acad. Sci. U. S. A.* 2009, *106* (30), 12311–12316.

(39) Johnson, M. P.; Ruban, A. V. Photoprotective Energy Dissipation in Higher Plants Involves Alteration of the Excited State Energy of the Emitting Chlorophyll(s) in the Light Harvesting Antenna II (LHCII). *J. Biol. Chem.* 2009, *284* (35), 23592–23601.

(40) Mimuro, M.; Tamai, N.; Ishimaru, T.; Yamazaki, I. Characteristic Fluorescence Components in Photosynthetic Pigment System of a Marine Dinoflagellate, *Protogonyaulax Tamarensis*, and Excitation Energy Flow among Them. Studies by Means of Steady-State and Time-Resolved Fluorescence Spectroscopy. *Biochim. Biophys. Acta* 1990, *1016*, 280.

(41) Schulte, T.; Hiller, R. G.; Hofmann, E. X-Ray Structures of the Peridinin-Chlorophyll-Protein Reconstituted with Different Chlorophylls. *FEBS Lett.* 2010, *584* (5), 973–978.

(42) Frank, H. A.; Cogdell, R. J. Carotenoids in Photosynthesis. *Photochem. Photobiol.* 1996, *63* (3), 257–264.

(43) Kohler, B. E. A Simple Model for Linear Polyene Electronic Structure. *J. Chem. Phys.* 1990, *93*, 5838–5942.

(44) Frank, H. A.; Cogdell, R. J. The Photochemistry and Function of Carotenoids in Photosynthesis. In *Carotenoids in Photosynthesis*; Young, A., Britton, G., Eds.; Springer-Verlag: London, 1993; pp 252–326.

(45) Vaswani, H. M.; Holt, N. E.; Fleming, G. R. Carotenoid-Chlorophyll Complexes: Ready-to-Harvest. *Pure Appl. Chem.* 2005, *77* (6), 925–945.

(46) Christensen, R. L.; Barney, E. A.; Broene, R. D.; Galinato, M. G. I.; Frank, H. A. Linear Polyenes: Models for the Spectroscopy and Photophysics of Carotenoids. *Arch. Biochem. Biophys.* 2004, *430* (1), 30–36.

(47) Polívka, T.; Sundström, V. Ultrafast Dynamics of Carotenoids Excited States—from Solution to Natural and Artificial Systems. *Chem. Rev.* 2004, *104* (4), 2021–2071.

(48) Cosgrove, S. A.; Guite, M. A.; Burnell, T. B.; Christensen, R. L. Electronic Relaxation in Long Polyenes. *J. Phys. Chem.* 1990, *94*, 8118–8124.

(49) DeCoster, B.; Christensen, R. L.; Gebhard, R.; Lugtenburg, J.; Farhoosh, R.; Frank, H. A. Low-Lying Electronic States of Carotenoids. *Biochim. Biophys. Acta* 1992, *1102* (1), 107–114.

(50) Frank, H. A.; Farhoosh, R.; Decoster, B.; Christensen, R. L. *Molecular Features That Control the Efficiency of Carotenoid-to-Chlorophyll Energy Transfer in Photosynthesis*; Proc. Int. Congr. Photosyn.; Montpellier, France, 1992; Vol. 1.

(51) Frank, H. A.; Christensen, R. L. Singlet Energy Transfer from Carotenoids to Bacteriochlorophylls. In *Anoxygenic Photosynthetic Bacteria*; Blankenship, R. E., Madigan, M. T., Bauer, C. E., Eds.; Adv. Photosynth.; Kluwer Academic Publishers: Dordrecht, The Netherlands, 1995; pp 373–384.

(52) Christensen, R. L. The Electronic States of Carotenoids. In *The Photochemistry of Carotenoids*; Frank, H. A., Young, A. J., Britton, G., Cogdell, R. J., Eds.; Advances in Photosynthesis; Kluwer Academic Publishers: Dordrecht, 1999; pp 137–159.

(53) Cherry, R. J.; Chapman, D.; Langelaar, J. Fluorescence and Phosphorescence of β-Carotene. *Trans. Faraday Soc.* 1968, *64*, 2304–2307.

(54) van Riel, M.; Kleinen-Hammans, J.; van de Ven, M.; Verwer, W.; Levine, Y. Fluorescence Excitation Profiles of β-Carotene in Solution and in Lipid/water Mixtures. *Biochem. Biophys. Res. Commun.* 1983, *113*, 102–107.

(55) Haley, L. V.; Koningstein, J. A. Space and Time-Resolved Resonance-Enhanced Vibrational Raman Spectroscopy from Femtosecond-Lived Singlet Excited State of β-Carotene. *Chem. Phys.* 1983, *77*, 1–9.

(56) Watanabe, J.; Kinoshita, S.; Kushida, T. Non-Motional Narrowing Effect in Excitation Profiles of Second-Order Optical Processes: Comparison between Stochastic Theory and Experiments in β-Carotene. *Chem. Phys. Lett.* 1986, *126*, 197–200.

(57) Bondarev, S. L.; Dvornikov, S. S.; Bachilo, S. M. Fluorescence of β-Carotene at 77 and 4.2 K. *Opt. Spectrosc.* 1988, *64*, 268–270.

(58) Gillbro, T.; Cogdell, R. J. Carotenoid Fluorescence. *Chem. Phys. Lett.* 1989, *158* (3-4), 312–316.

(59) Koyama, Y.; Kuki, M.; Andersson, P. O.; Gillbro, T. Singlet Excited States and the Light-Harvesting Function of Carotenoids in Bacterial Photosynthesis. *Photochem. Photobiol.* 1996, *63* (3), 243–256.

(60) Frank, H. A.; Young, A. J.; Britton, G.; Cogdell, R. J. The Photochemistry of Carotenoids. In *Advances in Photosynthesis*; Govindjee, Ed.; Kluwer Academic Publishers: Dordrecht, 1999.

(61) Frank, H. A.; Bautista, J. A.; Josue, J.; Pendon, Z.; Hiller, R. G.; Sharples, F. P.; Gosztola, D.; Wasielewski, M. R. Effect of the Solvent Environment on the Spectroscopic Properties and Dynamics of the Lowest Excited States of Carotenoids. *J. Phys. Chem. B* 2000, *104* (18), 4569–4577.

(62) Birge, R. R. Two Photon Spectroscopy of Protein-Bound Chromophores. *Acc. Chem. Res.* 1986, *19*, 138–146.

(63) Mimuro, M.; Nagashima, U.; Takaichi, S.; Nishimura, Y.; Yamazaka, I.; Katoh, T. Molecular Structure and Optical Properties of Cartenoids for the *in Vivo* Energy Transfer Function in Algal Photosynthetic Pigment System. *Biochim. Biophys. Acta* 1992, *1098*, 271–274.

(64) Mimuro, M.; Nishimura, Y.; Yamazaki, I.; Katoh, T.; Nagashima, U. Fluorescence Properties of the Allenic Carotenoid Fucoxanthin: Analysis of the Effect of Keto Carbonyl Group by Using a Model Compound, All-Trans-B-Apo-8'-Carotenal. *J. Lumin.* 1991, *50*, 1–10.

(65) Katoh, T.; Nagashima, U.; Mimuro, M. Fluorescence Properties of the Allenic Carotenoid Fucoxanthin: Implication for Energy Transfer in Photosynthetic Pigment Systems. *Photosynth. Res.* 1991, *27* (3), 221–226.

(66) Andersson, P. O.; Gillbro, T.; Asato, A. E.; Liu, R. S. H. Dual Singlet State Emission in a Series of Mini-Carotenes. *J. Lumin.* 1992, *51* (1-3), 11–20.

(67) Fujii, R.; Onaka, K.; Kuki, M.; Koyama, Y.; Watanabe, Y. The $2A_g^-$ Energies of All-*trans*-Neurosporene and Spheroidene as Determined by Fluorescence Spectroscopy. *Chem. Phys. Lett.* 1998, *288* (5,6), 847–853.

(68) Koyama, Y. Structures, Excited-State Properties and Functions of Carotenoids in Photosynthesis. *Spectrosc. Biol. Mol., Eur. Conf., 6th* 1995, 183–186.

(69) Onaka, K.; Fujii, R.; Nagae, H.; Kuki, M.; Koyama, Y.; Watanabe, Y. The State Energy and the Displacements of the Potential Minima of the $2A_g^-$ State in All-*trans*-β-Carotene as Determined by Fluorescence Spectroscopy. *Chem. Phys. Lett.* 1999, *315* (1,2), 75–81.

(70) Watanabe, Y.; Kameyama, T.; Miki, Y.; Kuki, M.; Koyama, Y. The 2 ^{1} A\textsubscript{g}- State and Two Additional Low-Lying Electronic States of Spheroidene Newly Identified by Fluorescence and Fluorescence-Excitation Spectroscopy at 170 K. *Chem. Phys. Lett.* 1993, *206* (1-4), 62–68.

(71) Cogdell, R. J.; Andersson, P. O.; Gillbro, T. Carotenoid Singlet States and Their Involvement in Photosynthetic Light-Harvesting Pigments. *J. Photochem. Photobiol. B* 1992, *15* (1-2), 105–112.

(72) Gillbro, T.; Andersson, P. O.; Liu, R. S. H.; Asato, A. E.; Takaishi, S.; Cogdell, R. J. Location of the Carotenoid $2A_g^-$ State and Its Role in Photosynthesis. *Photochem. Photobiol.* 1993, *57* (1), 44–48.

(73) Bondarev, S. L.; Knyukshto, V. N. Fluorescence from the S_1 (2^1A_g) State of All-*trans*-β-Carotene. *Chem. Phys. Lett.* 1994, *225*, 346–350.

(74) Bautista, J. A.; Connors, R. E.; Raju, B. B.; Hiller, R. G.; Sharples, F. P.; Gosztola, D.; Wasielewski, M. R.; Frank, H. A. Excited State Properties of Peridinin: Observation of a Solvent Dependence of the Lowest Excited Singlet State Lifetime and Spectral Behavior Unique among Carotenoids. *J. Phys. Chem. B* 1999, *103* (41), 8751–8758.

(75) Vaswani, H. M.; Hsu, C. P.; Head-Gordon, M.; Fleming, G. R. Quantum Chemical Evidence for an Intramolecular Charge-Transfer State in the Carotenoid Peridinin of Peridinin-Chlorophyll-Protein. *J. Phys. Chem. B* 2003, *107* (31), 7940–7946.

(76) Zigmantas, D.; Polívka, T.; Hiller, R. G.; Yartsev, A.; Sundström, V. Spectroscopic and Dynamic Properties of the Peridinin Lowest Singlet Excited States. *J. Phys. Chem. A* 2001, *105* (45), 10296–10306.

(77) Zigmantas, D.; Hiller, R. G.; Polívka, T.; Sundström, V. Carotenoid to Chlorophyll Energy Transfer in the Peridinin–chlorophyll-*a*–protein Complex Involves an Intramolecular Charge Transfer State. *Proc. Natl. Acad. Sci. U. S. A.* 2002, *99*, 16760–16765.

(78) Zigmantas, D.; Hiller, R. G.; Yartsev, A.; Sundström, V.; Polívka, T. Dynamics of Excited States of the Carotenoid Peridinin in Polar Solvents: Dependence on Excitation Wavelength, Viscosity, and Temperature. *J. Phys. Chem. B* 2003, *107*, 5339–5348.

(79) Zigmantas, D.; Hiller, R. G.; Sharples, F. P.; Frank, H. A.; Sundström, V.; Polívka, T. Effect of a Conjugated Carbonyl Group on the Photophysical Properties of Carotenoids. *Phys. Chem. Chem. Phys.* 2004, *6* (11), 3009–3016.

(80) Herek, J. L.; Wendling, M.; He, Z.; Polívka, T.; Garcia-Asua, G.; Cogdell, R. J.; Hunter, C. N.; van Grondelle, R.; Sundström, V.; Pullerits, T. Ultrafast Carotenoid Band Shifts: Experiment and Theory. *J. Phys. Chem. B* 2004, *108* (29), 10398–10403.

(81) Papagiannakis, E.; Larsen, D. S.; van Stokkum, I. H. M.; Vengris, M.; Hiller, R. G.; van Grondelle, R. Resolving the Excited State Equilibrium of Peridinin in Solution. *Biochemistry* 2004, *43* (49), 15303–15309.

(82) Wild, D. A.; Winkler, K.; Stalke, S.; Oum, K.; Lenzer, T. Extremely Strong Solvent Dependence of the S_1 -> S0 Internal Conversion Lifetime of 12'-Apo-β-Caroten-12'-Al. *Phys. Chem. Chem. Phys.* 2006, *8* (21), 2499–2505.

(83) Stalke, S.; Wild, D. A.; Lenzer, T.; Kopczynski, M.; Lohse, P. W.; Oum, K. Solvent-Dependent Ultrafast Internal Conversion Dynamics of N'-Apo-Beta-Carotenoic-N'-Acids (n = 8, 10, 12). *Phys. Chem. Chem. Phys.* 2008, *10* (16), 2180–2188.

(84) Kopczynski, M.; Ehlers, F.; Lenzer, T.; Oum, K. Evidence for an Intramolecular Charge Transfer State in 12'-Apo-β-Caroten-12'-Al and 8'-Apo-β-Caroten-8'-Al: Influence of Solvent Polarity and Temperature. *J. Phys. Chem. A* 2007, *111* (25), 5370–5381.

(85) Ehlers, F.; Wild, D. A.; Lenzer, T.; Oum, K. Investigation of the S_1/ICT → S0 Internal Conversion Lifetime of 4'-Apo-β-Caroten-4'-Al and 8'-Apo-β-Caroten-8'-Al: Dependence on Conjugation Length and Solvent Polarity. *J. Phys. Chem. A* 2007, *111* (12), 2257–2265.

(86) Papagiannakis, E.; Vengris, M.; Larsen, D. S.; van Stokkum, I. H. M.; Hiller, R. G.; van Grondelle, R. Use of Ultrafast Dispersed Pump-Dump-Probe and Pump-Repump-Probe Spectroscopies to Explore the Light-Induced Dynamics of Peridinin in Solution. *J. Phys. Chem. B* 2006, *110* (1), 512–521.

(87) Linden, P. A.; Zimmermann, J.; Brixner, T.; Holt, N. E.; Vaswani, H. M.; Hiller, R. G.; Fleming, G. R. Transient Absorption Study of Peridinin and Peridinin–chlorophyll *a*–protein after Two-Photon Excitation. *J. Phys. Chem. B* 2004, *108*, 10340–10345.

(88) Shima, S.; Ilagan, R. P.; Gillespie, N.; Sommer, B. J.; Hiller, R. G.; Sharples, F. P.; Frank, H. A.; Birge, R. R. Two-Photon and Fluorescence Spectroscopy and the Effect of Environment on the Photochemical Properties of Peridinin in Solution and in the Peridinin-Chlorophyll-Protein from *Amphidinium Carterae*. *J. Phys. Chem. A* 2003, *107*, 8052–8066.

(89) Ghosh, S.; Bishop, M. M.; Roscioli, J. D.; Mueller, J. J.; Shepherd, N. C.; LaFountain, A. M.; Frank, H. A.; Beck, W. F. Femtosecond Heterodyne Transient-Grating Studies of Nonradiative Decay of the S_2 ($1^1B_u^+$) State of β-Carotene: Contributions from Dark Intermediates and Double-Quantum Coherences. *J. Phys. Chem. B* 2015, *119*, 14905–14924.

(90) Ghosh, S.; Bishop, M. M.; Roscioli, J. D.; LaFountain, A. M.; Frank, H. A.; Beck, W. F. Femtosecond Heterodyne Transient Grating Studies of Nonradiative Deactivation of the S_2 ($1^1B_u^+$) State of Peridinin: Detection and Spectroscopic Assignment of an Intermediate in the Decay Pathway. *J. Phys. Chem. B* 2016, *120*, 3601–3614.

(91) Ghosh, S.; Roscioli, J. D.; Bishop, M. M.; Gurchiek, J. K.; LaFountain, A. M.; Frank, H. A.; Beck, W. F. Torsional Dynamics and Intramolecular Charge Transfer in the S_2 ($1^1B_u^+$) Excited State of Peridinin: A Mechanism for Enhanced Mid-Visible Light Harvesting. *J. Phys. Chem. Lett.* 2016, *7*, 3621–3626.

(92) Ghosh, S.; Bishop, M. M.; Roscioli, J. D.; LaFountain, A. M.; Frank, H. A.; Beck, W. F. Excitation Energy Transfer by Coherent and Incoherent Mechanisms in the Peridinin–chlorophyll *a* Protein. *J. Phys. Chem. Lett.* 2017, *8*, 463–469.

(93) Polívka, T.; Sundström, V. Dark Excited States of Carotenoids: Consensus and Controversy. *Chem. Phys. Lett.* 2009, *477*, 1–11.

(94) Cerullo, G.; Polli, D.; Lanzani, G.; De Silvestri, S.; Hashimoto, H.; Cogdell, R. J. Photosynthetic Light Harvesting by Carotenoids: Detection of an Intermediate Excited State. *Science* 2002, *298* (5602), 2395–2398.

(95) Collini, E.; Wong, C. Y.; Wilk, K. E.; Curmi, P. M. G.; Brumer, P.; Scholes, G. D. Coherently Wired Light-Harvesting in Photosynthetic Marine Algae at Ambient Temperature. *Nature* 2010, *463*, 644.

(96) Hossein-Nejad, H.; Curutchet, C.; Kubica, A.; Scholes, G. D. Delocalization-Enhanced Long-Range Energy Transfer between Cryptophyte Algae PE545 Antenna Proteins. *J. Phys. Chem. B* 2010, *115*, 5243.

(97) Krueger, B. P.; Lampoura, S. S.; van Stokkum, I. H. M.; Papagiannakis, E.; Salverda, J. M.; Gradinaru, C. C.; Rutkauskas, D.; Hiller, R. G.; van Grondelle, R. Energy Transfer in the Peridinin Chlorophyll-*a* Protein of *Amphidinium Carterae* studied by Polarized Transient Absorption and Target Analysis. *Biophys. J.* 2001, *80*, 2843–2855.

(98) van Stokkum, I. H. M.; Papagiannakis, E.; Vengris, M.; Salverda, J. M.; Polívka, T.; Zigmantas, D.; Larsen, D. S.; Lampoura, S. S.; Hiller, R. G.; van Grondelle, R. Inter-Pigment Interactions in the Peridinin Chlorophyll Protein Studied by Global and Target Analysis of Time Resolved Absorption Spectra. *Chem. Phys.* 2009, *357*, 70–78.

Chapter 2: Experimental

Two-dimensional electronic spectroscopy (2DES), a third-order nonlinear spectroscopy (three light-matter interactions), is a powerful technique capable of elucidating excited state dynamics for any system. However, it is also a very complicated technique, both theoretically and in practice. The goal of this chapter is to introduce the density matrix of a molecular system and double-sided Feynman diagrams. Feynman diagrams aid in understanding how laser pulses interact with molecules. We will discuss the Feynman diagrams corresponding to *ground state bleaching*, *stimulated emission*, and *excited state absorption* third-order responses for a three level system to build up an understanding of third-order nonlinear spectroscopy. The chapter concludes with a full description of 2DES spectroscopy and how it was implemented in our laboratory.

2.1 Nonlinear Optical Spectroscopy

This section will briefly cover the theory required to understand the density matrix of molecular systems. A density matrix is a matrix representation of a system's wavefunction, or quantum state. Using the density matrix is required here to account for the evolution of an ensemble, or a large collection of molecules, because the ensemble can be distributed among many states. The density matrix formalism can account for the statistical distribution. The content is based on that presented by Hamm and Zanni.[1] A more complete coverage of nonlinear optical spectroscopy is covered by Mukamel.[2] We will follow up the description of the density matrix with an introduction to double-sided Feynman diagrams, which are used to express third-

order responses using arrows and the elements of the density matrix.

2.1.1 Density Matrix of a System

The density matrix provides a set of all of the possible states a system can occupy. Using a density matrix along with the transition dipole moment operator allows one to follow the evolution of a system after field-matter interactions.[2–4] More details are provided in the following text, but first, a density matrix is represented as:

$$\rho \equiv |\psi\rangle\langle\psi| = \sum_{n,m} c_n c_m^* |n\rangle\langle m| \tag{2.1}$$

Equation 2.1 is the density matrix for a single isolated system, such as a molecule in the gas phase. When studying biological systems that exist in the condensed phase, the density matrix needs to be rewritten to account for an ensemble. Simply incorporating a population distribution coefficient into Equation 2.1, allows for the density matrix to represent the whole ensemble:

$$\rho = \sum_{s} p_s |\psi_s\rangle\langle\psi_s| \tag{2.2}$$

In Equation 2.2, p_s accounts for any distribution of the molecules among the states in the density matrix. Both Equations 2.1 and 2.2 use the Dirac notation or *bra-ket* notation often used while describing quantum states. The wavefunction $\langle\psi_s|$ is the *bra* term, and $|\psi_s\rangle$ is the *ket* term. The bra and ket terminology becomes useful when discussing which term the dipole moment operator acts upon in the density matrix. The density matrix for a three level system composed of a ground state *g*, the first excited state, *e*, and the second excited state, *f*, can be expressed as:

$$\rho = \begin{pmatrix} gg & eg & fg \\ ge & ee & fe \\ gf & ef & ff \end{pmatrix} \tag{2.3}$$

The on-diagonal elements, *gg*, *ee*, and *ff*, are *populations*, where as the off-diagonal elements are termed *coherences*. A single action of light on a population creates a coherence, or an oscillating charge density between two states, and an action of light on a coherence creates a population. Therefore, single actions of light on the density matrix can only make transitions between states horizontally, or vertically in the density matrix. In order to drive molecules from the ground state, *gg*, to the excited states, *ee*, two actions of light are required. It should be noted that coherences emit light resonant to the energy gap and populations evolve nonradiatively. Remember, a coherence is an oscillating charge density and as Maxwell's equations express, oscillating charges emit electromagnetic waves at the frequency of the oscillation. As will be discussed in the next section, the third-order signals are actually emissions from coherences.

2.1.2 Third-Order Nonlinear Optical Response

Nonlinear spectroscopy on the systems discussed in this thesis include three types of signals: *ground state bleaching*, *stimulated emission*, and *excited-state absorption*. As shown in the following discussion, these signals can be easily understood by employing two types of diagrams: wave mixing energy level diagrams (WMEL) and double-sided Feynman diagrams, with the latter especially helpful for *resonant* systems, where the incident electromagnetic radiation is tuned to match the gap between the energy levels. A three level system is required to discuss the excited state absorption signal. WMEL diagrams show the three states as horizontal

lines labelled *g* for the ground state, *e* for the first excited state, and *f* for the second excited state. The three laser actions are shown by red arrows with time increasing to the right. Dashed arrows act on the right side or bra side of the Feynman diagram. Solid arrows act on the left side or ket side of the Feynman diagram. The evolution of the density matrix is shown in between arrows. Feynman diagrams are similar in that they show the evolution of the density matrix, but instead of showing the actual energy levels, it simply shows two parallel vertical lines. The left side vertical line is the ket side of the density matrix, and the right side vertical line is the bra side of the density matrix. For Feynman diagrams, time increase vertically along the diagram. Arrows pointing toward the center of the Feynman diagram are absorptive processes and arrows point outwards are emissive processes. The final wavy arrow is the emitted third-order signal.

Before we get into the description of the different types of signals, it is important to point out that due to choice made in our 2DES spectrometer, each action of light has a fixed direction. That is to say that one pump arrow in the following diagrams always points to the left and the other pump arrow always points to the right. The probe arrow always points to the right, as well. The directions of the arrows has implications on the total number of possible signals. Fixing the arrow direction through experimental design greatly minimizes the total number of permutations of light-matter interactions available in the diagrams. The experimental setup that enforces the directionality is described at the end of this chapter.

Ground state bleaching (GSB) occurs when the first two actions of light create a ground state population and the probe pulse re-excites that ground state population. As shown in Figures 2.1 and 2.2, prior to any actions both the WMEL (left) and Feynman diagram (right) show the equilibrium ground state population *gg*. The first pump pulse can create a *ge* coherence

as shown in Figure 2.1 or a *eg* coherence as shown in Figure 2.2. The type of coherence created is only dependent upon what pump actions happens first due to the fixed directions and time ordering of the field-matter interactions. At this point, if no further actions were to occur, the coherence would simply decay in time, emitting light until the coherence vanished. However, in 2DES, after a short coherence time, τ, the second pump pulse acts on the coherence and can create a nonequilibrium population in the ground state. The ground state is different than the equilibrium ground state because it has been acted on by two actions of light and the momentum of those photons must be conserved within the molecules. The third action of light after the waiting time T then acts on the ground state to create another coherence *eg* or *ge*. That coherence is allowed to decay and emit a signal after an emission time, t. The emission from the final coherence is the third-order signal that we are interested in collecting for 2DES.

If the coherence created by the first field-matter interaction is different than the coherence created by the third field-matter interaction (as in Figure 2.1), the third-order response is considered to be a *rephasing* signal. If they are the same (Figure 2.2), the third-order response is considered to be a *nonrephasing* signal. For nonrephasing signals, the coherence decays as the the electric polarization created by the light-matter interaction decays due to macroscopic dephasing. In other words, the oscillating charge densities of the molecules in the ensemble are initially in phase as created by the laser field, but fluctuations of the local electric field cause the molecular polarizations to get out of phase (dephasing). While the coherence is decaying the amplitude of emitted light also decreases. A coherent detector would measure a damped electromagnetic wave at the frequency of the energy gap, a *free induction decay* (FID). Rephasing signals emit a *photon echo*, essentially a rising FID followed by a falling FID. As the

first coherence dephases, a second action of light can flip the phase of the polarization so that the dephasing reverses and the electric polarization begins to rephase. Rephasing increases the electric polarization until the polarization reaches a maximum before it begins to dephase again. The increasing and decreasing of the electric polarization is the emitted the photon echo.

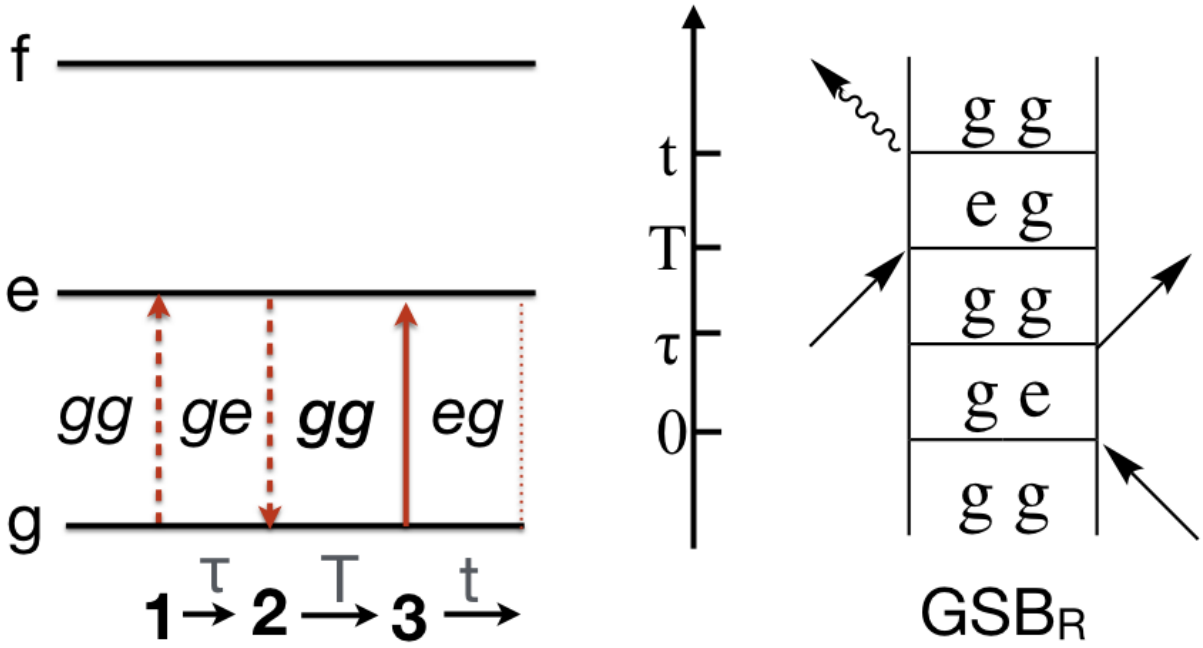

Figure 2.1. WMEL diagram (left) and Feynman diagram (right) corresponding to a rephasing ground-state bleaching response. In the WMEL diagram, time increased from left to right. The dashed arrows act on the right side of the Feynman diagrams and the solid arrows act on the left side of the Feynman diagrams. The dashed line in the WMEL and the wavy arrow in the Feynman diagram represent the emission of the signal.

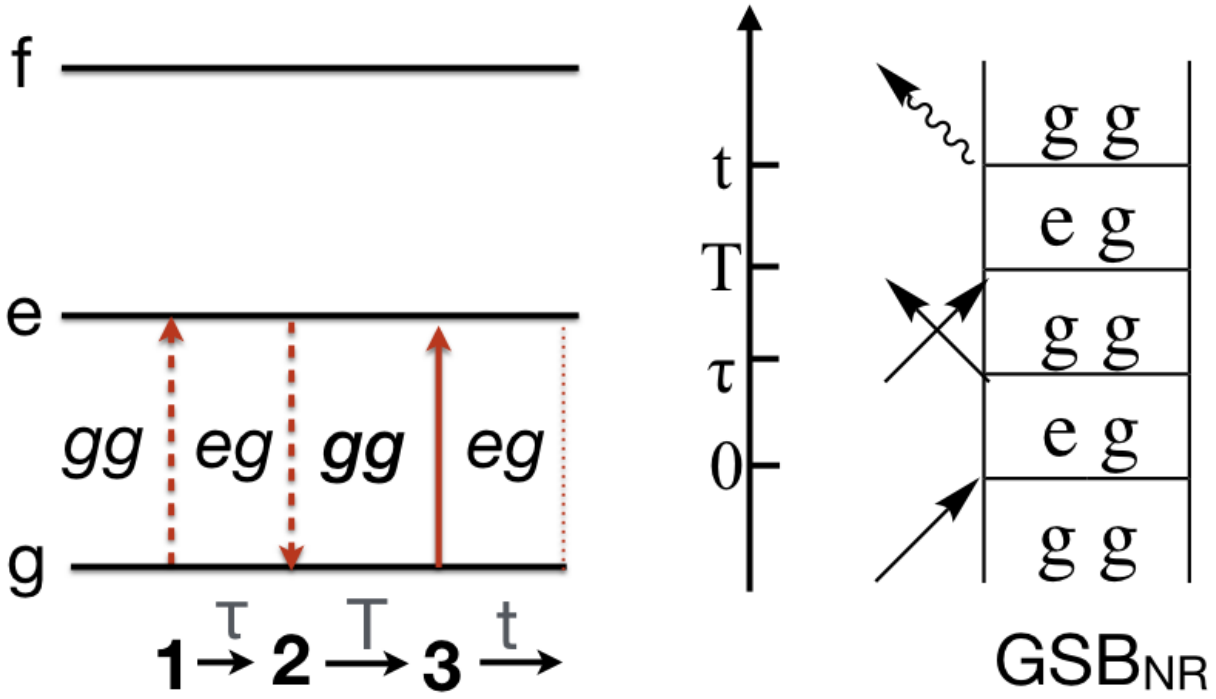

Figure 2.2. WMEL diagram (left) and Feynman diagram (right) corresponding to a nonrephasing ground-state bleaching response. In the WMEL diagram, time increased from left to right. The dashed arrows act on the right side of the Feynman diagrams and the solid arrows act on the left side of the Feynman diagrams. The dashed line in the WMEL and the wavy arrow in the Feynman diagram represent the emission of the signal.

Stimulated emission (SE) is similar to GSB in that only the ground state and the first excited state are involved, but it differs in that the first two pump pulses create a population in the excited state. Again, in Figures 2.3 and 2.4, prior to any actions the ensemble is in the equilibrium ground state population *gg*. The first pump pulse creates a *ge* coherence in Figure 2.3 and a *eg* coherence in Figure 2.4. Then, after the coherence time τ, the second pump pulse acts on the coherence and creates a population in the excited state *ee*. The third action of light after the waiting time *T* then acts on the excited state to, again, create the *eg* coherence. That coherence emits a signal after an emission time *t*. Figure 2.3 shows the rephasing stimulated emission pathway and Figure 2.4 shows the nonrephasing stimulated pathway.

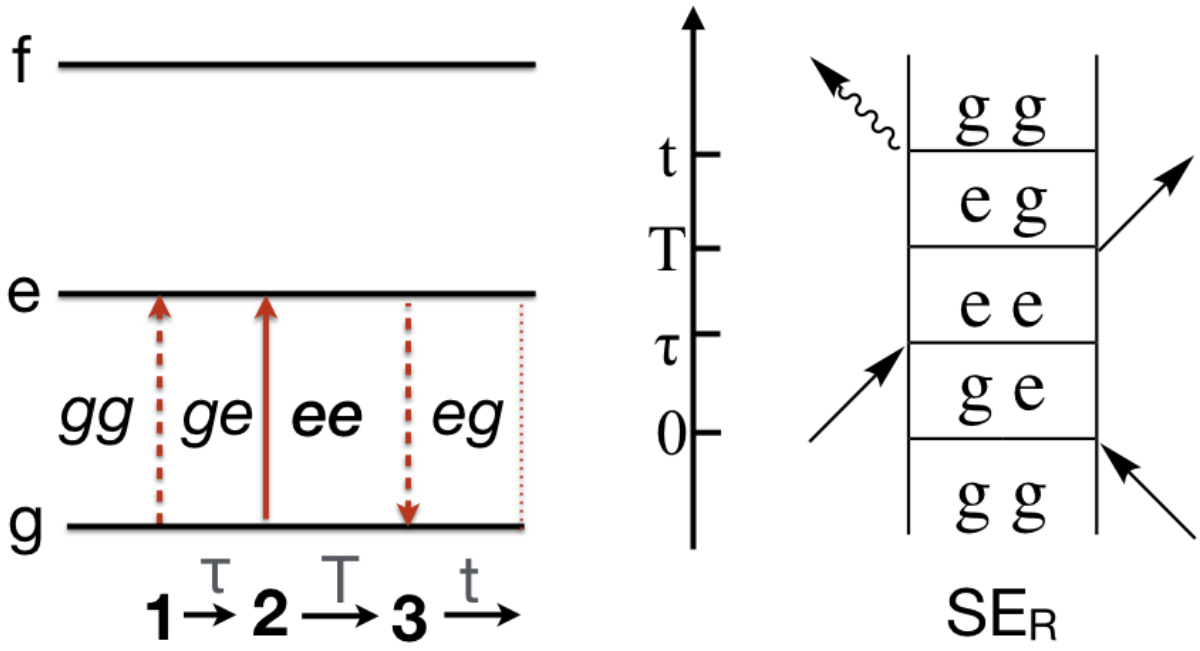

Figure 2.3. WMEL diagram (left) and Feynman diagram (right) corresponding to a rephasing stimulated emission response. In the WMEL diagram, time increased from left to right. The dashed arrows act on the right side of the Feynman diagrams and the solid arrows act on the left side of the Feynman diagrams. The dashed line in the WMEL and the wavy arrow in the Feynman diagram represent the emission of the signal.

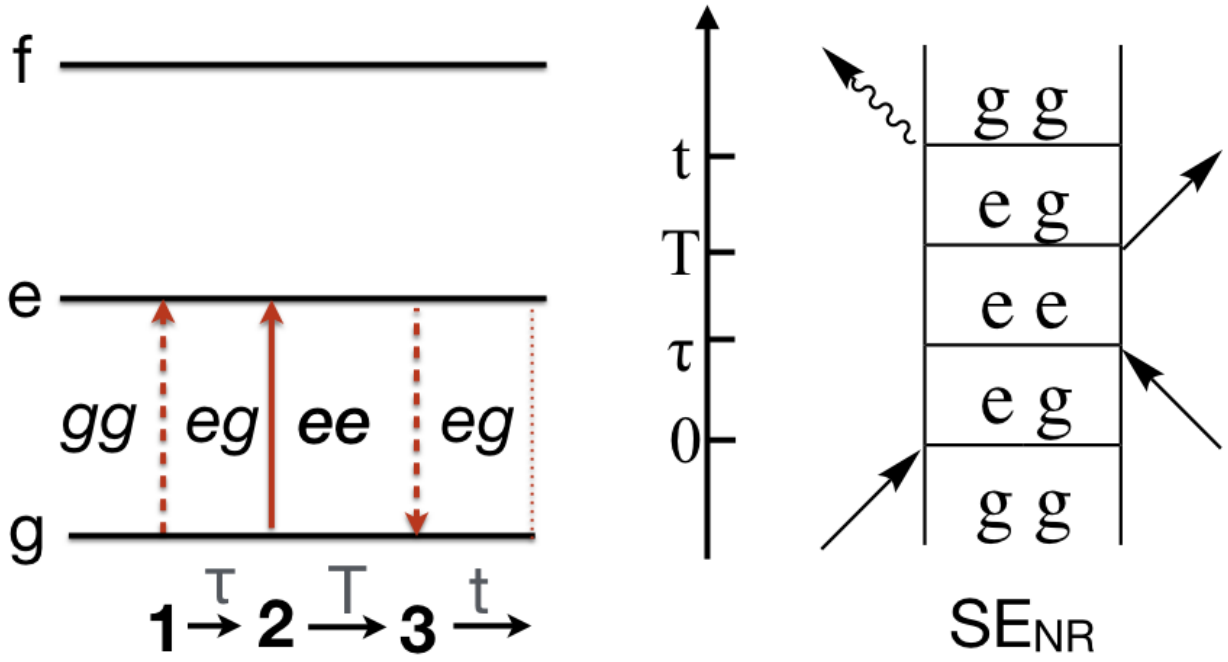

Figure 2.4. WMEL diagram (left) and Feynman diagram (right) corresponding to a nonrephasing stimulated emission response. In the WMEL diagram, time increased from left to right. The dashed arrows act on the right side of the Feynman diagrams and the solid arrows act on the left side of the Feynman diagrams. The dashed line in the WMEL and the wavy arrow in the Feynman diagram represent the emission of the signal.

Excited-state absorption (ESA) differs from SE and GSB because it involves the second excited state *f* (Figures 2.5 and 2.6). The first two actions are similar to that of SE, but the probe pulse actually excites the first excited state, creating the *ef* coherence. The *ef* coherence is the signal emitting coherence for ESA pathways. Here, the exact coherence can not be regenerated by the pulse because the probe action acts on a different energy gap. However, we still label Figure 2.5 as the rephasing pathway and Figure 2.6 as the nonrephasing pathway based upon which pump pulse acts first on the density matrix. If the pump action acts on the bra side of the density matrix first, it is a rephasing pathway, whereas an action on the ket side of the density matrix it is a nonrephasing pathway, consistent with SE and GSB pathways.

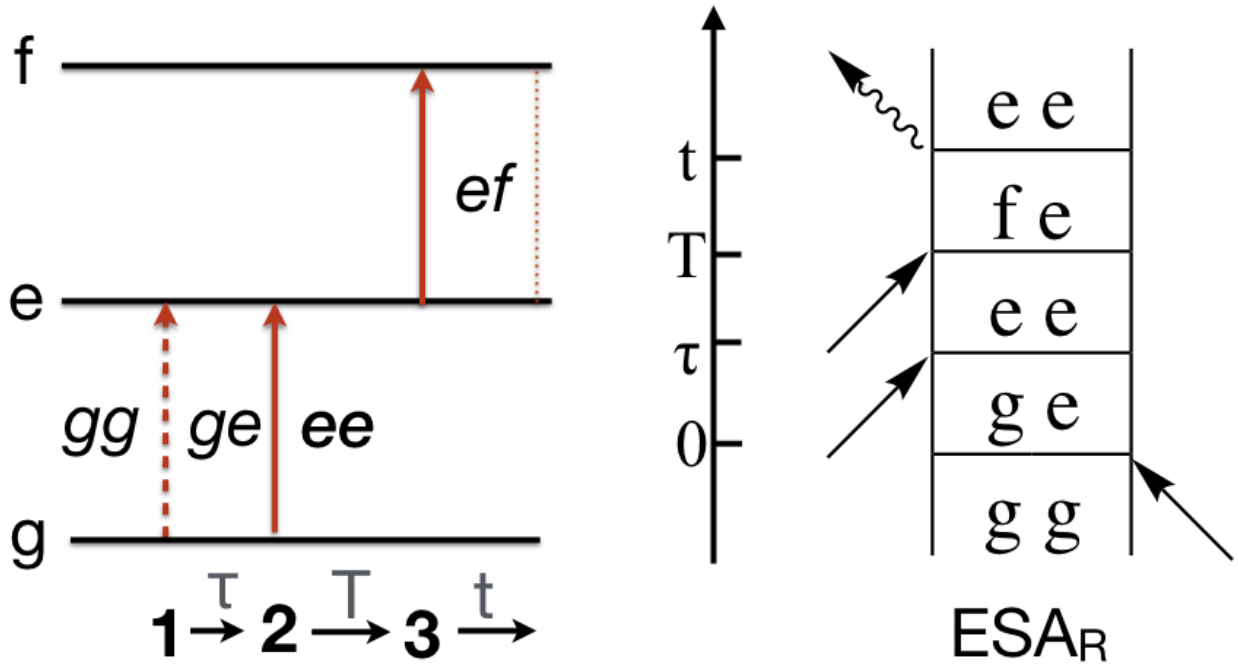

Figure 2.5. WMEL diagram (left) and Feynman diagram (right) corresponding to a rephasing excited-state absorption response. In the WMEL diagram, time increased from left to right. The dashed arrows act on the right side of the Feynman diagrams and the solid arrows act on the left side of the Feynman diagrams. The dashed line in the WMEL and the wavy arrow in the Feynman diagram represent the emission of the signal.

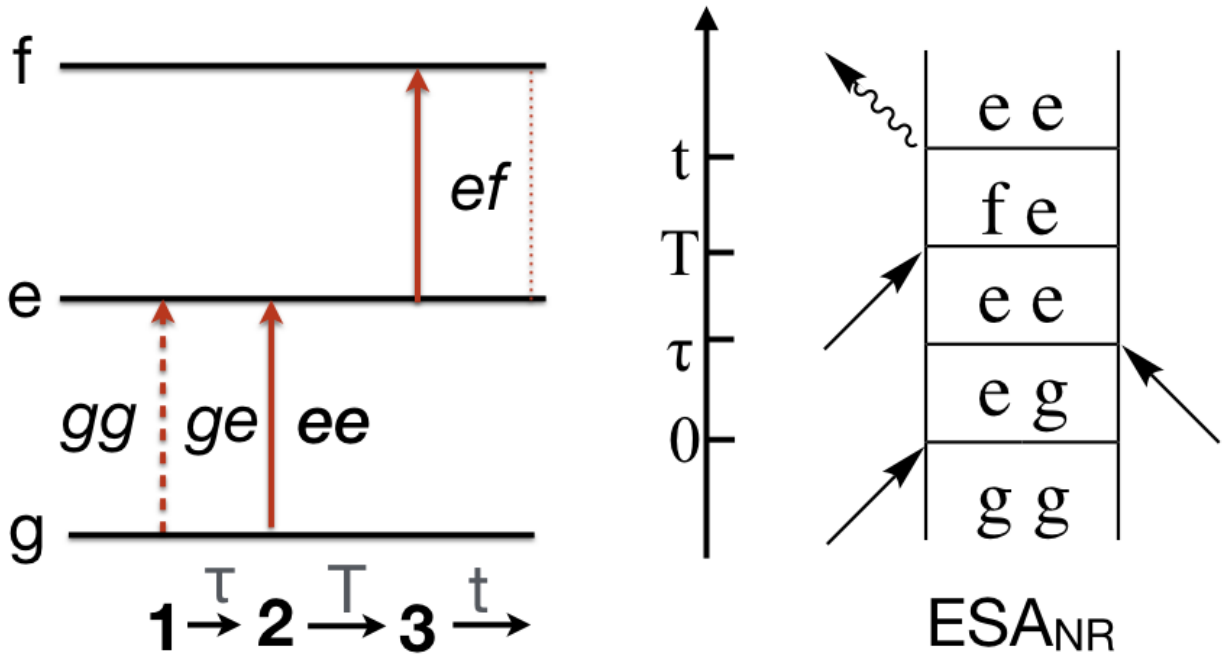

Figure 2.6. WMEL diagram (left) and Feynman diagram (right) corresponding to a nonrephasing excited-state absorption response. In the WMEL diagram, time increased from left to right. The dashed arrows act on the right side of the Feynman diagrams and the solid arrows act on the left side of the Feynman diagrams. The dashed line in the WMEL and the wavy arrow in the Feynman diagram represent the emission of the signal.

2.2 Two-Dimensional Electronic Spectroscopy

The experiments employed in this dissertation project to measure electronic coherences and energy transfer pathways used the broadband two-dimensional electronic spectroscopy (2DES) method, which is based on the pioneering work by Jonas and coworkers.[5] The first 2DES experiments in the Jonas laboratory used a conventional Michelson interferometer to split a single pulse train from a cavity dumped Ti:sapphire laser into four pulses and to control their times of arrival at the sample position with conventional time-of-flight delay lines.[6] A technique like this causes difficulty because the phase between all of the experimental pulses is difficult to control. Subsequent work in the Fleming[7] and Miller[8,9] laboratories established the now standard approach of using a diffractive optic and that allows for passively phase stabilized optical geometry using wedge-shaped prisms to control time delays.[10] Both approaches use spectral interferometry to measure the amplitude and phase of the third-order signal.[6,11–14]

In all of the above 2DES implementations, the pump pulse is split into two pulses and the time delay between the pump pulses (coherence time, τ) is scanned with a fixed waiting time T between the second pump pulse and the probe pulse (Figure 2.7). A series of τ dependent spectra at a fixed time T are directly detected using a spectrograph and charge coupled device (CCD) to generate the first wavelength axis, termed the detection axis. The second axis is generated by Fourier transformation of the τ axis, creating the excitation wavelength axis. These spectra are to be interpreted as correlation spectra that allow one to connect an excitation event with a detected event after some waiting time, T, allowing for the elucidation of energy transfer pathways in photosynthetic light harvesting proteins.[15–17]

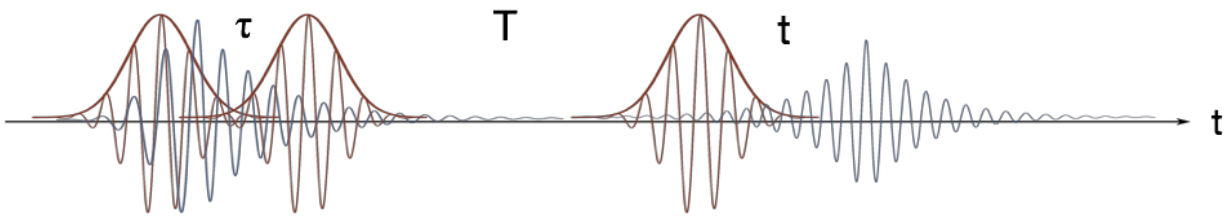

Figure 2.7. Pulse sequence used in the 2DES experiments. The red Gaussians are each of the three experimental pulses. The first pulse creates a coherence, as shown by the blue damped cosine. After some coherence time, τ, a second pulse acts on the coherence to create a population. The population is allowed to propagate for a waiting time, T, before the third pulse (probe) creates a coherence that emits the signal, in this case a photon echo (blue rising and decay cosine).

The following section explains how we implemented these methods in our laboratory. Our experimental design allowed for us to have three pulses with two time delays, τ and T, that controlled the time ordering (as discussed in Section 2.1.2). We also used the boxcars geometry and placed the detector in the $k_s = -k_1 + k_2 + k_3$ direction to ensure conservation of momentum and the directionality of pulse actions on the density matrix (phase matching).

2.2.1 Laser and Instrumentation for 2DES

The femtosecond excitation pulses required for the 2DES experiment were produced by a Yb oscillator and amplifier (Spectra-Physics Spirit) that has a 100 kHz output at 1.04 μm with 4 W total output power. The laser beam pumped a noncollinear optical parametric amplifier (NOPA, Spectra-Physics Spirit-NOPA-3H) that split the input beam into two beams for generation of a white light continuum (WL) and third harmonic light (THG). The THG and WL were mixed at two amplification stages responsible for generating the laser spectrum used in the experiments reported in the remainder of the dissertation. The NOPA output was then split into pump and probe beams which each were temporally compensated by two adaptive pulse shapers

(FemtoJock and FemtoJock P, Biophotonic Solutions Inc.). The collection of these four devices allowed for a laser spectrum that spanned 520 nm-690 nm with a central wavelength of 600 nm (100 nm FWHM) and a 7 fs transform limited pulse duration. The adaptive pulse shapers use multi-photon intrapulse interferometric phase scanning (MIIPS)[18] to measure the pulse duration at the sample. MIIPS is used to generate a phase function to apply across the laser spectrum to ensure that all of the different wavelengths reach the sample at the same time, resulting in our 8 fs pulses used in the experiments.

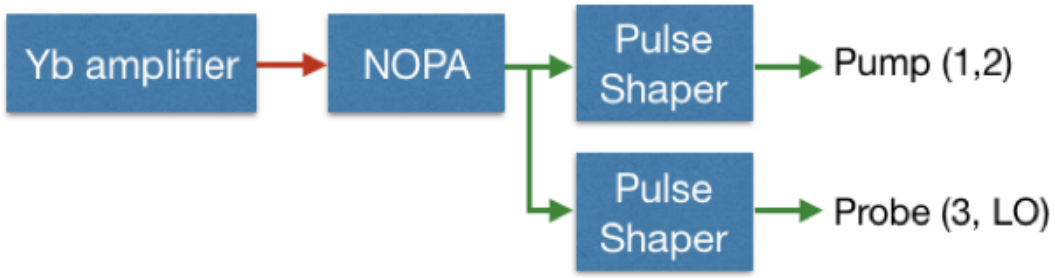

Figure 2.8. Laser and instrumentation used for our 2DES experiments. The Yb amplifier is a 100 kHz, 1.04 μm, 4 W output laser used to pump the NOPA. The NOPA was used to generate the laser spectra reported in Chapters 3 and 4 from the Yb laser output. The NOPA output was split into pump and probe beams, and each beam was processed with the pulse shapers to minimize pulse duration at the sample position.

The following describes the passively phase-stabilized photon echo spectrometer based on the designs of Brixner et al.[7] and Moran and Scherer.[19] The probe beam passed through a time-of-flight delay line to control the time interval between the second pump pulse and the probe pulse, or waiting time T. Both beams were focused onto a single spot on a transmissive diffractive optic (DO, 30 lines/mm) to disperse the beam into different orders. A mask blocked all the light except for the first and negative first orders of the pump and probe beams. The fours beams were collimated with a spherical mirror (SM) where they propagated in a boxcars geometry (upper left of Figure 2.9). The three experimental beams k_1, k_2, and k_3 passed through

wedge pairs (WP) so that the time delay between pump pulse k_1 and k_2, $\tau_{1,2}$, could be controlled and the time delay between the probe k_3 and the reference beam (local oscillator, LO) k_{LO}, $\tau_{3,LO}$, could also be controlled. The wedge pairs were on lateral translation stages to adjust the amount of the glass that was inserted into the beam, causing a time delay due to the difference in the speed of light in air and in glass. The delay between the probe and the local oscillator is required for the heterodyned spectral interferometric detection scheme[6,11–14] that is described in the next section. The local oscillator passed through a neutral density (ND) filter to attenuate the intensity. The four beams focus onto the sample (80 μm spot size, 5 nJ/pulse) where the three experimental pulses generate a signal that was emitted along the same direction as the local oscillator (pulse sequence is shown in Figure 2.7). The boxcars geometry allowed us to place the detector in the $k_s = -k_1 + k_2 + k_3$ direction to ensure phase matching. The signal and LO were then spatially isolated and dispersed onto a CCD through a monochromator. The CCD (Ocean Optics Flame-T, 450-700 nm, 3500 pixels, 0.1 nm bandpass) is a square law detector so every spectrum collected is the square of the sum of the local oscillator and the signal:

$$(E_{LO} + E_{sig})^2 = E_{LO}^2 + 2E_{LO}E_{sig} + E_{sig}^2 \tag{2.4}$$

Spectral interferometry allowed for for the collection of the $2E_{LO}E_{sig}$ term and isolation of the signal electric field through Fourier transform spectral interferometry.[20]

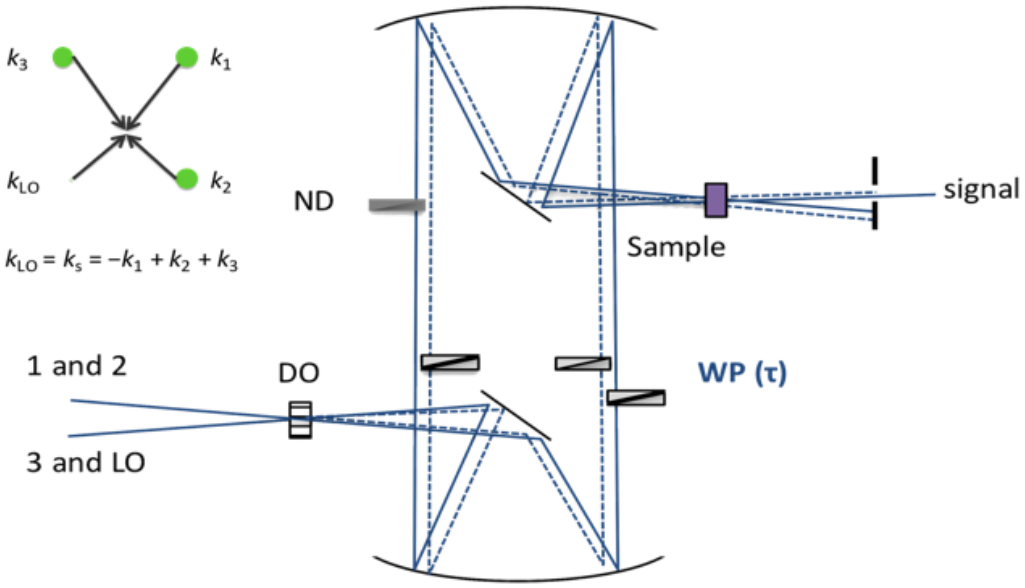

Figure 2.9. Diffractive optics (DO) based two-dimensional electronic spectrometer that allowed for time ordering and phase matching. The pump beam (1 and 2) and the probe beam (3 and LO) focused onto a DO to generate the four beams used in the experiment. The diverging beams were collimated using a SM where they propagated along the telescope to another SM. In the telescope, the three experimental beams passed through WP to control the relative time delays between the pump pulses and between the probe pulses. The LO was passed through ND filter to be attenuated by 10^{-4} as to not interfere with the sample. The four beams were focused onto the sample to generate the signal. The signal and LO were isolated and sent to the detector. The upper left shows the boxcar geometry from the perspective of the sample.

2.2.2 Detection of 2DES Signals with Spectral Interferometry

In order to ensure the detected signal was truly the $2E_{LO}E_{sig}$ term, a beam-shuttering protocol introduced by Brixner et al.[7] was implemented to isolate the third-order signal from any background scattering. For each spectrum collected, a spectrum of the pump scattering and the probe scattering was collected to be subtracted out of the collected signal. Figure 2.10 shows an example of an interferogram with the laser spectrum used in the experiments.

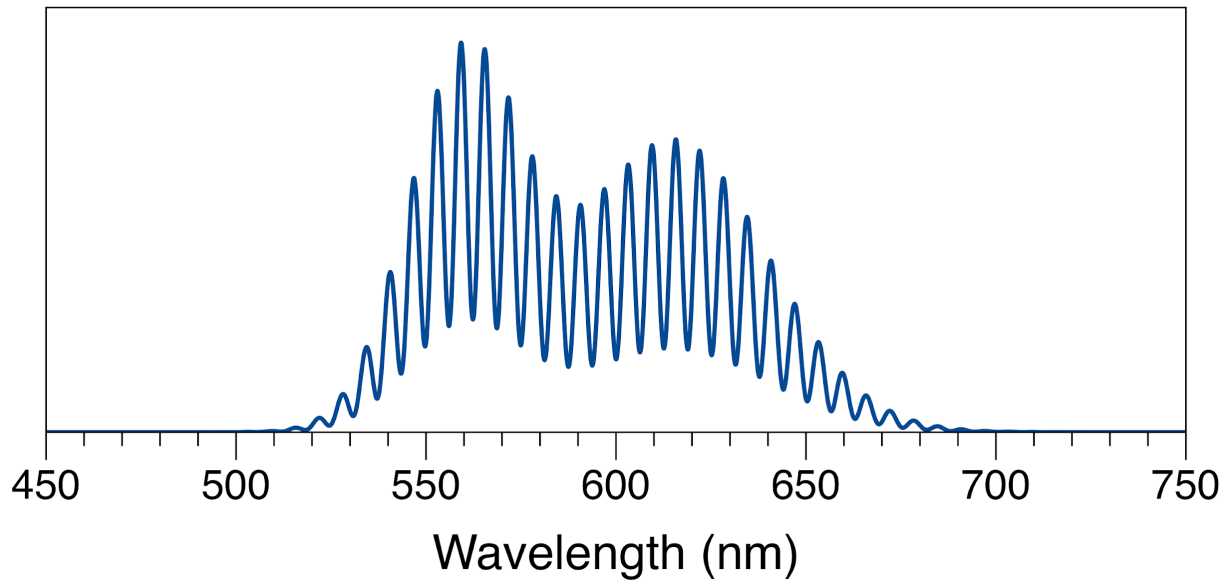

Figure 2.10. Background and scatter corrected interferogram collected at the CCD. The envelope of the spectrum is due to the laser spectrum and the oscillatory feature is due to the interference of the third-order signal with the laser spectrum.

In order to extract the signal from the interferogram the spectra were processed using an algorithm discussed by Jonas and coworkers[20] called Fourier transform spectral interferometry. The first step is to perform an inverse Fourier transform to separate out the signal from the local oscillator on a time axis (Figure 2.11). The peaks near time zero are due to the laser spectrum envelope and the peak at ~250 fs is the from the third-order signal. The time between the local oscillator and the third-order signal is chosen by the experimentalist using the wedge pair previously discussed. The only requirement is to be sure that the signal is fully resolved from the local oscillator. The signal is windowed (shown by shading) and the rest of values outside of the window are set to zero. Fourier transformation back into wavelength space the gives the extracted complex signal (Figure 2.12).

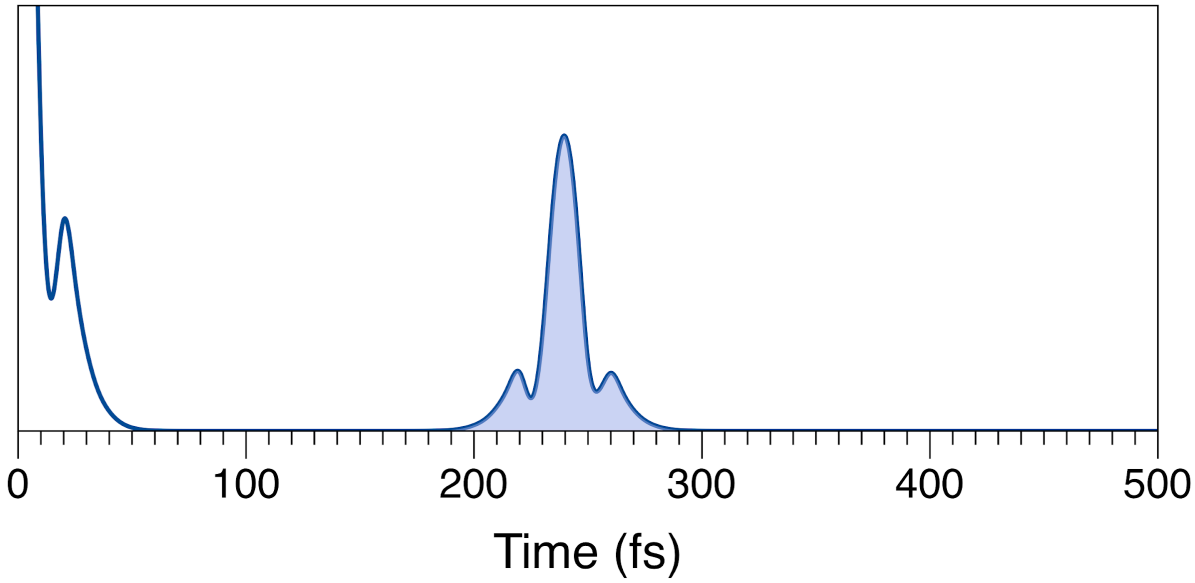

Figure 2.11. Collected third-order signal in the time domain after inverse Fourier transformation of the interferogram in Figure 2.10. The feature at 0 fs is due to the local oscillator and the feature at ~250 fs is from the third-order signal. The time domain is used to separate the signal from the local oscillator. The secondary features on the left and right of the main peak are due to the Fourier transformation of the two peaks in the envelope on the interferogram. The signal is windowed and Fourier transformed back into the wavelength domain (Figure 2.12).

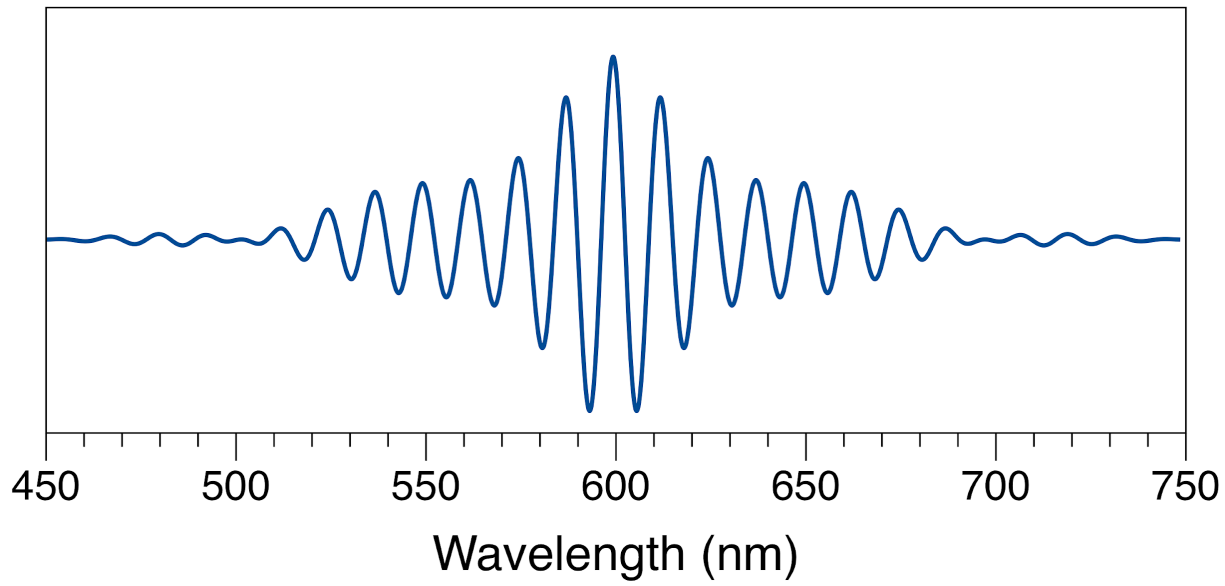

Figure 2.12. Complex third-order signal in the wavelength domain after Fourier transformation of the signal in Figure 2.11. The complex, oscillatory signal can be treated with a phase factor $e^{-i\omega\tau_{sig,LO}-\phi}$ to separate out absorptive (real) and dispersive (imaginary) components, where the dispersive component is ignored and the absorptive component is used to generate the 2DES spectra in the following chapters.

The signal then needs to be phased to separate out the absorptive (real) and dispersive (imaginary) components of the complex signal. In order to separate the signal into the two components, a phase factor $e^{-i\omega\tau_{sig,LO}-\phi}$ is applied. The $\tau_{sig,LO}$ term is the time delay between the local oscillator and third-order signal and is estimated by the peak position of the signal in Figure 2.11. It also requires an unknown phase factor ϕ that is the phase difference between the local oscillator and the signal. The phase factor is unknown and needs to be determined through the projection slice theorem[7] using pump-probe spectra, as described in the next section.

2.2.3 Phasing of 2DES Signals Using Pump-Probe Signals

Pump-probe spectra were collected using the same experimental apparatus to ensure the signals are emitted under the same optical preparations. One of the pump beams and the local oscillator were blocked to leave a single pump beam and the probe beam to detect the pump induced change in absorption. The pump and probe were modulated using a dual slot blade at 700 and 1000 Hz, respectively. The probe beam was isolated and detected by a single channel lock in detection scheme that was detecting at sum frequency. The home-built spectrograph provided a 4 nm bandpass and the signal was detected using a silicon photodiode connected to two lock-in channels to simultaneously measure the probe beam and signal intensities. Pump probe signals are phase independent absorptive components. That allowed us to manually adjusted the phase factor until the projection of the 2DES (integrated signal over the excitation axis) spectrum matched the pump probe signal for identical population times, T (Figure 2.13). The projection slice theorem ensured that the 2DES signal was fully absorptive and did not have any artifacts due to the imaginary component being mixed in with the absorptive component.

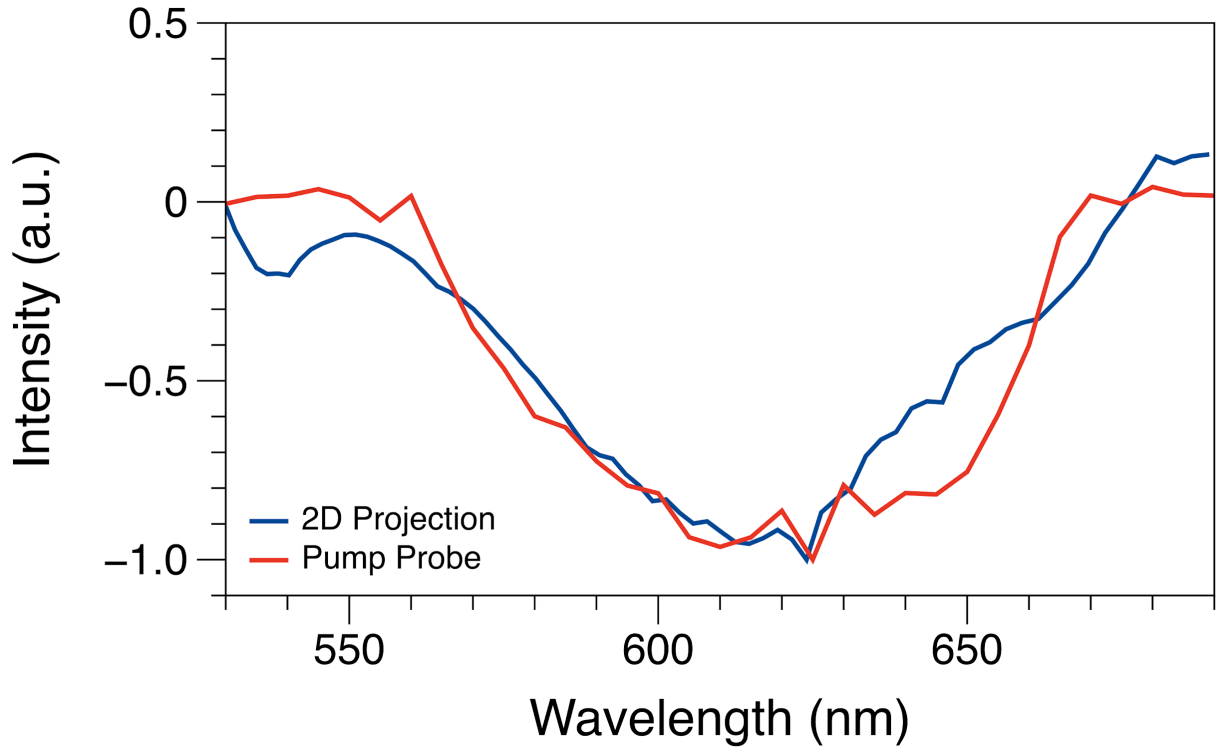

Figure 2.13. The 2DES projection (integration over excitation axis) and overlaid pump-probe spectrum for an identical population time, T. Plots of this kind are used to apply the projection slice theorem. The unknown phase factor was manually adjusted and then applied to the complex signal so that the 2DES projection matched the pump probe spectrum to ensure the 2DES signal was fully absorptive.

REFERENCES

REFERENCES

(1) Hamm, P.; Zanni, M. *Concepts and Methods of 2D Infrared Spectroscopy*; Cambridge University Press: Cambridge, 2011.

(2) Mukamel, S. *Principles of Nonlinear Optical Spectroscopy*; Oxford University Press: New York, 1995.

(3) Blum, K. *Density Matrix Theory and Applications*; Springer Science & Business Media, 2012.

(4) Boyd, R. W. *Nonlinear Optics*; Elsevier, 2003.

(5) Jonas, D. M. Two-Dimensional Femtosecond Spectroscopy. *Annu. Rev. Phys. Chem.* **2003**, *54*, 425.

(6) Gallagher, S. M.; Albrecht, A. W.; Hybl, J. D.; Landin, B. L.; Rajaram, B.; Jonas, D. M. Heterodyne Detection of the Complete Electric Field of Femtosecond Four-Wave Mixing Signals. *J. Opt. Soc. Am. B* **1998**, *15*, 2338–2345.

(7) Brixner, T.; Mančal, T.; Stiopkin, I. V.; Fleming, G. R. Phase-Stabilized Two-Dimensional Electronic Spectroscopy. *J. Chem. Phys.* **2004**, *121*, 4221.

(8) Goodno, G. D.; Dadusc, G.; Miller, R. J. D. Ultrafast Heterodyne-Detected Transient-Grating Spectroscopy Using Diffractive Optics. *J. Opt. Soc. Am. B* **1998**, *15*, 1791–1794.

(9) Goodno, G. D.; Miller, R. J. D. Femtosecond Heterodyne-Detected Four-Wave-Mixing Studies of Deterministic Protein Motions. 1. Theory and Experimental Technique of Diffractive Optics-Based Spectroscopy. *J. Phys. Chem. A* **1999**, *103*, 10619–10629.

(10) Park, J. S.; Joo, T. Coherent Interactions in Femtosecond Transient Grating. *J. Chem. Phys.* **2004**, *120*, 5269–5974.

(11) de Boeij, W. P.; Pshenichnichov, M. S.; Wiersma, D. A. Phase-Locked Heterodyne-Detected Stimulated Photon Echo. A Unique Tool to Study Solute-Solvent Interactions. *Chem. Phys. Lett.* **1995**, *238*, 1.

(12) Tokmakoff, A.; Lang, M. J.; Larsen, D. S.; Fleming, G. R. Intrinsic Optical Heterodyne Detection of a Two-Dimensional Fifth Order Raman Response. *Chem. Phys. Lett.* **1997**, *272* (1/2), 48–54.

(13) de Boeij, W. P.; Pschenichnikov, M. S.; Wiersma, D. A. Heterodyne-Detected Stimulated Photon Echo: Applications to Optical Dynamics in Solution. *Chem. Phys.* **1998**, *233*, 287–309.

(14) Lepetit, L.; Joffre, M. Two-Dimensional Nonlinear Optics Using Fourier-Transform Spectral Interferometry. *Opt. Lett.* **1996**, *21*, 564.

(15) Ostroumov, E. E.; Mulvaney, R. M.; Cogdell, R. J.; Scholes, G. D. Broadband 2D Electronic Spectroscopy Reveals a Carotenoid Dark State in Purple Bacteria. *Science* **2013**, *340* (6128), 52–56.

(16) Brixner, T.; Stenger, J.; Vaswani, H. M.; Cho, M.; Blankenship, R. E.; Fleming, G. R. Two-Dimensional Spectroscopy of Electronic Couplings in Photosynthesis. *Nature* **2005**, *434* (7033), 625–628.

(17) Harel, E.; Engel, G. S. Quantum Coherence Spectroscopy Reveals Complex Dynamics in Bacterial Light-Harvesting Complex 2 (LH2). *Proc. Natl. Acad. Sci. U. S. A.* **2012**, *109* (3), 706–711.

(18) Lozovoy, V. V.; Pastirk, I.; Dantus, M. Multiphoton Intrapulse Interference 4: Characterization and Compensation of the Spectral Phase of Ultrashort Laser Pulses. *Opt. Lett.* **2004**, *29*, 775–777.

(19) Moran, A. M.; Nome, R. A.; Scherer, N. F. Resolving the Emission Times of Solute and Solvent Four-Wave Mixing Signals by Spectral Interferometry. *J. Chem. Phys.* **2006**, *125* (3), 31101.

(20) Hybl, J. D.; Ferro, A. A.; Jonas, D. M. Two-Dimensional Fourier Transform Electronic Spectroscopy. *J. Chem. Phys.* **2001**, *115* (14), 6606–6622.

Chapter 3: Quantum Coherent Excitation Energy Transfer by Carotenoids in Photosynthetic Light Harvesting

It remains an open question whether quantum coherence and molecular excitons created by delocalization of electronic excited states are essential features of the mechanisms that enable efficient light capture and excitation energy transfer to reaction centers in photosynthetic organisms. The peridinin–chlorophyll a protein from marine dinoflagellates is an example of a light-harvesting system with tightly clustered antenna chromophores in which quantum coherence has long been suspected, but unusually it features the carotenoid peridinin as the principal light absorber for mid-visible photons. We report that broadband two-dimensional electronic spectroscopy indeed reveals the initial presence of exciton relaxation pathways that enable transfer of excitation from peridinin to chlorophyll a in <20 fs, but the quantum coherence that permits this is very short lived. Strongly coupled excited-state vibrational distortions of the peridinins trigger a dynamic transition of the electronic structure of the system and a rapid conversion to incoherent energy transfer mechanisms.

The work presented in this chapter has been adapted with permission from *J. Phys. Chem. Lett.* **2018**, *8*, 5141–5147. Copyright (2018) American Chemical Society.

3.1 Introduction

Photosynthetic light-harvesting protein complexes[1] incorporate intricate arrays of organic chromophores as antenna structures to capture the energy from solar photons. A large fraction of the absorbed excitation energy is transferred to reaction centers, where electron-transfer reactions store the energy as a transmembrane electrochemical gradient.[2] The structure of a light-harvesting protein arranges the interchromophore distances and orientations to control nonradiative decay processes[3] and to protect against photodamage.[4] When the interchromophore electronic interactions are relatively strong, optical excitations prepare exciton states, which are collective, delocalized excitations arising from quantum coherence, a quantum mechanical mixing of the excited states of two or more chromophores.[5] The excitation energy transfer processes that result are coherent or wavelike in character rather than an incoherent, particle-like hopping between individual chromophores.[6] The presence of quantum coherence in a light-harvesting protein may improve the fitness of a photosynthetic organism by directing the flow of energy along the most efficient pathway,[7] but how this is accomplished and whether or not it is essential to proper function is the subject of continuing interest and controversy.

In the peridinin–chlorophyll *a* protein (PCP), the nanocrystal-like cluster of eight peridinin and two chlorophyll (Chl) a chromophores that assembles inside a basket of α helices[8] (Figures 3.1a and 3.1b) exhibits a circular dichroism spectrum[9] and fast energy transfer pathways[10–13] that imply significant contributions from quantum coherence. Compared to other light-harvesting proteins, PCP exhibits an unusually high (90%) quantum yield for excitation energy transfer from carotenoids to Chl acceptors.[10] This efficiency arises from several levels of structural engineering in addition to the physical arrangement of chromophores. Considerable

attention has focused on the electronic effects of the carbonyl substitution of the conjugated polyene backbone[14] (Figure 3.1c) and of the strained conformations assumed in the PCP structure,[15] both of which are thought to enhance peridinin's function as an energy donor by enhancing its excited-state intramolecular charge-transfer (ICT) character.[16,17]

We report here results from broadband two-dimensional electronic spectroscopy (2DES)[20] that show directly that extraordinarily fast excitation energy transfer processes in PCP are initially mediated by quantum coherent mechanisms and mixed peridinin–Chl exciton states at room temperature. 2DES provides a crucial tool for studies of excitation energy transfer processes in light-harvesting proteins and chromophore aggregates because it identifies the pathways of energy transfer between donor and acceptor states.[21] In the present studies, however, the 2DES spectra also report the rapid decay of quantum coherence owing to the excited-state vibrational distortions that the peridinin molecules suffer after optical excitation, which transform the electronic structure of the peridinin–Chl cluster from the delocalized to the localized regime. The results make it clear, nevertheless, that quantum coherence provides a functional advantage for the light-harvesting function of PCP when illuminated incoherently by solar photons. The loss of quantum coherence accompanies a slowing of the excitation energy transfer rate by two orders of magnitude to the rate allowed by the incoherent, Förster mechanism.[22]

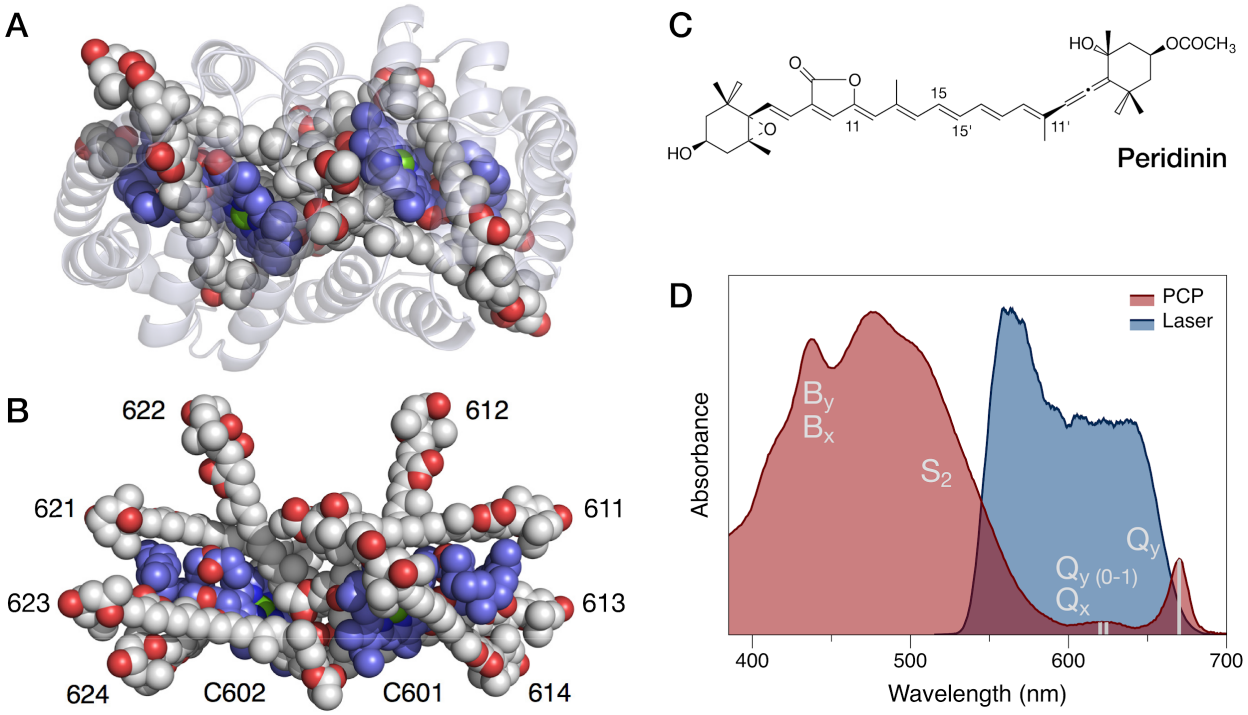

Figure 3.1. Structure of the peridinin–chlorophyll *a* light-harvesting protein (PCP) complex from *Amphidinium carterae* (PDB entry 1PPR).[8] (a) Bottom view, along the two-fold symmetry axis for a single subunit, with the polypeptide backbone of the protein displayed with ribbons and with the enclosed chromophore cluster of eight peridinins (carbon atoms, white; oxygen atoms, red) and two chlorophyll a chromophores (carbon atoms, blue; oxygen atoms, red; Mg^{II} ions, green) in a space-filling rendering. (b) Side view of the chromophore cluster, with the symmetry axis oriented vertically; the numbering identifies the peridinins and chlorophylls (C) as listed in the 1PPR structure. (c) Structure of peridinin. (d) Room-temperature absorption spectrum of the PCP complex (red) and the intensity of the femtosecond laser excitation pulses (blue) used in the 2DES experiment; the spectral regions for the chlorophyll Soret (B_x, B_y) and peridinin (S_2 ($1^1B_u^+$)) absorption transitions are labeled, and vertical lines mark approximate positions for the chlorophyll Q-band transitions: Q_y (0–0) (670 nm), Q_x (0–0) (624 nm, 1100 cm^{-1} shift),[18,19] and Q_y (0–1) (620 nm, 1200 cm^{-1} shift).

3.2 Experimental

3.2.1 Sample Preparation

Peridinin chlorophyll *a* protein (PCP) preparations were isolated from *Amphidinium carterae* cells using a previously published method in the laboratory of Roger Hiller (Macquarie University.[23] For the 2DES experiments, PCP samples were suspended in a buffer solution containing 50 mM tricine–NaOH, 20 mM KCl, pH 7.5, to obtain an optical density of 0.3 at 540 nm for a 1 mm pathlength. Linear absorption spectra were recorded at room temperature with a Varian Cary 50 spectrophotometer. The absorption spectrum was measured before and after the femtosecond spectroscopy experiments to assess whether there were any changes due to photochemistry or decomposition of the sample. There were no changes noted during these experiments.

3.2.2 Nonlinear Spectroscopy

We performed a series of broadband 2DES experiments at room temperature (23 °C) with wild-type PCP samples obtained from cultures of *Amphidinium carterae*. The experiments were carried out with a passively phase-stabilized, diffractive-optic based photon-echo spectrometer.[24] The 2DES experiment is a third-order nonlinear optical spectroscopy performed with three very short light pulses.[20] An initial pair of pulses is prepared with a scanned interval, τ, between them. Fourier transformation of the signal with respect to τ obtains the excitation axis of the two-dimensional spectrum. Then, after a fixed waiting (or population) interval, T, a third pulse arrives at the sample to probe the time evolution of the system. The sample then emits a coherent pulse of light, either a free-induction decay (nonrephasing signal) or a photon echo (rephasing signal), depending on which of the first two excitation pulses arrives first. The detection axis of the two-

dimensional spectrum is obtained directly by measuring the amplitude and phase of the emitted light using interferometry[25] with a spatially overlapped and attenuated local oscillator pulse, which arrives at a fixed interval prior to the third pulse of the experiment.

In the present experiments, the spectrally broad laser pulses for the 2DES experiments were prepared by a 100 kHz amplified Yb laser and a noncollinear optical parametric amplifier (NOPA). The output was split into excitation and probe pulses prior to being processed separately by two channels of adaptive pulse shapers; pulse durations of 8 fs were detected at the sample position (see Figure A3.1 in the Appendix for the residual optical phase spectrum). Figure 3.1d shows that the laser spectrum chosen for these experiments overlaps with the lowest energy absorption transitions from the ground state, S_0 ($1^1A_g^-$), to the S_2 ($1^1B_u^+$) state of peridinin, which are principally located in the 520–580 nm region, but additional peridinins with distorted ground-state conformations contribute to a broad tail extending out at least to 600 nm. The laser spectrum is broad enough to overlap with the Q_x and Q_y absorption transitions from Chl a (Figure 3.1d) in the 620 nm and 670 nm regions of the spectrum.[9] In 2DES experiments, as discussed below, this laser spectrum excites and detects energy transfer pathways in PCP between the peridinin donors and Chl a acceptors by two distinct mechanisms and timescales, with quantum coherence confined to the $T < 50$ fs regime. The 2DES spectra can be interpreted qualitatively as correlation spectra:[20] at a given (x, y) coordinate in the plotted contours, one can identify signals that were produced by the sequential action of a specific wavelength x from the excitation pulses followed by the action of a certain wavelength y of the probe pulse, which arrived at the indicated waiting time T.

3.3 Results and Discussion

In Figure 3.2, the formation and decay of strong stimulated emission (SE) signals off the diagonal of the 2DES spectrum allow one to follow the relaxation of population to the low-lying Chl Q_x and Q_y exciton states in <20 fs after excitation. Exciton states prepared by absorption transitions in the <580 nm peridinin region of the excitation axis relax by populating a range of intermediate Chl exciton states, including those in the overlapping Q_x and Q_y ($v = 1$) region,[18] as shown by the appearance of a SE cross peak over the 600–660 nm range of the detection axis in the $T = 10$ fs spectrum. The intensity profile as a function of T for this cross peak is shown in Figure 3.3a. By $T = 20$ fs, population in Q_x or Q_y ($v = 1$) has relaxed further to reach the $v = 0$ level of Q_y, as detected by SE in the 650–680 nm region of the detection axis. Peridinin exciton states prepared by absorption in the 580–600 nm region apparently relax by first populating Q_x or Q_y ($v = 1$) but arrive at Q_y ($v = 0$) in <10 fs. The fast evolution of a 630 nm SE feature initially on the diagonal of the spectrum shows that direct optical preparation of exciton states in the Q_x and Q_y ($v = 1$) region is also followed by fast relaxation to the $v = 0$ level of Q_y. By the $T = 25$ fs spectrum, SE signals are detected in the 680 nm detection region corresponding to Q_y ($v = 0$) all the way across the excitation axis.

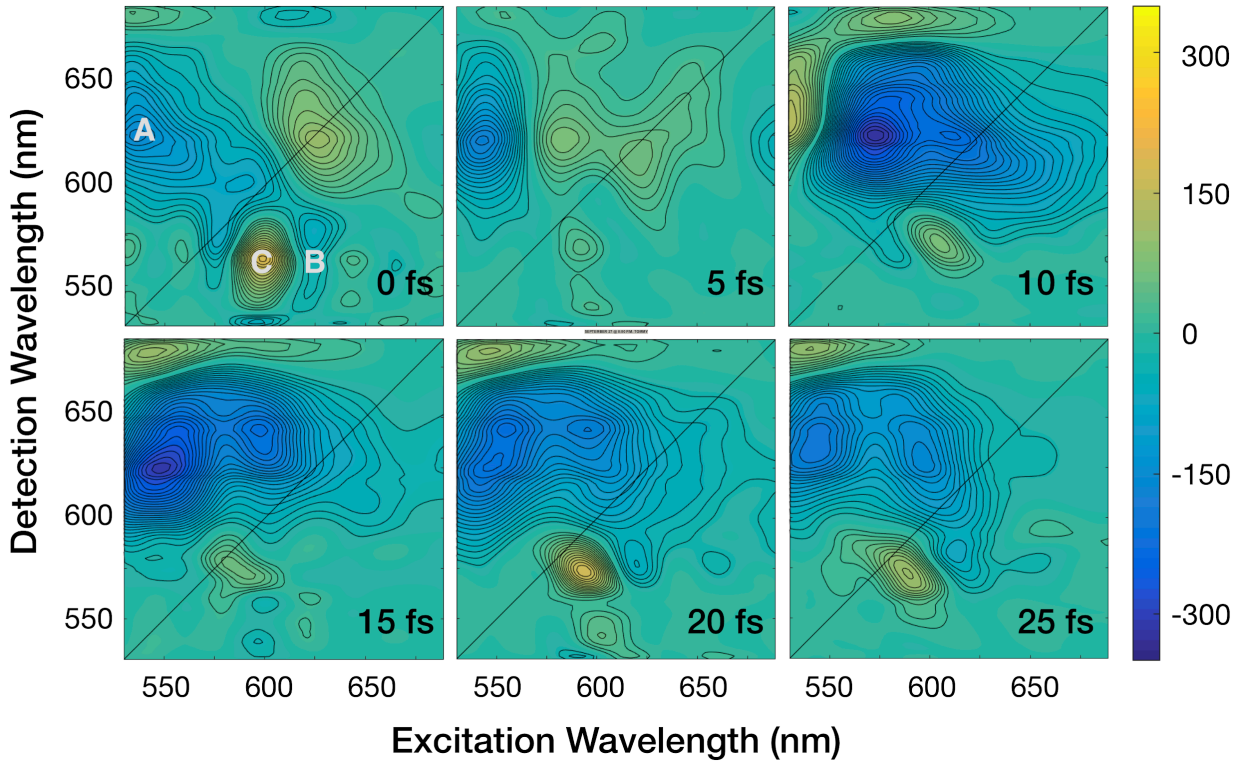

Figure 3.2. Time evolution of the phased absorptive 2DES spectra from PCP at room temperature, as shown for waiting times $T = 0\ldots25$ fs. The spectra are plotted as evenly spaced contours and filled with colors indicating positive (yellow, ground-state bleaching and stimulated emission) and negative (blue, excited-state absorption or photoinduced absorption) signals. The intensity profile as a function of T for the three marked coordinates is shown in Figures 3.3a–c: (a) exciton relaxation from peridinin to Chl a (Q_x or Q_y (0–1)), $\lambda_{ex} = 537$ nm, $\lambda_{det} = 625$ nm; (b) quantum beating between Chl a (Q_x or Q_y (0–1)) and peridinin, $\lambda_{ex} = 625$ nm, $\lambda_{det} = 570$ nm; (c) quantum beating between peridinins, $\lambda_{ex} = 600$ nm, $\lambda_{det} = 565$ nm.

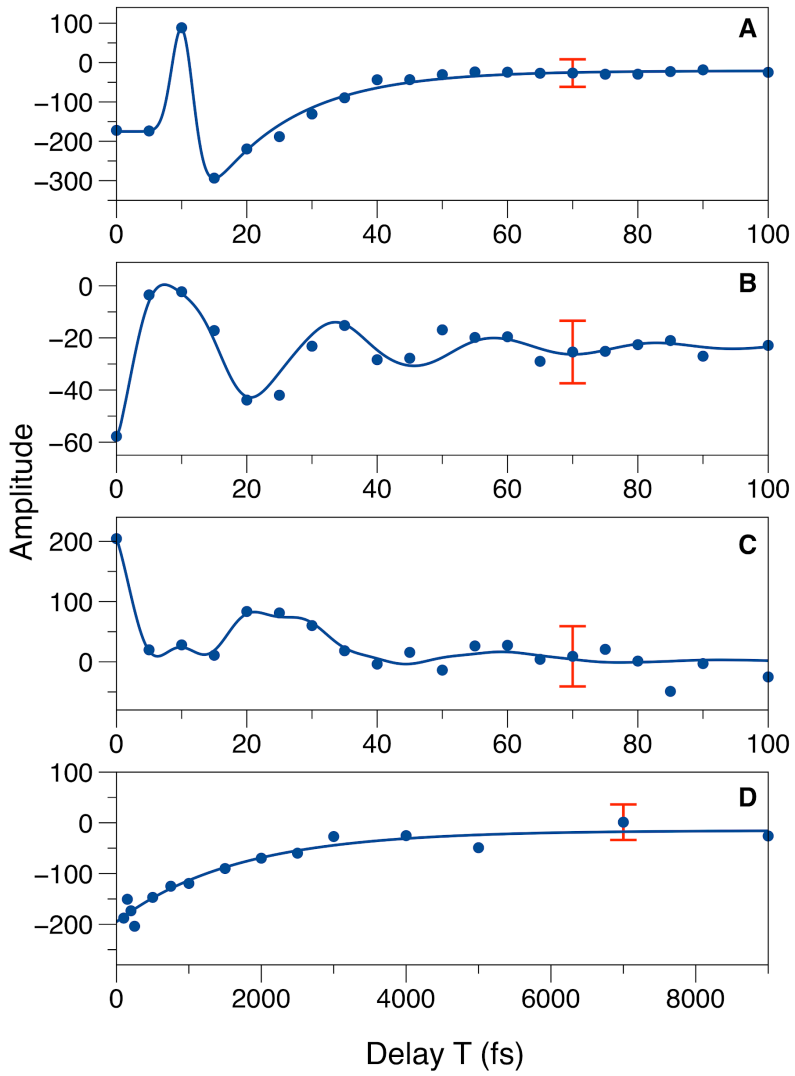

Figure 3.3. Amplitudes and fitted models for the marked cross peaks in the 2DES spectra from PCP (Figures 3.2 and 3.5) as a function of the waiting time T: (a) exciton relaxation from peridinin to Chl *a* (Q_x or Q_y (0–1)), $\lambda_{ex} = 537$ nm, $\lambda_{det} = 625$ nm; (b) quantum beating between Chl a (Q_x or Q_y (0–1)) and peridinin, $\lambda_{ex} = 625$ nm, $\lambda_{det} = 570$ nm; (c) quantum beating between peridinins, $\lambda_{ex} = 600$ nm, $\lambda_{det} = 565$ nm; (d) decay of the localized peridinin cross peak due to Förster energy transfer to Q_y ($v = 0$) and nonradiative decay to the S_1 state, $\lambda_{ex} = 600$ nm, $\lambda_{det} = 624$ nm. The models for (a) and (d) were obtained from linear least squares optimization; the models for (b) and (c) were obtained from a linear-prediction, singular value decomposition (LPSVD) program. Error bars are plotted to indicate the uncertainty in the measurements, which were obtained from the average of five 2DES spectra. The model parameters are listed in the Appendix as Tables A3.1–A3.3. The intensity profiles for additional features in the 2DES spectra are presented as Figures A3.4–A3.10.

During the relaxation of population from the peridinin to the Chl exciton states, the 2DES spectra from PCP shown in Figure 3.2 exhibit a broad region of blue, negative-going signals arising from excited-state absorption (ESA) transitions driven by the probe pulses. These signals are best explained by absorption transitions from singly excited exciton states, as initially prepared optically or from those populated as intermediates during the exciton relaxation process, to a manifold of doubly excited states, which correspond to the excitation of two chromophores in the delocalized cluster (Figure 3.4).[21,26] These transitions would be expected to gain additional strength from admixture of the doubly excited states with the bright S_n states of the peridinin chromophores, which lie at similar energies.[27] In Figure 3.2, the $T = 0$ fs spectrum shows that peridinin exciton states prepared by excitation wavelengths <580 nm instantaneously make strong transitions to the doubly excited exciton manifold when probed near 630 nm, which corresponds to an excitation of a Chl's Q_x or Q_y (0–1) transition. Similarly, the $T = 15$ fs spectrum indicates that Chl exciton states in the doubly excited manifold are populated by ESA transitions after optical preparation of peridinins (at excitation wavelengths below 600 nm) or of Chls (above 600 nm). The latter observation is especially important because it supports the conclusion that delocalization spans at least the two Chls in a given subunit of PCP, perhaps by being strengthened by bridging interactions with the surrounding peridinins.

The 2DES spectra also indicate coherence between Chls and peridinins in terms of quantum beating of cross peaks just below the diagonal. Figure 3.2 marks two cross peaks, arising from Chl–peridinin and peridinin–peridinin electronic coherences prepared by the excitation pulses at 625 nm and 600 nm, respectively. The intensities of these cross peaks are plotted as a function of waiting time T in Figures 3.3b and 3.3c; the intensity of a weaker cross

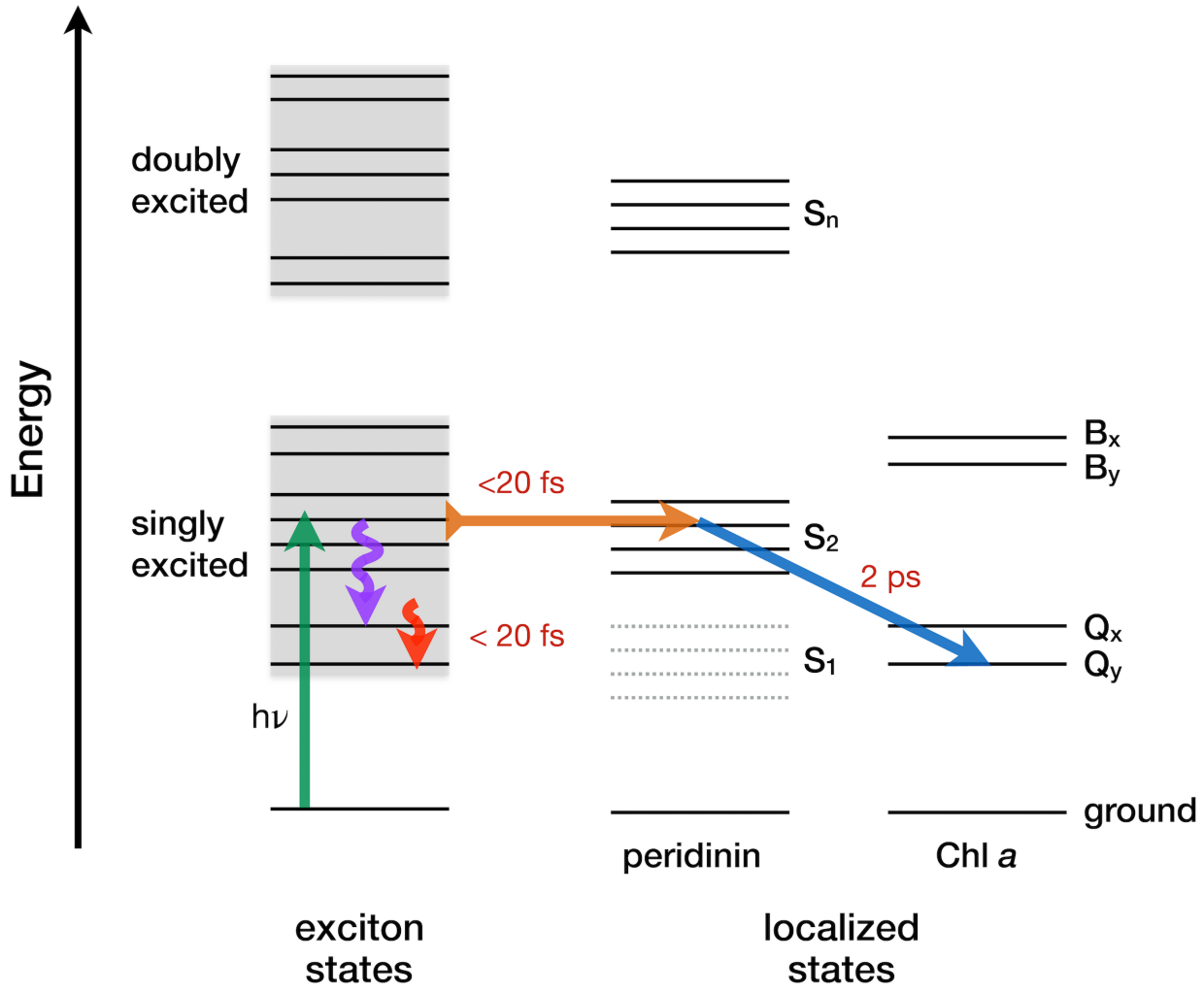

Figure 3.4. Exciton (delocalized, of mixed peridinin–Chl character) and localized (single chromophore) energy levels for the peridinin–chlorophyll *a* cluster, showing excitation energy transfer pathways after optical preparation of the S_2 state of peridinin. The decay of the intensity of the localized peridinin cross peak at the marked coordinate (d), $\lambda_{ex} = 600$ nm, $\lambda_{det} = 624$ nm, due to Förster energy transfer to Q_y ($v = 0$), is plotted as a function of delay T in Figure 3.3d.

peak from a Chl–peridinin coherence at 670 nm is presented as Figure A3.4. The quantum beats are modulated at difference frequencies corresponding to the successive actions of the two excitation pulses on the two photoselected chromophores. In all three cases, the beating is rapidly damped by a exponentially decaying envelope with a <20 fs time constant, which determines the rate at which the electronic coherence decays. Such a short dephasing time effectively rules out an assignment of the quantum beating to stimulated Raman transitions, which produce ground state vibrational coherences that characteristically dephase much more slowly, with >500 fs damping times usually observed. In contrast, relatively strong quantum beating signals from slowly damped stimulated Raman vibrational coherences are readily observed in solutions of carotenoids[28] and in light-harvesting proteins where the rate of energy transfer from the carotenoid to a Chl acceptor is much slower than in PCP.[29] The apparent lack of strong vibrational coherence in the 2DES spectra shown in Figure 3.2 is consistent with an ultrafast nonadiabatic transfer of the electronic wavepacket prepared by the first excitation pulse from peridinin to Chl on the <20 fs timescale inferred from the dynamics of the SE cross peaks. Fast damping of the resonant electronic coherence created by the action of the first excitation pulse attenuates the ground state vibrational coherence that would be created by the action of the second excitation pulse.[30–32]

It is important to note that the <20 fs dephasing time obtained from the damping of the electronic quantum beating observed in PCP closely matches the time constant for the decay of the ESA to the doubly excited exciton states observed in the 2DES spectra shown in Figure 3.2. The ESA progressively disappears over the $T = 15\ldots50$ fs range, as shown by the intensity profiles sampled at several positions (Figures 3.3a, A3.5, and A3.6). The oscillator strength for

the ESA transitions vanishes because the doubly excited exciton manifold is destroyed as the excited state wavefunctions collapse onto single chromophores, mainly Chls. This dynamic exciton localization process can be attributed to a torsional and/or out-of-plane distortion of the conjugated polyene backbone of peridinin, which follows optical excitation to the S_2 state and an initial displacement along the C–C/C=C bond-stretching coordinates.[17] This structural evolution mixes the bright S_2 and dark S_1 ($2^1A_g^-$) states[15] and results in a marked decrease in the strength of interaction, J, between the peridinins and between the peridinins and Chls. Simultaneously, the system–bath reorganization energy, λ, increases owing to the enhanced ICT character that peridinin develops as it twists and bends.[16,27] The transition from the quantum coherent to the localized regime occurs when $J \leq \lambda$.[33] As discussed previously,[17] this condition accompanies formation of an intermediate state of peridinin, S_x,[29,34] which we assign to distorted S_2 structures relaxing with respect to out-of-plane coordinates down the steep potential energy gradient towards an conical intersection (or seam) with the S_1 state, where nonradiative decay occurs.[16,27,35]

At waiting times $T > 50$ fs, after the decay of the ESA signal arising from transitions to doubly excited exciton states, the 2DES spectrum from PCP (Figure 3.5) exhibits a distinct, more slowly decaying ESA signal as an off-diagonal cross peak spanning the 560–640 nm region of the detection axis. This spectrum is comparable to that observed in 2DES spectra from β-carotene[36] or peridinin in solution. Examples of 2DES spectra from peridinin in methanol solvent over the $T = 0\ldots3000$ fs range are shown in Figures A3.11–A3.15. These signals can be attributed to the fraction of peridinins that survive the initial period of quantum coherence in PCP to end up as localized peridinin S_x states. They are chiefly produced by excitation of red-shifted

absorption transitions in the 580–610 nm region, which correspond to direct vertical excitations of peridinins to the torsional gradient just past the barrier that divides planar and distorted species on the S_2 potential surface.[16,27] These peridinin excited states would be expected to localize more rapidly than those excited at shorter wavelengths because they exhibit an especially large ICT character immediately upon optical excitation.[17] Over the $T = 100…9000$ fs range, the peridinin ESA peak decreases in intensity with a time constant of 1.7 ps (Figure 3.3d) as S_x transfers excitation energy to Q_y ($v = 0$) incoherently, via the the Förster mechanism.[10–12] The fit returns an estimate for the long-lived amplitude offset arising from the residual S_1 state of peridinin. In our model, the lifetime of S_x is determined by two processes, decay of S_x via Förster energy transfer to Chl *a* and nonradiative decay of S_x to S_1. The rate of energy transfer from peridinin to Chl *a* was previously determined in pump–probe measurements with 100 fs pulses to fall in the 2.3–3.2 ps range.[10–13,37,38] The revised estimate for the lifetime of S_x in PCP determines the intrinsic lifetime of S_x to fall in the 3.9–6.5 ps range, which is in line with our previous estimate of 4.4 ps from heterodyne transient grating spectroscopy with 40 fs pulses.[17]

The 2DES spectra shown in Figure 3.5 directly resolve the connectivity for the Förster energy transfer process between the donor S_x state and the acceptor $v = 0$ level of Q_y in terms of the appearance of a cross peak at centered at 680 nm on the detection axis. A comparable Förster excitation transfer process between a distorted carotenoid excited state and a bacteriochlorophyll acceptor was observed previously in the purple bacterial LH2 system.[29] As shown in Figures A3.7–A3.10, the plotted intensity of the Chl Q_y region of the detection axis exhibits a complicated time profile with respect to delay T owing to spectrally overlapping contributions

from absorptive pathways with different timescales. The initial <20 fs rise of SE reports the arrival of population in Q_y due to relaxation from the optically prepared peridinin or Chl exciton state, as discussed above. The intensity is then modulated over $T > 50$ fs, which would be consistent with recovery of the red-shifted photoinduced absorption spectrum from a nonequilibrium ground state peridinin species following exciton relaxation and localization. Lastly, nonradiative decay of the S_x state in 1.7 ps obtains a very broad ESA spectrum from S_1 that overlaps with the Q_y transition.[10,12] These peridinins correspond to those that fail to transfer excitation to Chl acceptors during the lifetime of the S_x state.[17]

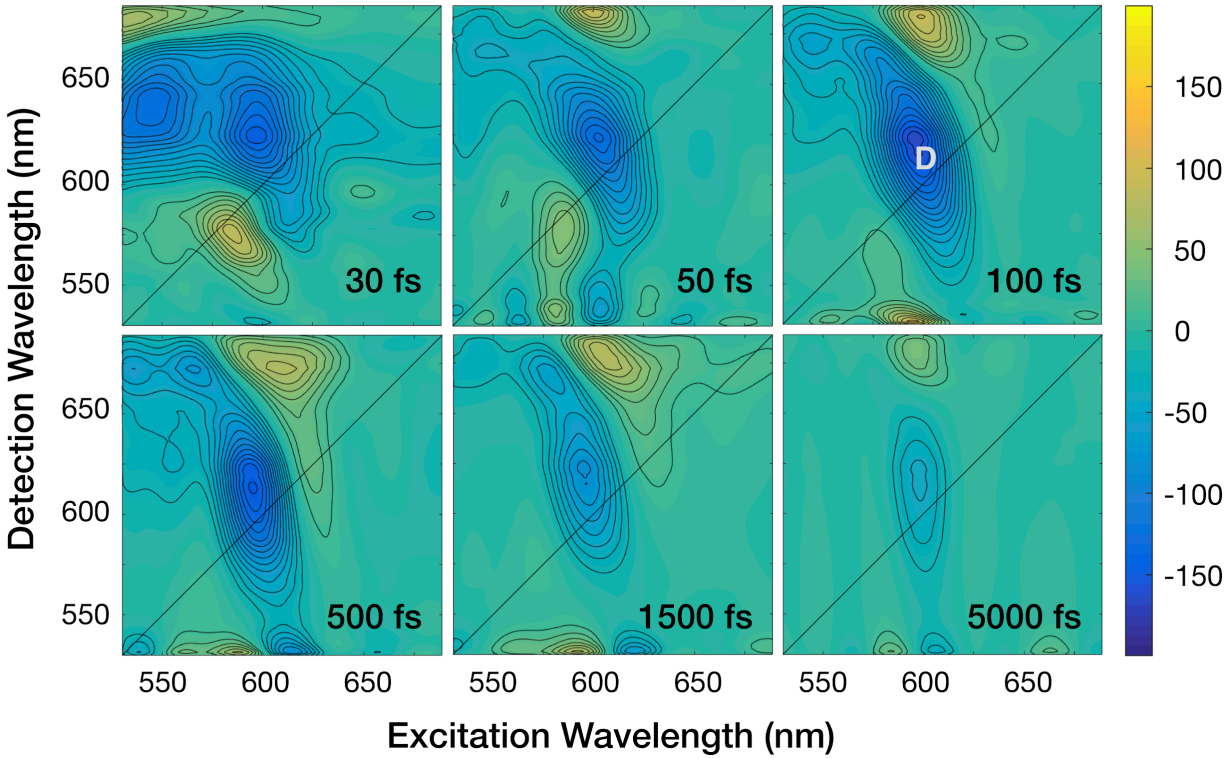

Figure 3.5. Time evolution of the phased absorptive 2DES spectra from PCP at room temperature, as shown for waiting times $T = 30\ldots5000$ fs. The intensity scaling used for the contours and color bar is twice that used for the spectra in Figure 3.2 in order to make weaker signals more visible. The intensity profile for the marked coordinate is plotted in Figure 3.3c.

3.4 Conclusions

The overall efficiency for excitation energy transfer from peridinin to Chl a acceptors in PCP is significantly enhanced by the initial presence of quantum coherence. The main channel of energy transfer involves exciton relaxation in <20 fs from the optically prepared peridinin exciton states to low-lying Chl exciton states. Similar ultrafast nonradiative decay processes between exciton states have been observed in light-harvesting proteins,[39–41] the primary electron donor in purple bacterial photosynthetic reaction centers,[42] and in model chromophore dimers.[43] Even though the rate of this process is ultrafast, its quantum yield is limited by the comparable rate for dynamic exciton localization arising from the excited state vibrational motions of the peridinin chromophores. The strained ground-state conformations that the peridinins assume in the chromophore cluster[15] result in longer lifetimes for the S_2 state due to their enhanced ICT character, which increases the friction for the out-of-plane distortions that result in formation of S_x and localization. As pointed out previously, the lifetime of S_x is also increased by solvent friction due to the increasing ICT character that accompanies relaxation on the torsional gradient. The initial presence of quantum coherence significantly increases the overall yield of excitation transfer because the effective rate of energy transfer via the coherent process from S_2 is at least two orders of magnitude faster than that of the Förster process from S_x.[17]

Note that the quantum coherent mechanism of energy transfer that operates in PCP would be expected to be just as effective in living organisms under solar illumination as in the present experiments with femtosecond laser pulses. The observation in the present work of the ESA transitions between the singly and doubly excited exciton manifolds is the crucial point that establishes the initial presence of quantum coherence in PCP. The exciton manifolds are

determined by the electronic structure of the chromophore cluster, from the details of the relatively strong *J* couplings between the chromophores.[44] Population in the exciton energy levels can be optically prepared even by incoherent light sources, such as a beam of sunlight. In contrast, the quantum beating observed in PCP and in other light-harvesting complexes[45] is an interference phenomenon produced only by phase-coherent optical excitations of more than one energy level by a broadband, femtosecond light source. But by showing that the decay of the ESA and quantum beating signals occurs at the same rate and accompanies vibrational distortions of the coupled chromophores, we establish with some certainty that the mechanism that transfers population from peridinin to Chl on the <20 fs timescale in PCP is quantum coherent, involving the exciton levels that are initially present. As also observed previously in a strongly coupled cyanine dimer,[46] the short timescale for the persistence of quantum coherence in PCP is fully consistent with the line broadening timescale implied by the breadth of the linear absorption spectrum.[16,17,27] In future work, it will be interesting to determine how the electronic and vibrational structure of the peridinin–Chl cluster is optimized[47–49] in order to take advantage of the enhanced rates of excitation transfer that are apparently possible in the short lived quantum coherent regime.

APPENDIX

APPENDIX

Additional experimental details, laser intensity and residual optical phase spectra, phasing of 2DES spectra, model parameters and intensity analysis of additional points of interest in PCP 2DES spectra, and 2DES spectra from peridinin samples in methanol solution are all presented in the appendix.

A3.1 Experimental Details for 2DES Measurements

Femtosecond excitation pulses for use in broadband two-dimensional electronic spectroscopy (2DES) were generated by a 100 kHz amplified Yb laser (Spectra-Physics Spirit) that pumped a noncollinear optical parametric amplifier (NOPA, Spectra-Physics Spirit-NOPA-3H), which was adjusted to obtain an output spectrum centered at 600 nm (100 nm FWHM) and spanning the 520–690 nm range baseline to baseline. The NOPA output was split into pump and probe beams prior to being processed by a pair of adaptive pulse shapers (FemtoJock and FemtoJock P, Biophotonic Solutions Inc.). The pulse shapers used the multiphoton intrapulse interference phase scan procedure (MIIPS)[50] with a β-barium borate second-harmonic generation crystal at the sample position to compress the pump and probe pulses separately to 8 fs. The residual optical phase (Figure A3.1) is flat and close to zero across the spectrum, which indicates that nearly transform limited pulses were obtained.

2DES was performed with a passively phase-stabilized photon echo spectrometer based on the designs of Brixner et al.[24] and Moran and Scherer.[51] Spectral interferometry[52] was used to calibrate the time delays between the three excitation pulses, which were controlled by lateral translation of wedge-shaped fused silica prisms for the coherence delay τ between the first two pulses and by a conventional time-of-flight delay for the waiting (or population) time delay T

between the second and third pulses. The excitation pulses were focused by a 20 cm focal length mirror to a 100 μm beam waist at the sample position and attenuated to energies of less than 5 nJ by fused silica neutral density filters. The local oscillator pulse, which was set to arrive 250 fs prior to the probe pulse, was attenuated by 4.0 OD using a fused silica neutral density filter. 2DES signals were detected by spectral interferometry using a compact spectrograph and CCD detector (Ocean Optics Flame-T, 450–700 nm, 3500 pixels, 0.1 nm bandpass); a beam-shuttering protocol[24] was implemented to isolate the third-order signal from background scattering.

2DES spectra were processed using the algorithm discussed by Jonas and coworkers to resolve the real (absorptive) and imaginary (dispersive) components.[53] The 2DES spectra plotted in Figures 3.2 and 3.3 and for peridinin in methanol (Figures A3.11-A3.13) are sums of the absorptive components from rephasing and nonrephasing pathways. The spectra were phased using the projection slice algorithm[24] using pump-probe spectra acquired under the same optical conditions (examples are shown for PCP in Figures A3.2 and A3.3).

A3.2 Laser Intensity and Residual Optical Phase Spectra, for PCP 2DES spectra

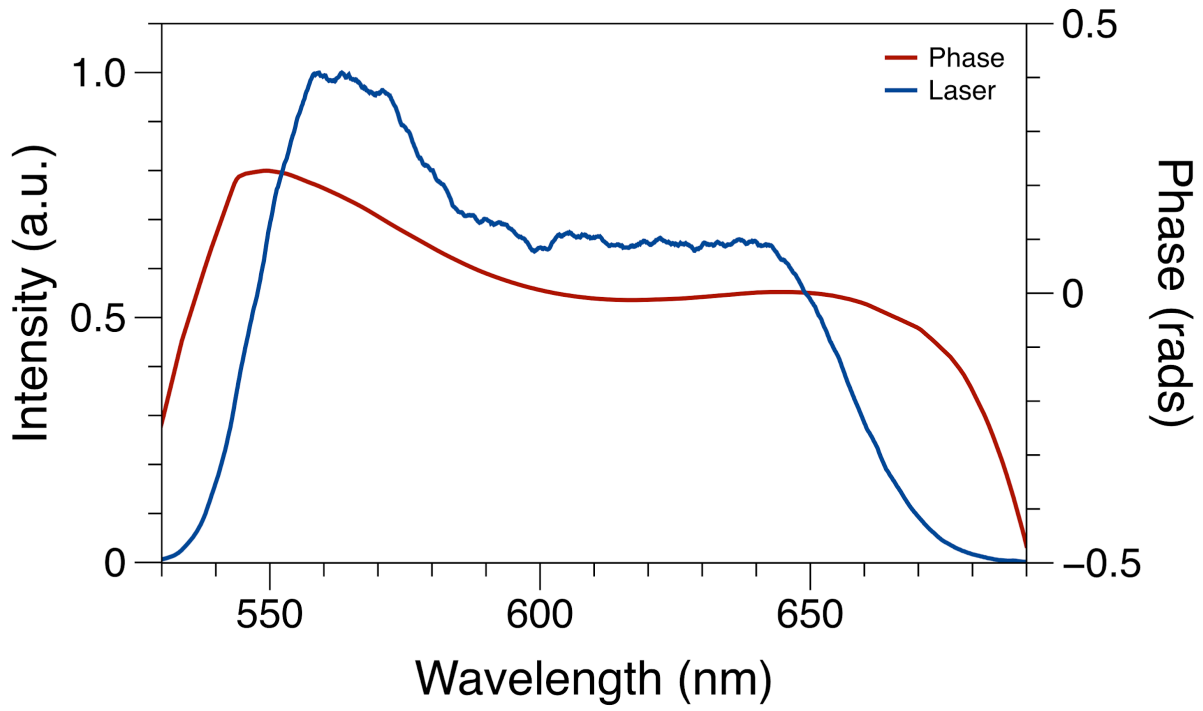

Figure A3.1. NOPA output spectrum (blue) for PCP 2DES experiments. Superimposed is the residual phase (red), as determined by the MIIPS scan.

A3.3 Phasing of PCP 2DES Spectra

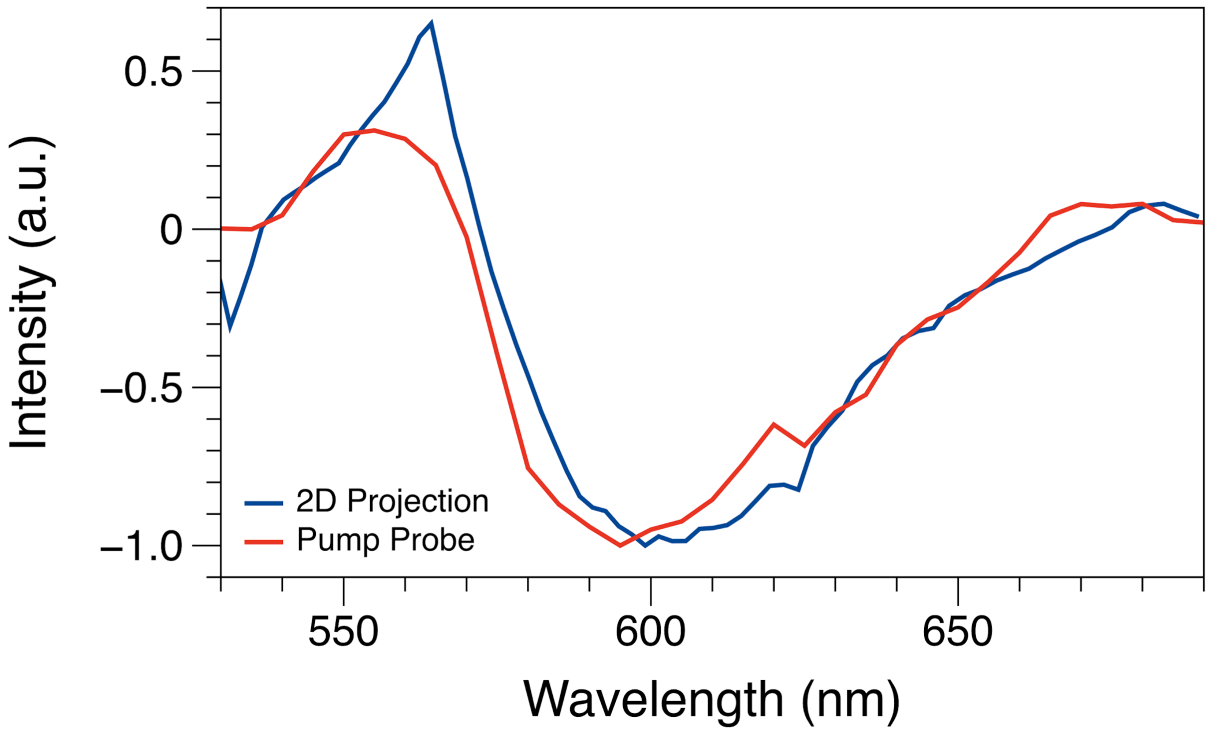

Figure A3.2. 2DES projection (blue) compared to the pump-probe spectrum (red) at waiting time $T = 0$ fs.

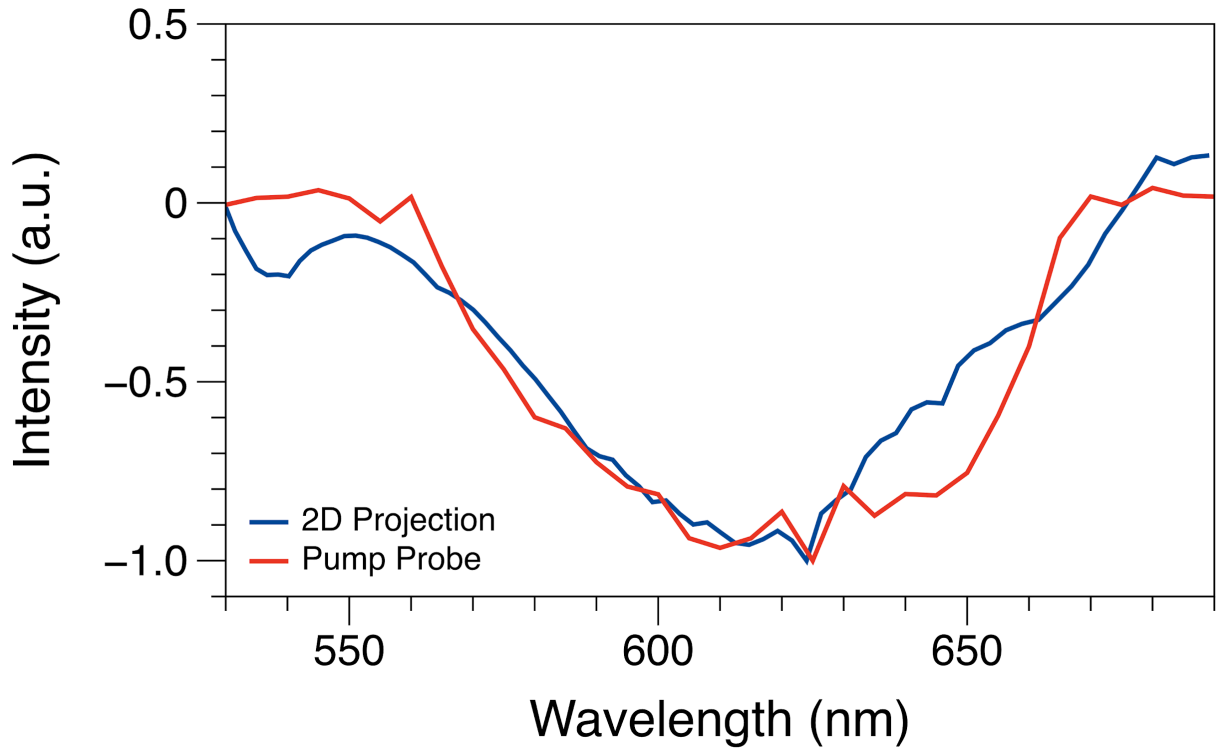

Figure A3.3. 2DES projection (blue) compared to the pump-probe spectrum (red) at waiting time $T = 500$ fs.

A3.4 Intensity analysis of PCP 2DES spectra

Figure 3.3 and the following figures present intensity profiles with respect to the waiting time of additional points of interest in the 2DES spectra. Non-oscillatory transients were modeled using iterative reconvolution with a Gaussian instrument response function to obtain curves that track the response at short time (<100 fs) followed by exponentials. LPSVD was used to model the oscillatory, quantum beating transients. For the long *T* transient (Figure 3.3d), a single exponential model was employed.

Table A3.1. Model parameters for PCP 2DES transient at λ_{ex} = 537 nm and λ_{det} = 625 nm, Figure 3.3, Panel A.

Component	Amplitude	Time Constant (fs)
Exponential	-445	13
Offset	154	—

Table A3.2. Model parameters for oscillations in the PCP 2DES transient at λ_{ex} = 625 nm and λ_{det} = 570 nm, Figure 3.3, Panel B.

Frequency (cm^{-1})	Time Constant (fs)
3300	12
1350	26

Table A3.3. Model parameters for oscillations in the PCP 2DES transient at λ_{ex} = 600 nm and λ_{det} = 565 nm, Figure 3.3, Panel C.

Frequency (cm^{-1})	Time Constant (fs)
3300	14
950	22

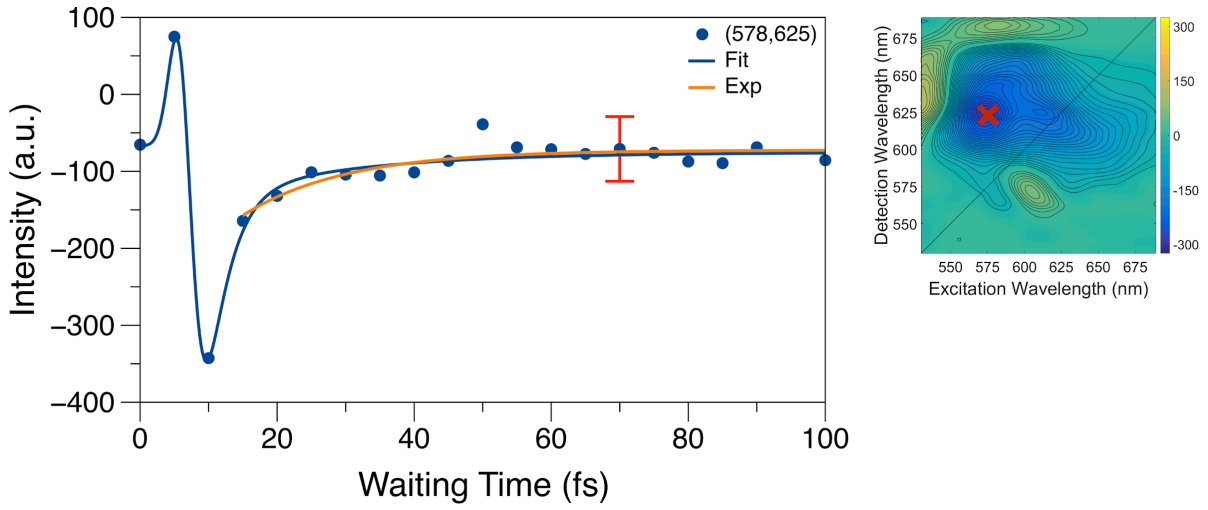

Figure A3.4. Intensity of the off-diagonal Chl Q_x-peridinin coherence peak at λ_{ex} = 643 nm and λ_{det} = 564 nm, as marked in the $T = 0$ fs spectrum. The fitted model (blue) was obtained from LPSVD, which includes a 1350 cm^{-1} oscillation with a 20 fs damping time.

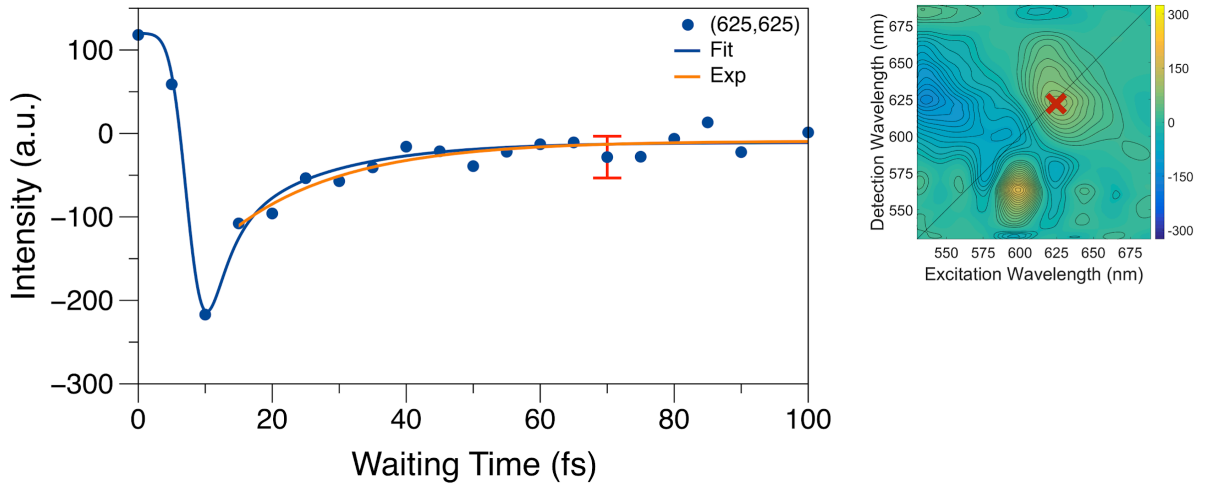

Figure A3.5. Intensity of the off-diagonal peridinin-Chl Q_x ESA peak at λ_{ex} = 578 nm and λ_{det} = 625 nm, as marked in the $T = 10$ fs spectrum. The fitted model (blue) was obtained from iterative reconvolution of a gaussian and three exponentials, which returned a 21 fs exponential for $T > 10$ fs. Overlaid is a 13 fs exponential (orange).

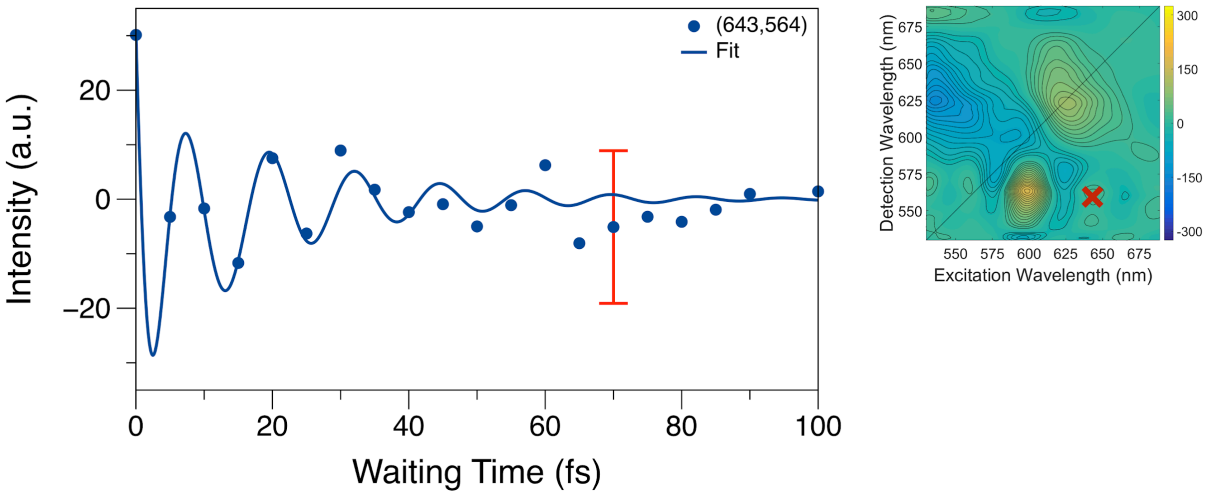

Figure A3.6. Intensity of the diagonal Chl Q_x-Chl Q_x SE peak at λ_{ex} = 625 nm and λ_{det} = 625 nm, as marked in the $T = 0$ fs spectrum. The fitted model (blue) was obtained from iterative reconvolution of a gaussian and two exponentials, which obtained a 15 fs exponential rise. Overlaid is a 13 fs exponential (orange).

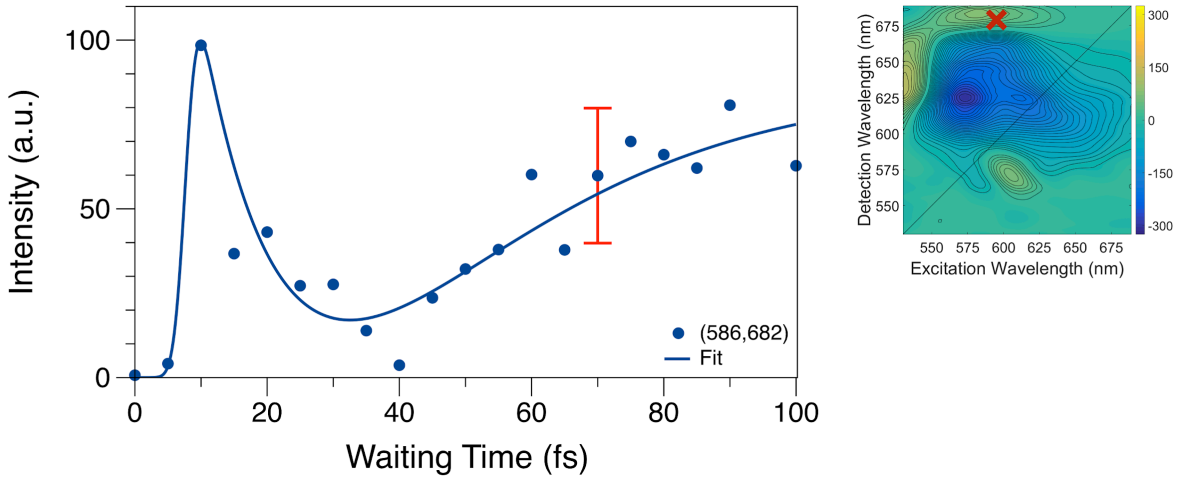

Figure A3.7. Intensity of the off-diagonal Per-Chl Q_y peak at λ_{ex} = 586 nm and λ_{det} = 682 nm, as marked in the $T = 10$ fs spectrum. The fitted model (blue) was obtained from iterative reconvolution of a gaussian and three exponentials, which obtained a 17 fs decay, a 25 fs rise, and a 700 fs decay. Figure A3.8 shows the data out to 9 ps.

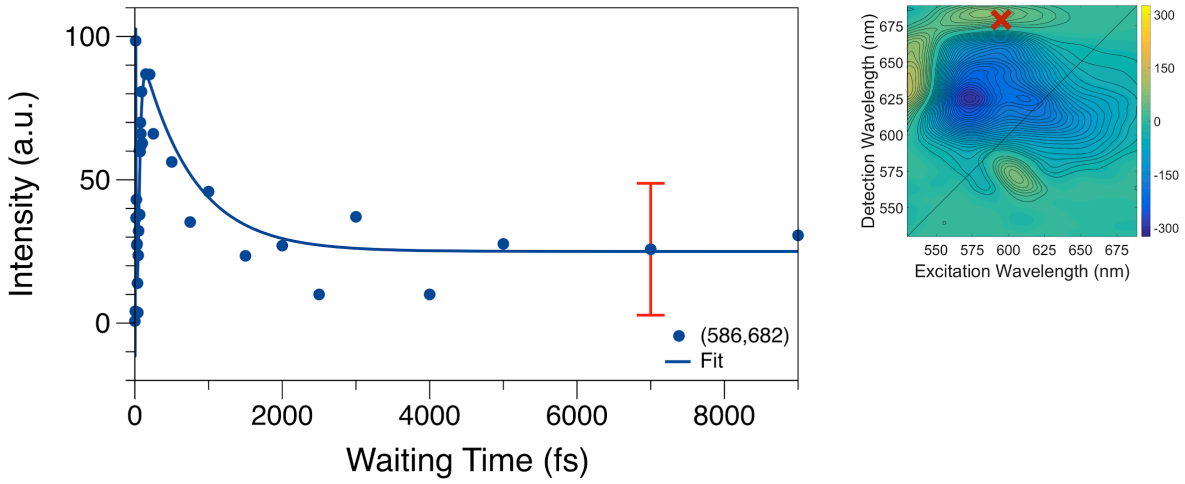

Figure A3.8. Intensity of the off-diagonal Per-Chl Q_y peak at λ_{ex} = 586 nm and λ_{det} = 682 nm, as marked in the $T = 0$ fs spectrum. The fitted model (blue) was obtained from iterative reconvolution of a gaussian and two exponentials, which obtained a 17 fs decay, a 25 fs rise, and a 700 fs decay.

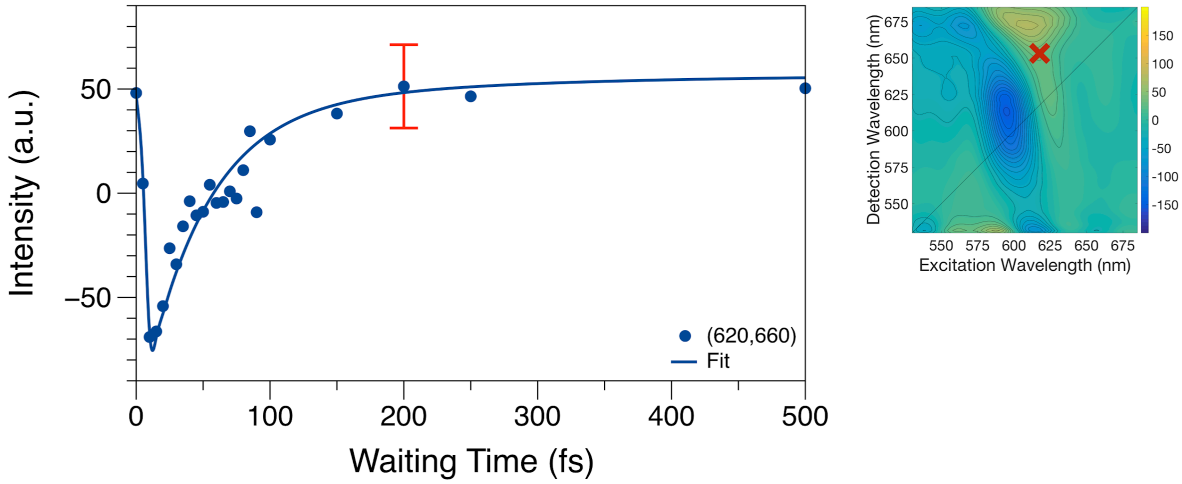

Figure A3.9. Intensity of the off-diagonal Chl Q_x-Chl Q_y peak at λ_{ex} = 620 nm and λ_{det} = 660 nm, as marked in the $T = 500$ fs spectrum. The fitted model (blue) was obtained from iterative reconvolution of a gaussian and two exponentials, which obtained 47 fs and 750 fs rises and a 1.5 ps decay. Figure A3.10 shows the data out to 9 ps.

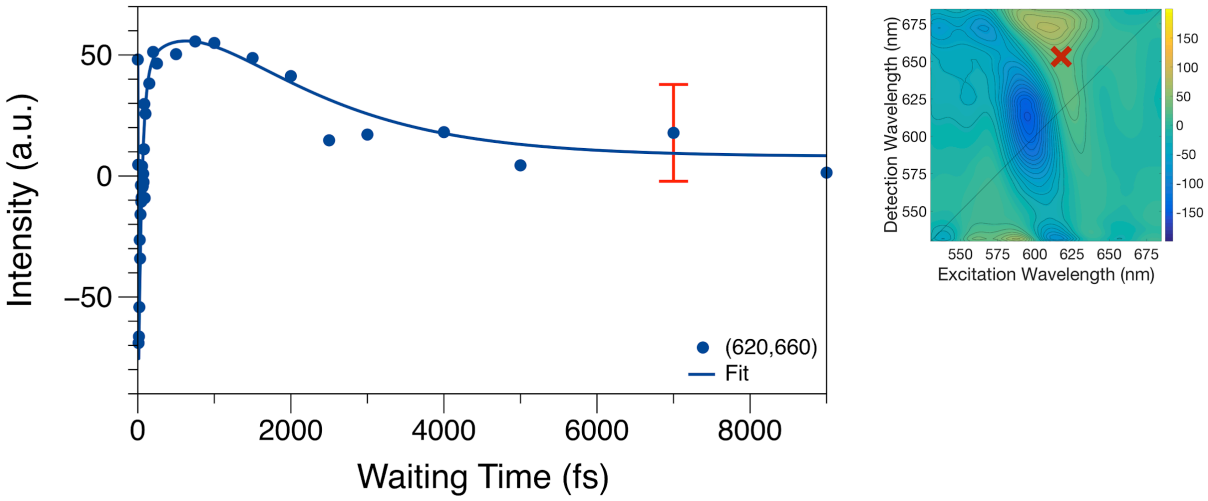

Figure A3.10. Intensity of the off-diagonal Chl Q_x-Chl Q_y peak at λ_{ex} = 620 nm and λ_{det} = 660 nm, as marked in the T = 500 fs spectrum. The fitted model (blue) was obtained from iterative reconvolution of a gaussian and two exponentials, which obtained 47 fs and 750 fs rises and a 1.5 ps decay.

A3.5 Laser Intensity and Residual Optical Phase Spectra for Peridinin 2DES Spectra

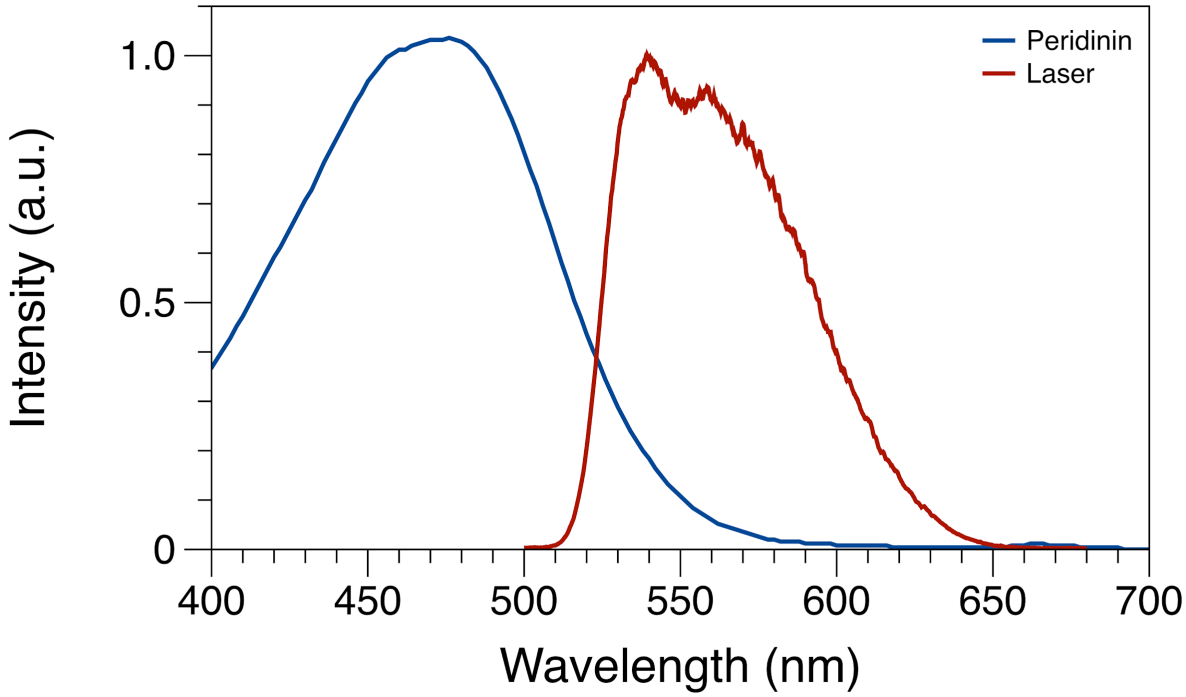

Figure A3.11. Room temperature absorption spectrum (blue) from peridinin in methanol. Superimposed is the spectrum of the NOPA output (red), as used in Figures A3.13-A3.16.

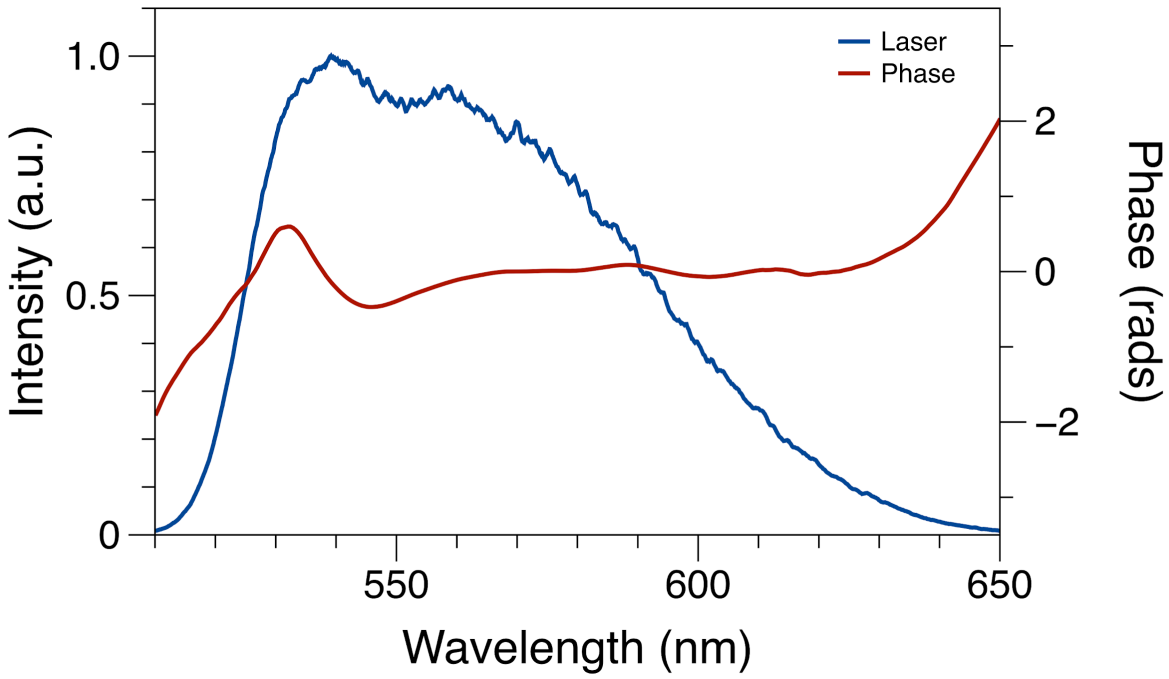

Figure A3.12. NOPA output spectrum (blue) used in peridinin 2DES experiments. Superimposed is the residual phase (red) determined by the MIIPS scan.

A3.6 2DES Spectra from Peridinin in Methanol

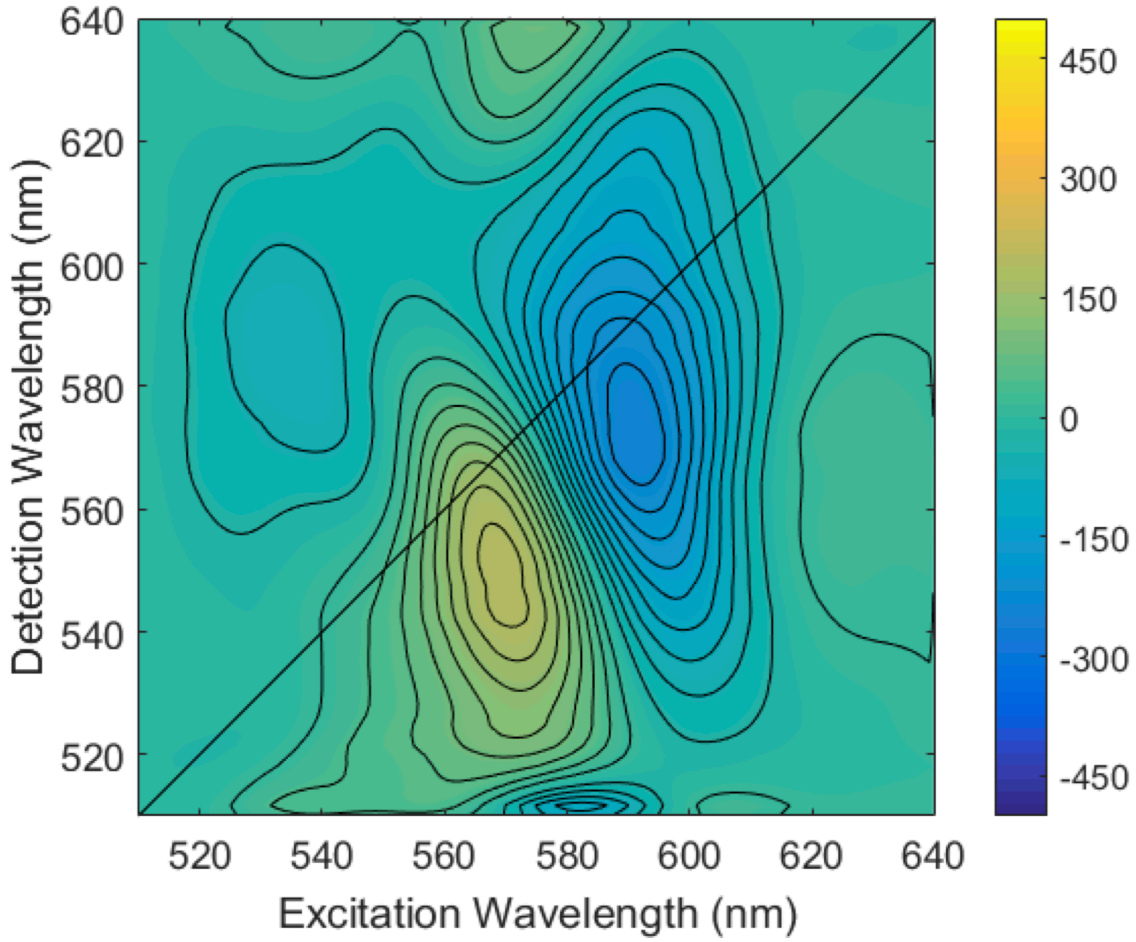

Figure A3.13. Absorptive 2DES spectrum from peridinin in methanol at waiting time $T = 0$ fs.

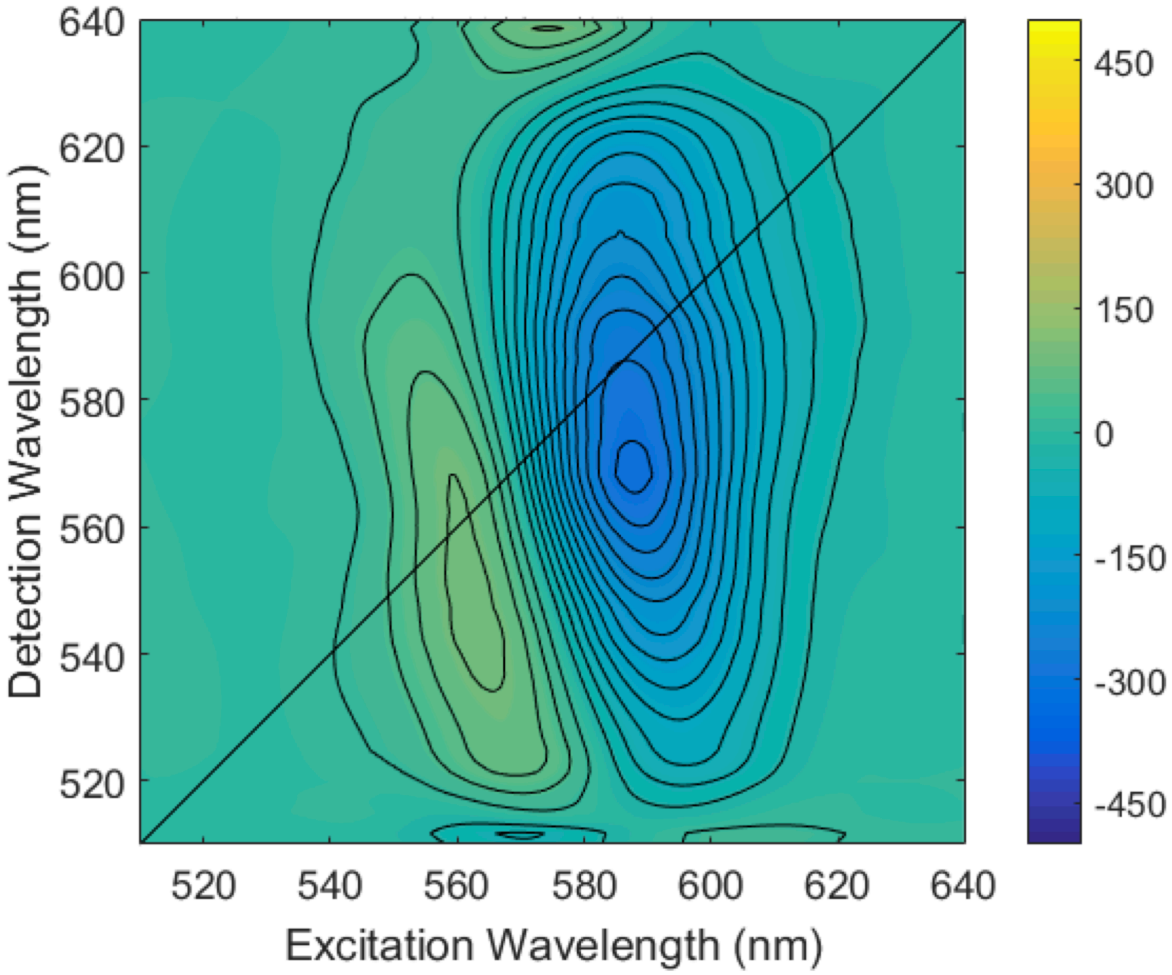

Figure A3.14. Absorptive 2DES spectrum from peridinin in methanol at waiting time $T = 60$ fs.

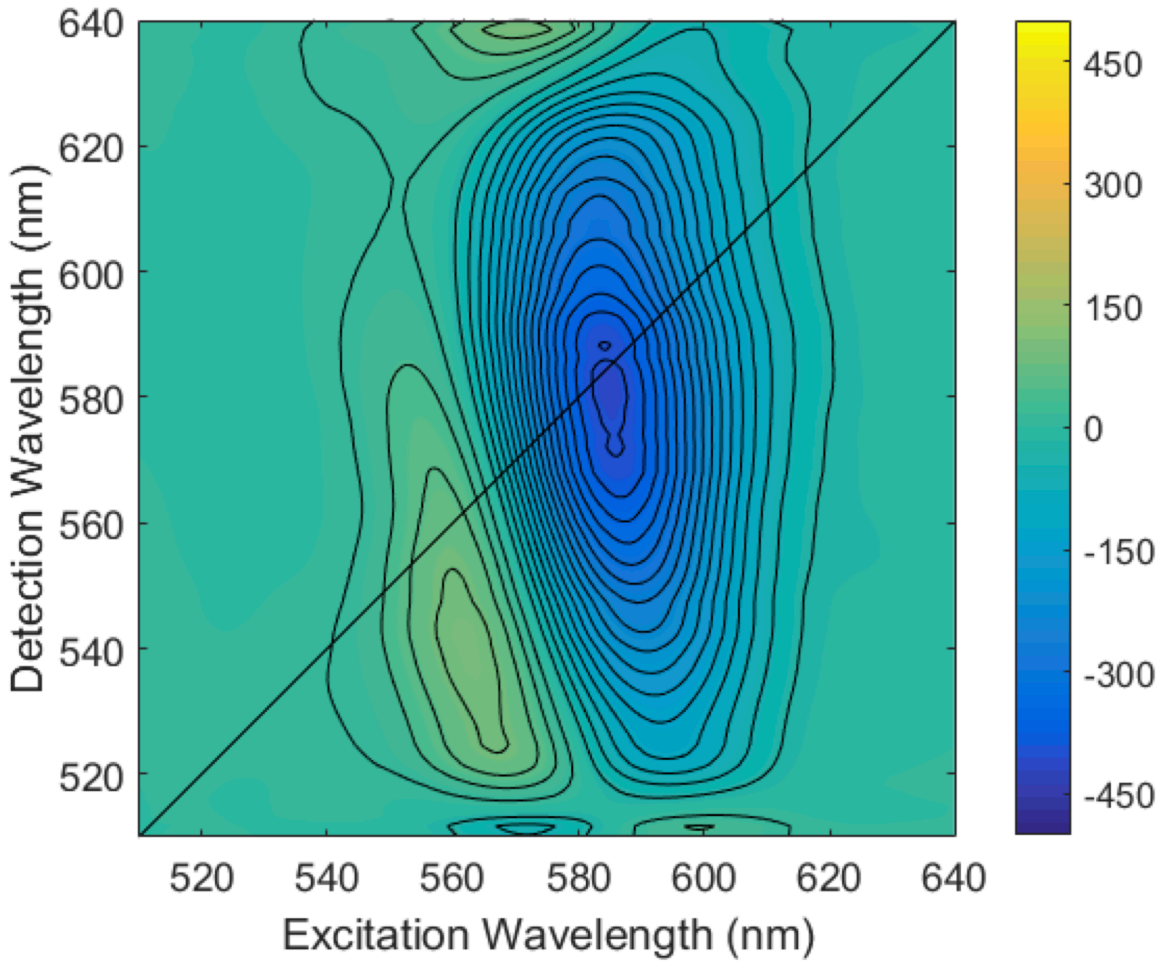

Figure A3.15. Absorptive 2DES spectrum from peridinin in methanol at waiting time $T = 500$ fs.

REFERENCES

REFERENCES

(1) Frank, H. A.; Cogdell, R. J. Light Capture in Photosynthesis. *Comp. Biophys.* **2012**, *8*, 94–114.

(2) Moore, G. F.; Brudvig, G. W. Energy Conversion in Photosynthesis: A Paradigm for Solar Fuel Production. *Annu. Rev. Condens. Matter Phys.* **2011**, *2* (1), 303–327.

(3) Beddard, G. S.; Porter, G. Concentration Quenching in Chlorophyll. *Nature* **1976**, *260*, 366.

(4) Pascal, A. A.; Liu, Z.; Broess, K.; van Oort, B.; van Amerongen, H.; Wang, C.; Horton, P.; Robert, B.; Chang, W.; Ruban, A. Molecular Basis of Photoprotection and Control of Photosynthetic Light-Harvesting. *Nature* **2005**, *436* (7047), 134–137.

(5) Chenu, A.; Scholes, G. D. Coherence in Energy Transfer and Photosynthesis. *Annu. Rev. Phys. Chem.* **2015**, *66*, 69–96.

(6) Engel, G. S.; Calhoun, T. R.; Read, E. L.; Ahn, T. K.; Mančal, T.; Cheng, Y. C.; Blankenship, R. E.; Fleming, G. R. Evidence for Wavelike Energy Transfer through Quantum Coherence in Photosynthetic Systems. *Nature* **2007**, *446*, 782–786.

(7) Hildner, R.; Brinks, D.; Nieder, J. B.; Cogdell, R. J.; van Hulst, N. F. Quantum Coherent Energy Transfer over Varying Pathways in Single Light-Harvesting Complexes. *Science* **2013**, *340* (6139), 1448–1451.

(8) Hofmann, E.; Wrench, P. M.; Sharples, F. P.; Hiller, R. G.; Welte, W.; Diederichs, K. Structural Basis of Light Harvesting by Carotenoids: Peridinin-Chlorophyll-Protein from *Amphidinium carterae*. *Science* **1996**, *272* (5269), 1788–1791.

(9) Kleima, F. J.; Wendling, M.; Hofmann, E.; Peterman, E. J.; van Grondelle, R.; van Amerongen, H. Peridinin Chlorophyll *a* Protein: Relating Structure and Steady-State Spectroscopy. *Biochemistry* **2000**, *39* (17), 5184–5195.

(10) Bautista, J. A.; Hiller, R. G.; Sharples, F. P.; Gosztola, D.; Wasielewski, M.; Frank, H. A. Singlet and Triplet Energy Transfer in the Peridinin-Chlorophyll *a*-Protein from *Amphidinium carterae*. *J. Phys. Chem. A* **1999**, *103* (14), 2267–2273.

(11) Krueger, B. P.; Lampoura, S. S.; van Stokkum, I. H. M.; Papagiannakis, E.; Salverda, J. M.; Gradinaru, C. C.; Rutkauskas, D.; Hiller, R. G.; van Grondelle, R. Energy Transfer in the Peridinin Chlorophyll-*a* Protein of *Amphidinium carterae* studied by Polarized Transient Absorption and Target Analysis. *Biophys. J.* **2001**, *80*, 2843–2855.

(12) Zigmantas, D.; Hiller, R. G.; Polívka, T.; Sundström, V. Carotenoid to Chlorophyll Energy Transfer in the Peridinin–chlorophyll-*a*–protein Complex Involves an Intramolecular Charge Transfer State. *Proc. Natl. Acad. Sci. U. S. A.* **2002**, *99*, 16760–16765.

(13) van Stokkum, I. H. M.; Papagiannakis, E.; Vengris, M.; Salverda, J. M.; Polívka, T.; Zigmantas, D.; Larsen, D. S.; Lampoura, S. S.; Hiller, R. G.; van Grondelle, R. Inter-Pigment Interactions in the Peridinin Chlorophyll Protein Studied by Global and Target Analysis of Time Resolved Absorption Spectra. *Chem. Phys.* **2009**, *357*, 70–78.

(14) Bautista, J. A.; Connors, R. E.; Raju, B. B.; Hiller, R. G.; Sharples, F. P.; Gosztola, D.; Wasielewski, M. R.; Frank, H. A. Excited State Properties of Peridinin: Observation of a Solvent Dependence of the Lowest Excited Singlet State Lifetime and Spectral Behavior Unique among Carotenoids. *J. Phys. Chem. B* **1999**, *103* (41), 8751–8758.

(15) Shima, S.; Ilagan, R. P.; Gillespie, N.; Sommer, B. J.; Hiller, R. G.; Sharples, F. P.; Frank, H. A.; Birge, R. R. Two-Photon and Fluorescence Spectroscopy and the Effect of Environment on the Photochemical Properties of Peridinin in Solution and in the Peridinin-Chlorophyll-Protein from *Amphidinium carterae*. *J. Phys. Chem. A* **2003**, *107* (40), 8052–8066.

(16) Ghosh, S.; Roscioli, J. D.; Bishop, M. M.; Gurchiek, J. K.; LaFountain, A. M.; Frank, H. A.; Beck, W. F. Torsional Dynamics and Intramolecular Charge Transfer in the S_2 ($1^1B_u^+$) Excited State of Peridinin: A Mechanism for Enhanced Mid-Visible Light Harvesting. *J. Phys. Chem. Lett.* **2016**, *7*, 3621–3626.

(17) Ghosh, S.; Bishop, M. M.; Roscioli, J. D.; LaFountain, A. M.; Frank, H. A.; Beck, W. F. Excitation Energy Transfer by Coherent and Incoherent Mechanisms in the Peridinin–chlorophyll *a* Protein. *J. Phys. Chem. Lett.* **2017**, *8*, 463–469.

(18) Reimers, J. R.; Cai, Z. L.; Kobayashi, R.; Ratsep, M.; Freiberg, A.; Krausz, E. Assignment of the Q-Bands of the Chlorophylls: Coherence Loss via Q_x - Q_y Mixing. *Sci. Rep.* **2013**, *3*, 2761.

(19) Carbonera, D.; Di Valentin, M.; Spezia, R.; Mezzetti, A. The Unique Photophysical Properties of the Peridinin-Chlorophyll-*a*-Protein. *Curr. Protein Pept. Sci.* **2014**, *15* (4), 332–350.

(20) Jonas, D. M. Two-Dimensional Femtosecond Spectroscopy. *Annu. Rev. Phys. Chem.* **2003**, *54*, 425–463.

(21) Brixner, T.; Stenger, J.; Vaswani, H. M.; Cho, M.; Blankenship, R. E.; Fleming, G. R. Two-Dimensional Spectroscopy of Electronic Couplings in Photosynthesis. *Nature* **2005**, *434* (7033), 625–628.

(22) Sener, M.; Strumpfer, J.; Hsin, J.; Chandler, D.; Scheuring, S.; Hunter, C. N.; Schulten, K. Förster Energy Transfer Theory as Reflected in the Structures of Photosynthetic Light-Harvesting Systems. *Chemphyschem* **2011**, *12* (3), 518–531.

(23) Sharples, F. P.; Wrench, P. M.; Ou, K.; Hiller, R. G. Two Distinct Forms of the Peridinin-Chlorophyll *a*-Protein from *Amphidinium carterae*. *Biochem. Biophys. Acta* **1996**, *1276*, 117–123.

(24) Brixner, T.; Mančal, T.; Stiopkin, I. V.; Fleming, G. R. Phase-Stabilized Two-Dimensional Electronic Spectroscopy. *J. Chem. Phys.* **2004**, *121*, 4221.

(25) Lepetit, L.; Joffre, M. Two-Dimensional Nonlinear Optics Using Fourier-Transform Spectral Interferometry. *Opt. Lett.* **1996**, *21* (8), 564–566.

(26) Ginsberg, N. S.; Cheng, Y.-C.; Fleming, G. R. Two-Dimensional Electronic Spectroscopy of Molecular Aggregates. *Acc. Chem. Res.* **2009**, *42* (9), 1352–1363.

(27) Ghosh, S.; Bishop, M. M.; Roscioli, J. D.; LaFountain, A. M.; Frank, H. A.; Beck, W. F. Femtosecond Heterodyne Transient Grating Studies of Nonradiative Deactivation of the S_2 ($1^1B_u^+$) State of Peridinin: Detection and Spectroscopic Assignment of an Intermediate in the Decay Pathway. *J. Phys. Chem. B* **2016**, *120*, 3601–3614.

(28) Fujiwara, M.; Yamauchi, K.; Sugisaki, M.; Gall, A.; Robert, B.; Cogdell, R. J.; Hashimoto, H. Energy Dissipation in the Ground-State Vibrational Manifolds of β-Carotene Homologues: A Sub-20-Fs Time-Resolved Transient Grating Spectroscopic Study. *Phys. Rev. B Condens. Matter* **2008**, *77* (20), 2021.

(29) Ostroumov, E. E.; Mulvaney, R. M.; Cogdell, R. J.; Scholes, G. D. Broadband 2D Electronic Spectroscopy Reveals a Carotenoid Dark State in Purple Bacteria. *Science* **2013**, *340* (6128), 52–56.

(30) Pollard, W. T.; Lee, S.; Mathies, R. A. Wave Packet Theory of Dynamic Absorption Spectra in Femtosecond Pump–probe Experiments. *J. Chem. Phys.* **1990**, *92* (7), 4012–4029.

(31) Pollard, W. T.; Dexheimer, S. L.; Wang, Q.; Peteanu, L. A.; Shank, C. V.; Mathies, R. A. Theory of Dynamic Absorption Spectroscopy of Nonstationary States. 4. Application to 12-Fs Resonant Impulsive Raman Spectroscopy of Bacteriorhodopsin. *J. Phys. Chem.* **1992**, *96* (15), 6147–6158.

(32) Pollard, W. T.; Mathies, R. A. Analysis of Femtosecond Dynamic Absorption Spectra of Nonstationary States. *Annu. Rev. Phys. Chem.* **1992**, *43*, 497–523.

(33) Ishizaki, A.; Calhoun, T. R.; Schlau-Cohen, G. S.; Fleming, G. R. Quantum Coherence and Its Interplay with Protein Environments in Photosynthetic Electronic Energy Transfer. *Phys. Chem. Chem. Phys.* **2010**, *12* (27), 7319–7337.

(34) Cerullo, G.; Polli, D.; Lanzani, G.; De Silvestri, S.; Hashimoto, H.; Cogdell, R. J. Photosynthetic Light Harvesting by Carotenoids: Detection of an Intermediate Excited State. *Science* **2002**, *298* (5602), 2395–2398.

(35) Beck, W. F.; Bishop, M. M.; Roscioli, J. D.; Ghosh, S.; Frank, H. A. Excited State Conformational Dynamics in Carotenoids: Dark Intermediates and Excitation Energy Transfer. *Arch. Biochem. Biophys.* **2015**, *572*, 175–183.

(36) Christensson, N.; Milota, F.; Nemeth, A.; Sperling, J.; Kauffmann, H. F.; Pullerits, T.; Hauer, J. Two-Dimensional Electronic Spectroscopy of Beta-Carotene. *J. Phys. Chem. B* **2009**, *113* (51), 16409–16419.

(37) Kleima, F. J.; Hofmann, E.; Gobets, B.; van Stokkum, I. H.; van Grondelle, R.; Diederichs, K.; van Amerongen, H. Förster Excitation Energy Transfer in Peridinin-Chlorophyll-*a*-Protein. *Biophys. J.* **2000**, *78* (1), 344–353.

(38) Lampoura, S. S.; Krueger, B. P.; Van Stokkum, I. H. M.; Salverda, J. M.; Gradinaru, C. C.; Rutkauskas, D.; Hiller, R. G.; Van Grondelle, R. Energy Transfer in the Peridinin Chlorophyll *a* Protein of *Amphidinium carterae* Studied by Polarized Absorption Measurements. *Int. J. Mod. Phys. B* **2001**, *15* (28n30), 3849–3852.

(39) Edington, M. D.; Riter, R. E.; Beck, W. F. Interexciton-State Relaxation and Exciton Localization in Allophycocyanin Trimers. *J. Phys. Chem.* **1996**, *100* (33), 14206–14217.

(40) van Grondelle, R.; Novoderezhkin, V. Dynamics of Excitation Energy Transfer in the LH1 and LH2 Light-Harvesting Complexes of Photosynthetic Bacteria. *Biochemistry* **2001**, *40* (50), 15057–15068.

(41) Dahlberg, P. D.; Ting, P.-C.; Massey, S. C.; Martin, E. C.; Hunter, C. N.; Engel, G. S. Electronic Structure and Dynamics of Higher-Lying Excited States in Light Harvesting Complex 1 from *Rhodobacter sphaeroides*. *J. Phys. Chem. A* **2016**, *120* (24), 4124–4130.

(42) Arnett, D. C.; Moser, C. C.; Dutton, P. L.; Scherer, N. F. The First Events in Photosynthesis: Electronic Coupling and Energy Transfer Dynamics in the Photosynthetic Reaction Center from *Rhodobacter sphaeroides*. *J. Phys. Chem. B* **1999**, *103* (11), 2014–2032.

(43) Jumper, C. C.; Anna, J. M.; Stradomska, A.; Schins, J.; Myahkostupov, M.; Prusakova, V.; Oblinsky, D. G.; Castellano, F. N.; Knoester, J.; Scholes, G. D. Intramolecular Radiationless Transitions Dominate Exciton Relaxation Dynamics. *Chem. Phys. Lett.* **2014**, *599*, 23–33.

(44) Novoderezhkin, V. I.; Romero, E.; Prior, J.; van Grondelle, R. Exciton-Vibrational Resonance and Dynamics of Charge Separation in the Photosystem II Reaction Center. *Phys. Chem. Chem. Phys.* **2017**, *19* (7), 5195–5208.

(45) Panitchayangkoon, G.; Voronine, D. V.; Abramavicius, D.; Caram, J. R.; Lewis, N. H.; Mukamel, S.; Engel, G. S. Direct Evidence of Quantum Transport in Photosynthetic Light-Harvesting Complexes. *Proc. Natl. Acad. Sci. U. S. A.* **2011**, *108* (52), 20908–20912.

(46) Halpin, A.; Johnson, P. J.; Tempelaar, R.; Murphy, R. S.; Knoester, J.; Jansen, T. L.; Miller, R. J. Two-Dimensional Spectroscopy of a Molecular Dimer Unveils the Effects of Vibronic Coupling on Exciton Coherences. *Nat. Chem.* **2014**, *6* (3), 196–201.

(47) Womick, J. M.; Moran, A. M. Vibronic Enhancement of Exciton Sizes and Energy Transport in Photosynthetic Complexes. *J. Phys. Chem. B* **2011**, *115* (6), 1347–1356.

(48) Tiwari, V.; Peters, W. K.; Jonas, D. M. Electronic Resonance with Anticorrelated Pigment Vibrations Drives Photosynthetic Energy Transfer Outside the Adiabatic Framework. *Proc. Natl. Acad. Sci. U. S. A.* **2013**, *110* (4), 1203–1208.

(49) Perlík, V.; Seibt, J.; Cranston, L. J.; Cogdell, R. J.; Lincoln, C. N.; Savolainen, J.; Šanda, F.; Mančal, T.; Hauer, J. Vibronic Coupling Explains the Ultrafast Carotenoid-to-Bacteriochlorophyll Energy Transfer in Natural and Artificial Light Harvesters. *J. Chem. Phys.* **2015**, *142*, 212434.

(50) Lozovoy, V. V.; Pastirk, I.; Dantus, M. Multiphoton Intrapulse Interference 4: Characterization and Compensation of the Spectral Phase of Ultrashort Laser Pulses. *Opt. Lett.* **2004**, *29*, 775–777.

(51) Moran, A. M.; Maddox, J. B.; Hong, J. W.; Kim, J.; Nome, R. A.; Bazan, G. C.; Mukamel, S.; Scherer, N. F. Optical Coherence and Theoretical Study of the Excitation Dynamics of a Highly Symmetric Cyclophane-Linked Oligophenylenevinylene Dimer. *J. Chem. Phys.* **2006**, *124*, 194904.

(52) Gallagher, S. M.; Albrecht, A. W.; Hybl, J. D.; Landin, B. L.; Rajaram, B.; Jonas, D. M. Heterodyne Detection of the Complete Electric Field of Femtosecond Four-Wave Mixing Signals. *J. Opt. Soc. Am. B* **1998**, *15*, 2338–2345.

(53) Hybl, J. D.; Albrecht, A. W.; Gallagher Faeder, S. M.; Jonas, D. M. Two-Dimensional Electronic Spectroscopy. *Chem. Phys. Lett.* **1998**, *297* (3), 307–313.

Chapter 4: Structural Tuning of Quantum Decoherence and Coherent Energy Transfer in Photosynthetic Light Harvesting

Photosynthetic organisms capture energy from solar photons by constructing light-harvesting proteins containing arrays of electronic chromophores. Collective excitations (excitons) arise when energy transfer between chromophores is coherent, or wavelike, in character. Here we demonstrate experimentally that coherent energy transfer to the lowest energy excitons is principally controlled in a light-harvesting protein by the temporal persistence of quantum coherence rather than by the strength of vibronic coupling. In the peridinin–chlorophyll protein from marine dinoflagellates, broad-band two-dimensional electronic spectroscopy reveals that replacing the native chlorophyll *a* acceptor chromophores with chlorophyll *b* slows energy transfer from the carotenoid peridinin to chlorophyll despite narrowing the donor–acceptor energy gap. The formyl substituent on the chlorophyll *b* macrocycle hastens decoherence by sensing the surrounding electrostatic noise. These findings demonstrate how quantum coherence enhances the efficiency of energy transfer despite being very short lived in light-harvesting proteins at physiological temperatures.

The work presented in this chapter has been adapted with permission from *J. Phys. Chem. lett.* **2018**, *8*, 5141–5147.

4.1 Introduction

The discovery that photosynthetic light-harvesting and reaction-center complexes exhibit quantum coherent excitation energy transfer processes[1–9] has renewed interest in their structures and photophysics and inspires the search for new materials incorporating strongly interacting electronic chromophores for the capture and conversion of solar energy to electricity or fuels.[10,11] Quantum coherence,[12] resulting in collective excitation of arrays of strongly interacting light-harvesting chromophores, is proposed to contribute to the enhanced rates and yields of energy transfer that have been detected in several light-harvesting systems by effectively choosing the most efficient route between donors and acceptors in the midst of a constantly fluctuating energy landscape.[13] Whether photosynthetic organisms really obtain a functional advantage from quantum coherence under physiological conditions, and how it is derived from the structure of a light-harvesting protein, however, have not yet been demonstrated experimentally.[14]

The peridinin–chlorophyll protein (PCP), a peripheral light-harvesting protein from marine dinoflagellates,[15] is a well-structurally characterized case in which it is now evident that coherent energy transfer is crucial to proper function.[16–19] The structure of PCP (Figure 4.1) contains eight peridinins nearly in van der Waals contact around two chlorophyll (Chl) chromophores and two lipids in a C_2 symmetric, two-domain nanocrystalline complex.[15] Femtosecond pump–probe measurements with 100 fs pulses established early on that excitation energy is transferred using the Förster mechanism in PCP from the peridinins to the Chl *a* acceptor with a 2.3–3.2 ps time constant.[20–25] Because the resonant S_2 state of peridinin was known to have a very short lifetime, <50 fs,[26] these investigations attributed most of the energy transfer yield in PCP to a form of the S_1 state of peridinin with an enhanced intramolecular

charge-transfer (ICT) character derived from its carbonyl substituent.[20,24,27,28] The results also indicated, however, that the short-lived S_2 state serves as the donor state for a much faster energy transfer process, possibly involving a quantum coherent mechanism.[20–25] Recent investigations in this laboratory using heterodyne transient grating spectroscopy with 40 fs pulses[16,29,30] focused on determining the nature of this faster process and on characterizing the nonradiative decay processes in peridinin that accompany it. At least two-thirds of the energy transfer yield in PCP was estimated to originate from the S_2 state of peridinin with a <30 fs time constant.[16] The assignment of the faster process to coherent energy transfer was then confirmed with broad-band two-dimensional electronic spectroscopy (2DES), as discussed below,[17,18] and this conclusion is supported by recent electronic structure calculations.[19] The remaining energy transfer yield was assigned to the slower, Förster process on the ps timescale but involving a distorted form of the S_2 state of peridinin, termed S_x, which is produced by large-amplitude out-of-plane (torsional and/or pyramidal) motions of the conjugated polyene backbone.[16] The S_x state is detected in heterodyne transient grating experiments in <20 fs after optical preparation of the S_2 state;[30–32] distortion of the conjugated polyene backbone results in an enhanced ICT character, which frictionally retards nonradiative decay to the S_1 state.[16] In PCP, the ICT character enhances the yield of the Förster process because it lengthens the lifetime of the S_x state of peridinin.[30] The scheme that emerges from these recent studies, then, accounts for all of the energy transfer yield in PCP using either the S_2 state or the S_x state of peridinin as the donor.[16] This hypothesis is in accord with the finding that the "dark" S_1 state in carotenoids lacks oscillator strength for transitions to or from the ground state, S_0, due to large excited-state displacements from the equilibrium ground-state structure following optical preparation of the S_2 state.[33]

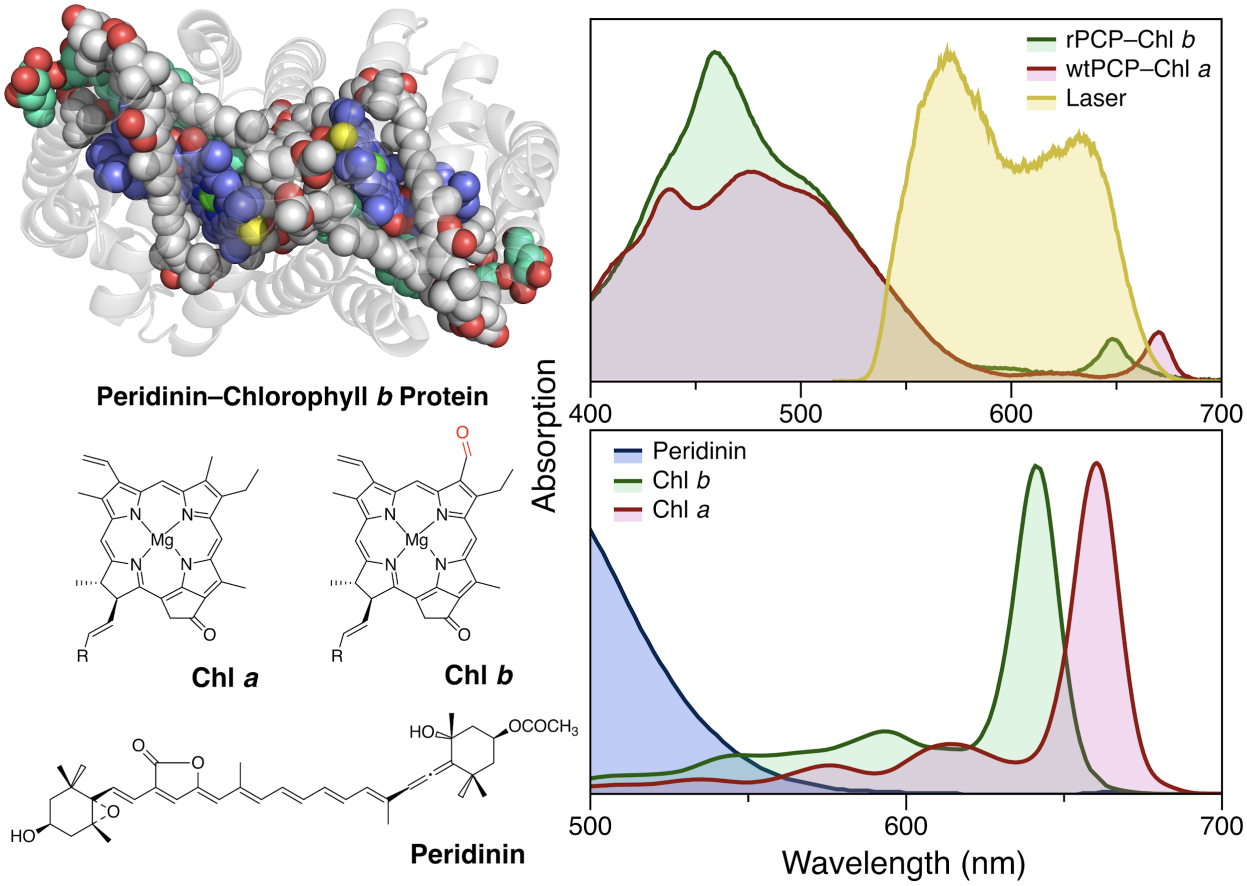

Figure 4.1. (*Left*) Structures of the reconstituted PCP complex containing Chl *b* (rPCP–Chl *b*, PDB structure 2X20[34]), chlorophyll *a* (Chl *a*), chlorophyll *b* (Chl b), and peridinin. In the space-filling structure of rPCP–Chl *b*, as viewed down the C_2 symmetry axis, the formyl substituents of the two Chl *b* (blue) chromophores are marked by gold spheres. Eight peridinin chromophores (grey) and two lipid molecules (digalactosyl diacylglycerol, cyan) complete the cluster. The surrounding protein is shown with transparent ribbons. Figure A4.1 in the Appendix shows the same rendering of the structure from a rotated vantage point. (*Right, top*) Room-temperature absorption spectra from rPCP–Chl *b* (green) and wtPCP–Chl *a* (red), overlaid with the spectrum of the laser pulses (yellow) used in the 2DES experiment. (*Right, bottom*) Absorption spectra of the chromophores in solution: peridinin in methanol (blue); Chl *b* (green) and Chl *a* (red) in diethyl ether.[35]

PCP offers a unique opportunity to study the nature of quantum coherence in a light-harvesting protein because it can be reconstituted with different Chl chromophores[36] without changing the structure of the peridinin–Chl cluster.[34] When Chl *b* is present, a formyl (–CH=O) group is substituted for a methyl ($–CH_3$) group on the Chl *a* macrocycle in a position that points outwardly (Figure 4.1); as shown in Figures A4.1 and A4.2 in the Appendix, the crystal structure of the reconstituted PCP complex with Chl *b* (rPCP–Chl *b*)[34] exhibits the same peridinin–Chl organization and interchromophore distances as found in that of the wild-type PCP complex with Chl *a* (wtPCP–Chl *a*).[15] But because the formyl group is in conjugation, its electron-withdrawing character significantly perturbs the π-electron system of the porphyrin ring. The energy of the Q_y state is shifted more than 500 cm^{-1} to higher energy from that of Chl *a*, significantly narrowing the peridinin S_2 to Chl Q_y donor–acceptor energy gap.[37] The vibronic structure in the absorption spectrum is also affected; progressions in low frequency normal modes make stronger contributions to the absorption spectrum of Chl *b* (Figure 4.1).[38]

Figure 4.2 examines the impact of reconstitution with Chl *b* on the vibronic interactions with the four neighboring peridinins in each domain of PCP by comparing the peridinin and Chl energy levels. For both Chl *a* and Chl *b*, the lowest vibrational levels of Q_x and Q_y lie well below the peridinin site energies estimated with electronic structure calculations.[19] The strongest interactions with peridinin involve the $v = 2$ and $v = 1$ levels of the resonance Raman-active C=C and C–C stretching modes of the Chl *a* and *b* macrocycles, respectively, which span the energies of the thermally distorted peridinins that contribute to the broad long-wavelength onset of the mid-visible absorption band.[39] The exciton splittings in the PCP complex are effectively intermediate in strength,[40] and admixture of the electronic and vibrational states[41–44] is clearly

implicated. Without inclusion of the vibrations in the excitonic wavefunctions, the large peridinin to Chl electronic energy gaps in both complexes would tend to produce localized excitations, which is inconsistent with detection of sub-ps peridinin–to-Chl energy transfer.

In short, the narrowing of the donor–acceptor energy gap and better matching with vibrations that accompanies reconstitution of PCP with Chl *b* would be expected to enhance the rate of energy transfer and slow the rate of decoherence. We have tested this hypothesis by carrying out a new set of 2DES experiments at room temperature (23 °C) with the rPCP–Chl *b* complex under the same optical conditions used previously with the wtPCP–Chl *a* complex.[17] The present results are in direct opposition to expectations, indicating a dominant role for the rate of quantum decoherence in determining the rate of energy transfer.

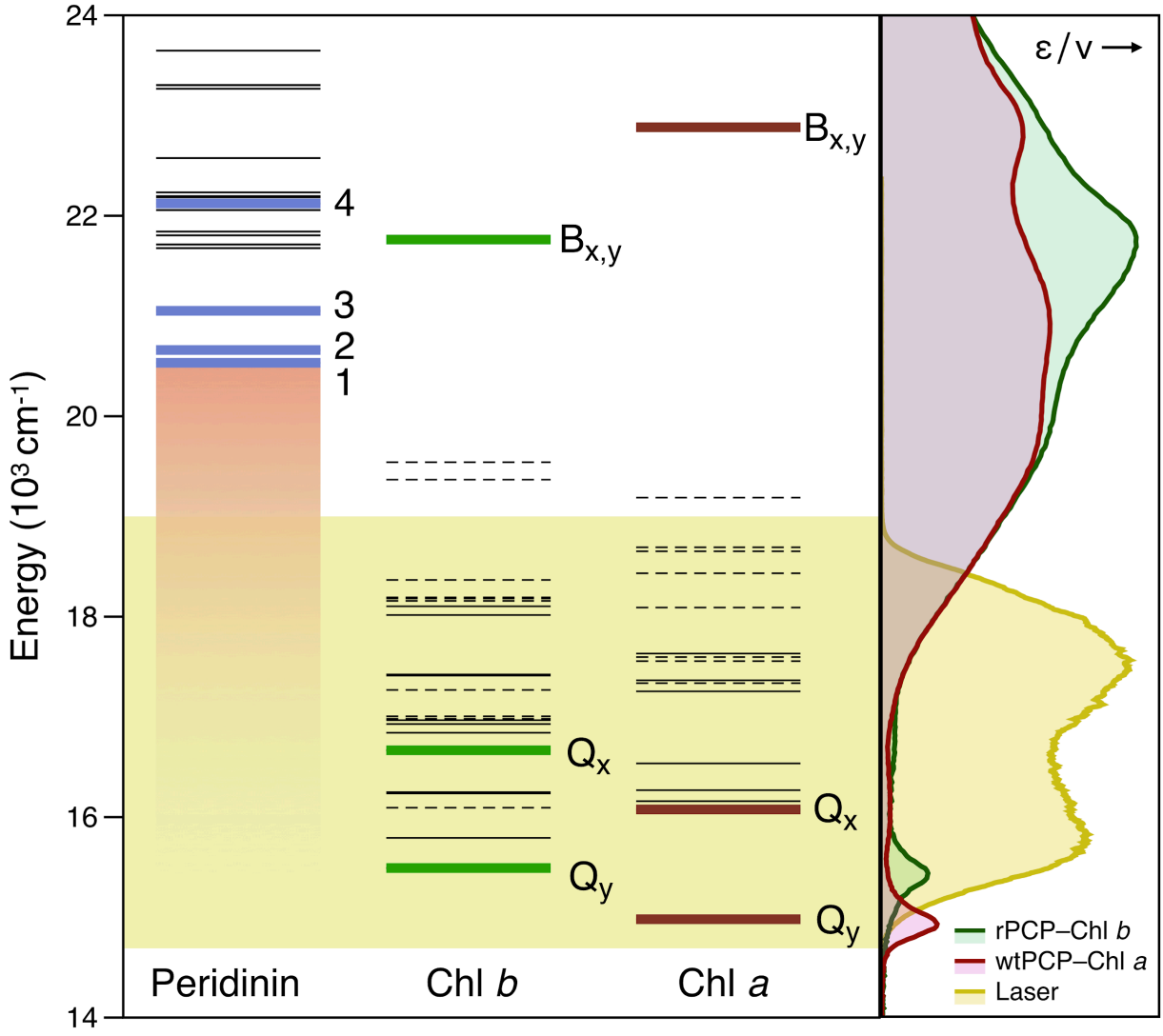

Figure 4.2. Electronic and vibrational energy levels for chromophore sites in the PCP complexes with Chl *a* and Chl *b*. Site energies (S_2, $v = 0$) for the four peridinin sites (1–4) (Table A4.1)[19] and for the Chls (B_x, B_y, Q_x, and Q_y)[45] are marked by colored bars (Table A4.2); thin and dashed bars mark the $v = 1$ and $v = 2$ levels, respectively, for the strongest resonance Raman-active vibrational modes[46] (Table A4.3). An orange gradient indicates the long-wavelength absorption region in PCP arising from peridinin conformers with distorted conjugated polyene backbones. The yellow filled region marks the energy levels spanned by the femtosecond excitation pulses used in the 2DES experiment. (*Right*) Absorption dipole-strength spectra, $\varepsilon(\nu)/\nu$, for wtPCP–Chl *a* and rPCP–Chl *b*, are overlaid with the laser spectrum.

4.2 Experimental

4.2.1 Sample Preparation

Preparation of reconstituted PCP complexes containing chlorophyll (Chl) *b* (rPCP–Chl *b*) employed N-terminal domain PCP apoprotein expressed in *Escherichia coli* and reconstituted with peridinin and Chl *b* using previously reported procedures.[36] The expression construct for the N-terminal domain apoprotein from PCP was generously provided by Dr. Roger Hiller (Macquarie University). The construct was transformed into *E. coli* JM109 cells (Sigma-Aldrich), and the protein was expressed and purified. Reconstitution of the apoprotein with Chl *b* was performed as described previously[36] with the minor exception that pre-packed HiTrap DEAE fast-flow columns (GE Healthcare) were used in place of DEAE Tris-acryl columns for the final purification step. Reconstituted complexes were concentrated using YM-30 Amicon Centriplus filters. Chl *b* was extracted and purified from spinach, and additional Chl *b* was purchased from Sigma-Aldrich. Peridinin was obtained as a gift from Dr. Roger Hiller.

For the 2DES experiments, rPCP–Chl *b* samples were suspended in a buffer solution containing 50 mM tricine–NaOH and 20 mM KCl at pH 7.5 to obtain an optical density of 0.3 at 540 nm for a 1 mm optical pathlength. Linear absorption spectra were recorded at room temperature with a Varian Cary 50 spectrophotometer. The absorption spectrum was measured before and after the femtosecond spectroscopy experiments to assess whether there were any changes due to photochemistry or decomposition of the sample. There were no changes noted during these experiments.

4.2.2 Nonlinear Spectroscopy

The 2DES experiment is a third-order nonlinear spectroscopy performed with a sequence of three femtosecond excitation pulses.[47] The sequence begins with an initial pair of pulses with a relatively short coherence time interval, τ, between them. Then, after a fixed waiting (or population) interval, T, a third pulse arrives at the sample to probe the time evolution of the system. This pulse stimulates the emission of either a free-induction decay (nonrephasing signal) or a photon echo (rephasing signal). The detection axis of the two-dimensional spectrum is acquired directly using a spectrograph and a CCD detector, which measures the wavelength-resolved amplitude and phase of the signal pulse through its spectral interference with an attenuated local oscillator pulse.[48] The excitation axis of the spectrum is obtained by Fourier transformation of the time series obtained by scanning the delay τ between the first two pulses. The 2DES spectrum can then be interpreted qualitatively as an excitation–detection correlation spectrum.[47] By repeating the 2DES measurements as a function of T, one can observe the time evolution of the populations and coherences that were prepared by the initial pair of excitation pulses. Figures 4.1 and 4.2 show that the spectrum of the excitation pulses (8 fs duration) used here is broad enough to excite the lowest energy peridinins in the 520–600-nm region and to probe the Q_y ($v = 0$) absorption transition from Chl *b* (Figure 4.1) in the 650 nm region of the spectrum.

The 2DES experiments with rPCP–Chl *b* were conducted with the same passively phase-stabilized, diffractive-optic based photon-echo spectrometer[48] used for the previously reported studies on wtPCP–Chl *a*.[17] The three broad-band excitation pulses for the 2DES experiment were obtained from an amplified Yb laser and a noncollinear optical parametric amplifier. The

excitation pulse pair and the delayed probe pulse were processed separately by adaptive pulse shapers; durations of 8 fs were detected at the sample position (see Figures A4.3 and A4.4 for the residual optical phase spectra). The 2DES spectra were phased using the projection-slice theorem.[48]

4.3 Results and Discussion

As observed previously for the wtPCP–Chl *a* complex,[17] the 2DES spectra observed with the rPCP–Chl *b* complex (Figure 4.3) report the initial presence and decay of quantum coherence in terms of quantum beating near the diagonal of the spectrum. The signal amplitudes at the coordinates marked A and B, respectively, are modulated with respect to the waiting time T (Figure 4.4) owing to successive optical field–matter actions of the excitation pulses on a pair of peridinins or on a Chl–peridinin pair. The modulation frequency determines the energy gap between the two photoselected sites, and the damping rate reports directly the decay of the coherence between them. The quantum beats are damped very rapidly, in <25 fs, indicating their predominant electronic character; vibrational coherences usually exhibit damping times > 500 fs. The decay of the peridinin–Chl coherence (Figure 4.4b) is much more rapid than observed previously with wtPCP–Chl *a*; the first recurrence of the beating, at $T = 35$ fs, is at least two times weaker for Chl *b* than for Chl *a*.

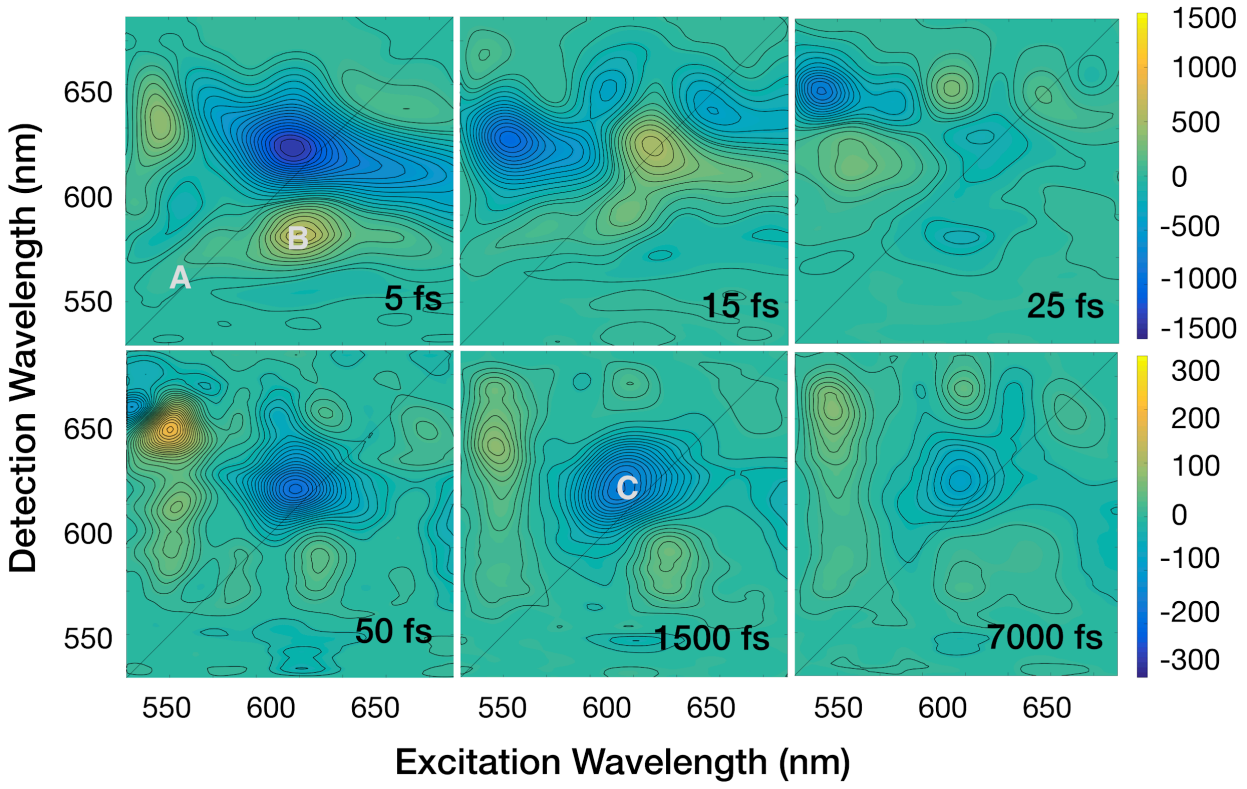

Figure 4.3. Phased absorptive 2DES spectra measured at room temperature (23 °C) at waiting times $T = 5$ fs to 7000 fs in preparations of the rPCP–Chl *b* complex. The amplitudes are plotted as evenly spaced contour lines, as tinted with a color bar ranging from yellow for positive signals (ground-state bleaching (GSB) and stimulated emission (SE)) to blue for negative (excited state absorption (ESA) and photoinduced absorption) signals. The intensity scaling for the $T > 50$ fs spectra (bottom row) is five times larger to reveal weaker features. The amplitude profile as a function of waiting time T for the marked coordinates A and B is plotted in Figure 4.4, whereas that for C is shown in Figure 4.5d.

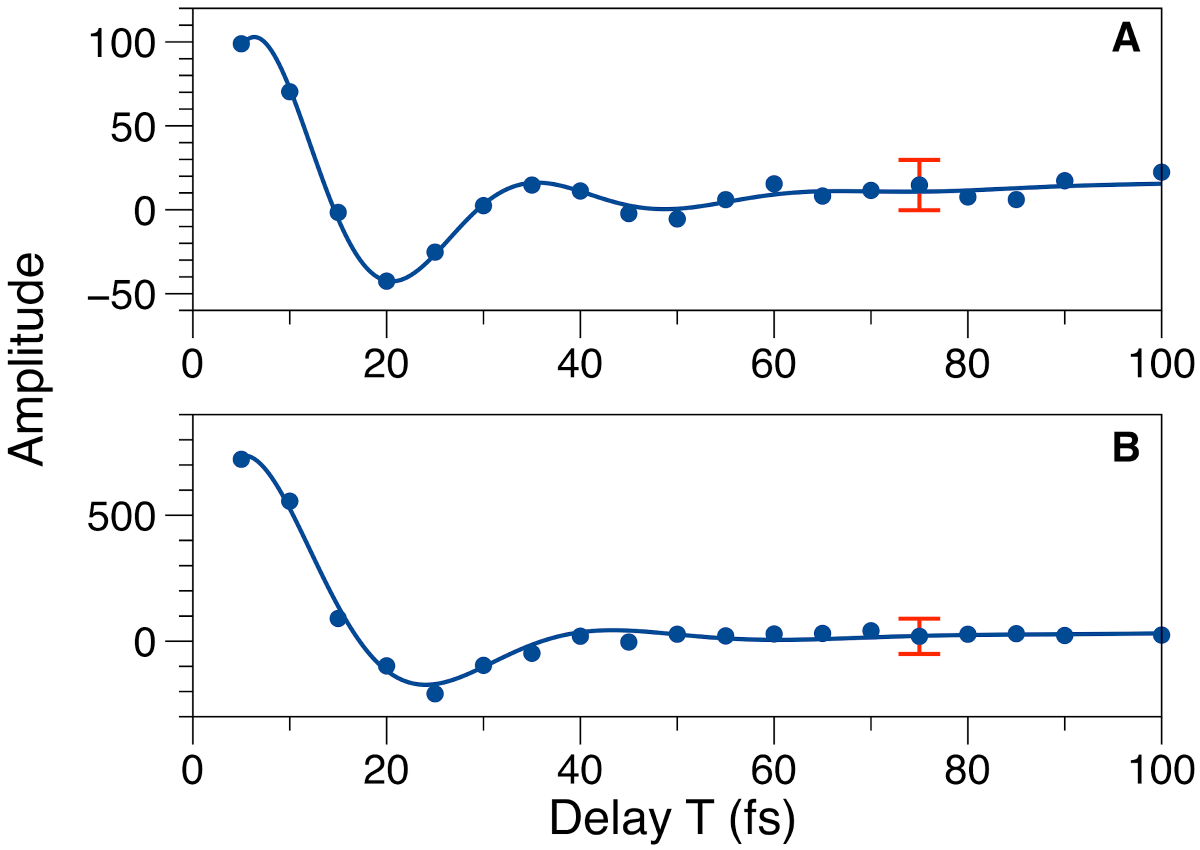

Figure 4.4. Detection of quantum beating at the coordinates marked A and B in the 2DES spectra from the rPCP–Chl *b* complex (Figure 4.3). (a) A: On-diagonal quantum beating between peridinins (1160 ± 30 cm^{-1} modulation frequency, 14 ± 1 fs damping time). (b) B: Off-diagonal quantum beating between Chl *b* (Q_x or Q_y ($v = 1$)) and peridinin (885 ± 41 cm^{-1} modulation frequency, 13 ± 1 fs damping time). The error bars report the estimated confidence intervals for the 2DES signal amplitudes. The plotted curves show fits to the sum of a fitted damped cosinusoid and an exponential decay; Tables A4.4 and A4.5 report the model parameters.

A direct spectroscopic measurement of quantum coherence, however, is obtained in the 2DES spectra from a broad band of excited-state absorption (ESA) transitions between singly and doubly excited exciton states.[49,50] These negative-going signals arise from excitation by the probe pulse of a second exciton in the peridinin–Chl cluster after the excitation pulse pair optically prepares population in a singly excited exciton level.[17] In Figure 4.3, this ESA band spans most of the $T = 5$ fs spectrum, but it has largely disappeared by the $T = 25$ fs spectrum. In the wtPCP–Chl *a* complexes, the doubly excited ESA signal was present until the $T = 50$ fs spectrum.[17] The lowest energy part of the doubly excited exciton manifold ($\lambda_{\mathrm{det}} > 600$ nm) mainly corresponds to excitation of a Chl exciton from any of the singly excited excitons. The doubly excited ESA signal overlaps extensively with positive-going, off-diagonal signals due to ground-state bleaching (GSB) transitions of the shared exciton ground state. The decay of the ESA amplitude integrated over the whole 2DES spectrum (Figure 4.5c) estimates the rate at which the doubly excited exciton manifold vanishes[17] owing to dynamic exciton localization, the decay of the collective excitation.[50] Additional amplitude traces from the 2DES spectra and analysis are presented in Figures A4.5-A4.9. The present results clearly indicate that quantum decoherence occurs more rapidly in the rPCP–Chl *b* complexes than in the wtPCP–Chl *a* complexes.

As summarized by Table 4.1, the present results establish that both measures of quantum coherence in the PCP complex decay faster in the presence of Chl *b*. The decay of the integral of the doubly excited ESA band, 12 ± 2 fs for Chl *a* vs. 10 ± 1 fs for Chl *b*, directly measures the rate of dynamic exciton localization. The damping time constants for the Chl–peridinin quantum beats, 24 ± 6 fs vs. 13 ± 1 fs, respectively, are longer than those for decay of the doubly excited

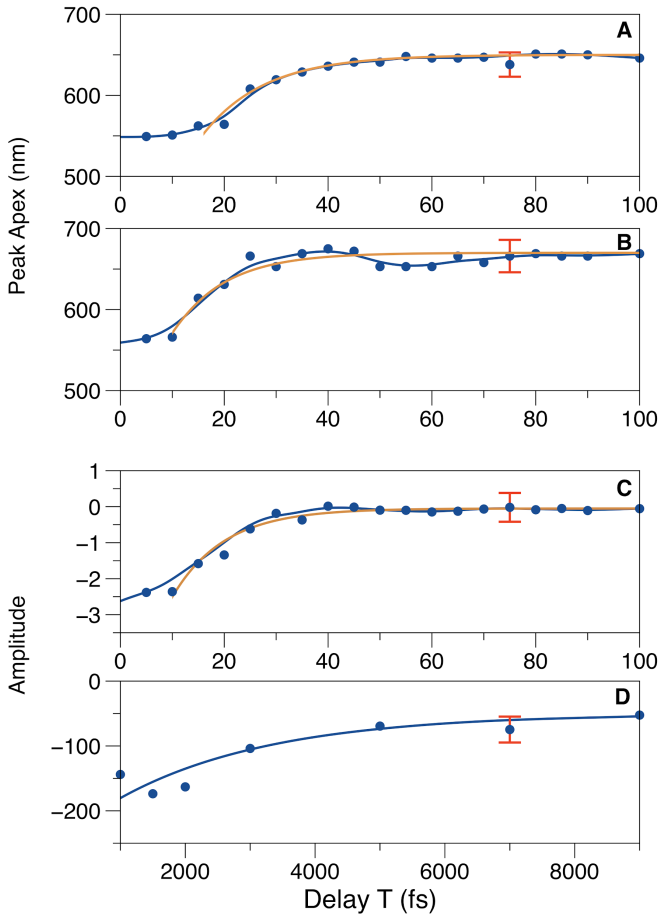

Figure 4.5. Determination of the rates of energy transfer and quantum decoherence using the 2DES spectra from the rPCP–Chl *b* complex (Figure 4.3). Relaxation of SE signals to the Chl *b* Q_y ($v = 0$) region of the detection axis: (a) at $\lambda_{ex} = 535$ nm and (b) at $\lambda_{ex} = 610$ nm. (c) Decay of the doubly excited ESA signal, as estimated from the total integral ($\times 10^{-6}$) of the 2DES signal. (d) Decay of the off-diagonal ESA cross peak assigned to the S_x state of localized peridinins, at $\lambda_{ex} = 595$ nm and $\lambda_{det} = 614$ nm (point C in Figure 4.3), over the $T > 1000$ fs range. The exponential curves plotted for (a–d) determine time constants of 14 ± 2 fs, 12 ± 2 fs, 10 ± 1 fs and 2.3 ± 0.5 ps, respectively; the model parameters are listed in Tables A4.6–A4.9. The plotted error bars report confidence intervals for the signal amplitudes. ESA in both cases. Note that the time constants compared here are as determined directly from the signal amplitudes in the 2DES spectra, without inclusion of compensation for the instrument response width. Because the optical conditions and excitation pulse widths are the same in both studies, the time constants can be directly compared.

Table 4.1. Comparison of time constants for decoherence and energy transfer in the PCP Chl *a*[17] and PCP Chl *b* complexes.

	PCP Chl *a*	**PCP Chl *b***
Quantum decoherence, determined by decay of the doubly excited exciton manifold[a]	12 ± 2 fs	10 ± 1 fs
Quantum decoherence, determined by damping of peridinin–peridinin quantum beats	24 ± 8 fs	14 ± 2 fs
Quantum decoherence, determined by damping of Chl–peridinin quantum beats	24 ± 6 fs	13 ± 1 fs
Exciton relaxation (coherent energy transfer) from peridinin to Chl Q_y	<10 fs[b]	12 ± 2 fs[c]
Decay of localized S_x state[d]	1.7 ± 0.4 ps	2.3 ± 0.5 ps

[a]Decay of the ESA signal integrated over the 2DES spectrum

[b]Rise of the SE peak amplitude at Q_y ($v = 0$)[17]

[c]Shift of the SE apex to Q_y (Figure 4.5b)

[d]Decay of the ESA cross peak from localized peridinins in the S_x state due to energy transfer to Chl and nonradiative decay to S_1[16]

The key and perhaps most surprising finding from the 2DES spectra, however, is that the rate of coherent energy transfer in PCP to Chl *b* is markedly slower than observed to Chl *a* under the same optical conditions. The energy transfer rate can be estimated in the 2DES spectra from the time evolution of stimulated emission (SE) signals, eventually moving from the diagonal to off-diagonal cross peaks in the Q_y region of the detection axis. Energy transfer in the wtPCP–Chl *a* complex is too fast to be resolved by the 8 fs pulses used in the experiment; a strong band of SE is already detected at Q_y ($v = 0$) fully across the excitation axis by $T = 15$ fs.[17] For the rPCP–Chl *b* complex, where the Q_y region partially overlaps with the doubly excited ESA band noted above, the progress of SE from the diagonal to the 650 nm region of the detection axis is slow enough to be followed temporally in terms of the apex of the net SE signal (the detection wavelength corresponding to the amplitude maximum of a slice of the 2DES signal).[51] As determined at two excitation wavelengths (Figure 4.5a,b), exciton relaxation to Q_y ($v = 0$) is essentially complete by $T = 30$ fs.

Incoherent energy transfer from localized peridinins to the Chl *a* or Chl *b* acceptors follows the decay of quantum coherence in PCP. A distinct band of ESA, assigned to transitions of the localized S_x state to a higher singlet state S_n,[29,30] is observed just above the diagonal of the 2DES spectrum at waiting times $T > 50$ fs. A corresponding feature is observed in the 2DES spectra from the wtPCP–Chl *a* complex.[17] It is resolved in these spectra in the long-wavelength tail of the mid-visible ground-state absorption spectrum, which arises from peridinins with distorted ground-state conformations.[26,39] Energy transfer from these localized peridinins to the Chl acceptor via the Förster mechanism is marked by the presence above the ESA cross peak from S_x of a SE cross peak in the Q_y ($v = 0$) region of the detection axis. In the 2DES spectra

from rPCP–Chl *b* samples, the rate of decay of the peridinin S_x ESA cross peak is 2.3 ± 0.5 ps (Figure 4.5d). A shorter time constant is observed in the wtPCP–Chl *a* samples, 1.7 ± 0.4 ps.[17] These time constants are determined by the rate of energy transfer to the Chl acceptor and the intrinsic rate of nonradiative decay from S_x to S_1 in the absence of a Chl acceptor but in the protein and peridinin-derived medium in the PCP complex. The presence of the residual S_1 state gives rise to a long-lived offset in the decay of the ESA cross peak. Assuming the S_x state exhibits a 4.4 ps intrinsic lifetime, the estimate we obtained previously from heterodyne transient grating measurements,[16] these time constants determine energy transfer time constants of 2.8 ps and 4.8 ps for the wtPCP–Chl *a* and rPCP–Chl *b* complexes, respectively. These energy transfer time constants are somewhat shorter than estimated previously[37] but have the expected trend.

4.4 Conclusions

The structural origin of the distinct energy transfer dynamics in the wtPCP–Chl *a* and rPCP–Chl *b* complexes in the coherent regime is the addition of the formyl group on the chlorophyll macrocycle that accompanies reconstitution with Chl *b* (Figures A4.10–A4.16). Its electron-withdrawing character polarizes the π-electron density of the Chl macrocycle and increases the permanent dipole moment.[52] The result is an increase in the strength of coupling to the electrostatic noise in the surroundings of the peridinin–Chl cluster, which arises mainly from the fast librational motions of the surrounding water molecules.[53,54] Even though Chls usually exhibit weak couplings to the surrounding bath, the addition of the formyl group to Chl *b* is apparently enough to shorten the decoherence timescale. These changes arise principally from an increase in the coupling strength to fast molecular motions in the surrounding bath, not from changes in their frequencies or character of motion.

The finding that shortening the decoherence timescale slows the rate of coherent energy transfer in the rPCP–Chl *b* complex represents a significant demonstration of the impact of structural features that maintain state correlation.[55] This factor is apparently more important in determining the rate of coherent energy transfer than the donor–acceptor energy gap or the vibronic coupling. The mechanism involves passage of an electronic wavepacket between the potential surfaces of the donor and acceptor excitons through a conical intersection.[17,56] Imperfect correlation of the two potential surfaces raises a fluctuating barrier,[13,57] which frictionally broadens the electronic wavepacket and slows its progress to the product surface.

The results also suggest a new perspective about the importance of quantum coherence in photosynthetic light harvesting. Even though the relevant timescales are very short indeed, certainly <100 fs, as determined here and in recent work on the Fenna–Matthews–Olson bacteriochlorophyll *a* complex,[58] the extraordinarily fast energy transfer rates that are possible in the coherent regime between strongly coupled chromophores will favor unidirectionality in the excitation transfer pathways towards the lowest-energy chromophores in a light-harvesting complex and overall to the primary electron donor in the associated reaction center.[59,60] Further, a light-harvesting system can alter the efficiency of excitation transfer in response to changes in incident light intensity or other environmental changes merely by varying the coupling of its chromophores to the surroundings, for example through a conformational change that modulates the exposure to the surrounding solvent, so that the rate of quantum decoherence increases. This hypothesis potentially connects mechanisms for nonphotochemical quenching[61] to a branching between coherent and incoherent mechanisms of excitation transfer, as mediated by structurally tuning the rate of quantum decoherence.

APPENDIX

APPENDIX

Additional experimental details, laser intensity and residual optical phase spectra, phasing of 2DES spectra, model parameters and intensity analysis of additional points of interest in PCP 2DES spectra, and 2DES spectra from peridinin samples in methanol solution are all presented in the appendix.

A4.1 Experimental Details for 2DES Measurements

The 2DES spectrometer and femtosecond laser system used in the present experiments were as described in detail in the previous work on the wild-type PCP preparations containing Chl *a* (wtPCP–Chl *a*).[17] A noncollinear optical parametric amplifier (NOPA, Spectra-Physics Spirit-NOPA-3H) was pumped by a amplified Yb laser (Spectra-Physics Spirit-4W, 400 fs pulses at 1.04 μm, with 4 W average power at a 100 kHz repetition rate) to generate an output spectrum centered at 600 nm (100 nm FWHM) and spanning the 520-690 nm range baseline to baseline. The NOPA's signal output beam was partially compressed temporally by the on-board pair of Brewster prisms and then split into pump and probe beams, which were then independently processed by a pair of adaptive pulse shapers (FemtoJock and FemtoJock P, respectively, Biophotonic Solutions Inc.). With a β-barium borate second-harmonic generation crystal mounted at the sample position in the 2DES spectrometer, the excitation pulses were compressed to durations of 8 fs by running the multiphoton intrapulse interference phase scan procedure (MIIPS)[62] sequentially on both pulse shapers. The residual optical phase (Figures A4.3 and A4.4) is close to zero over the entire spectral bandwidth, which indicates that nearly transform limited pulses were obtained for both the pump and probe pulses.

The 2DES signals were recorded using a diffractive-optic based, passively phase-

stabilized photon echo spectrometer based on the design of Brixner et al.[48] and Moran and Scherer.[63] Time delays between the three excitation pulses and the local oscillator pulse were calibrated using spectral interferometry. 2DES spectra were acquired by scanning the coherence time τ between the first two pulses from −30 fs to +30 fs with 0.5 fs steps with a fixed waiting time T maintained between the second and third pulses by translating wedge-shaped fused silica prisms across the pump beams. The spectra are presented as relaxation spectra (the sum of the rephasing and nonrephasing signals). Control experiments showed that the 2DES signal amplitude with the 8 fs pulses used here goes to zero in less than ±25 fs. Spectra acquired with longer τ scans than ±30 fs exhibited the same signal content and line shapes but a decreased signal/noise ratio. The waiting time T between the second excitation pulse and the third (probe) pulse was controlled by a conventional time-of-flight delay line equipped with a retroreflector mounted on a translation stage, which was scanned to a maximum of 9 ps in these experiments. The excitation pulses were attenuated to energies of <5 nJ with a fused silica neutral density filter. The local oscillator pulse was attenuated further by 4.0 OD using a fused silica neutral density filter and set to arrive 250 fs prior to the probe pulse. The excitation and local oscillator pulses were cofocused to a beam waist of 100 μm at the sample position by a spherical mirror with a 20 cm focal length using the forward boxcars configuration. Spectral interferograms between the local oscillator and the emitted third-order signal were detected using a compact spectrograph/CCD detector (Ocean Optics Flame-T, 450-700 nm, 3500 pixels, 0.1 nm bandpass). Scattered light was subtracted using a beam-shuttering protocol.[48] The isolated 2DES signal was then processed and phased using an algorithm to separate the real (absorptive) and imaginary (dispersive) components.[64]

As shown below (Figures A4.17-A4.22), phasing of the 2DES spectra was performed using the projection slice theorem in comparison to pump–probe spectra, which were measured using the same excitation beams and optical geometry used for the 2DES spectra with one of the pump beams and the local oscillator beam blocked. Because the Ocean-Optics spectrograph/ CCD detector did not have sufficient dynamic range and sensitivity to detect the $<1 \times 10^{-3}$ pump-induced transmission changes observed under the experimental conditions used in the 2DES spectra, the pump–probe spectra were acquired using a phase-sensitive detection scheme. The pump and probe beams were modulated using mechanical chopper with a dual-slot blade at 700 and 1000 Hz, respectively. The transmitted probe beam was isolated and directed to a separate monochromator; the probe intensity was then detected at the sum of the modulation frequencies using a silicon photodiode and a lock-in amplifier. The pump–probe spectra measured at a given waiting time T were accordingly sampled at different probe wavelengths than returned by the CCD detector used to acquire the 2DES spectra, but the same probe wavelength range was covered.

A4.2 Structure of the Chromophore Cluster in rPCP–Chl b

An alignment of the chromophore cluster from wild type PCP with Chl *a* (wtPCP–Chl *a*) with that from reconstituted PCP with Chl *b* (rPCP–Chl *b*) is shown in Figure A4.2. The two clusters are nearly isostructural with the exception of the formyl substituent on the Chl *b* macrocycle, which is oriented away from the other chromophores.

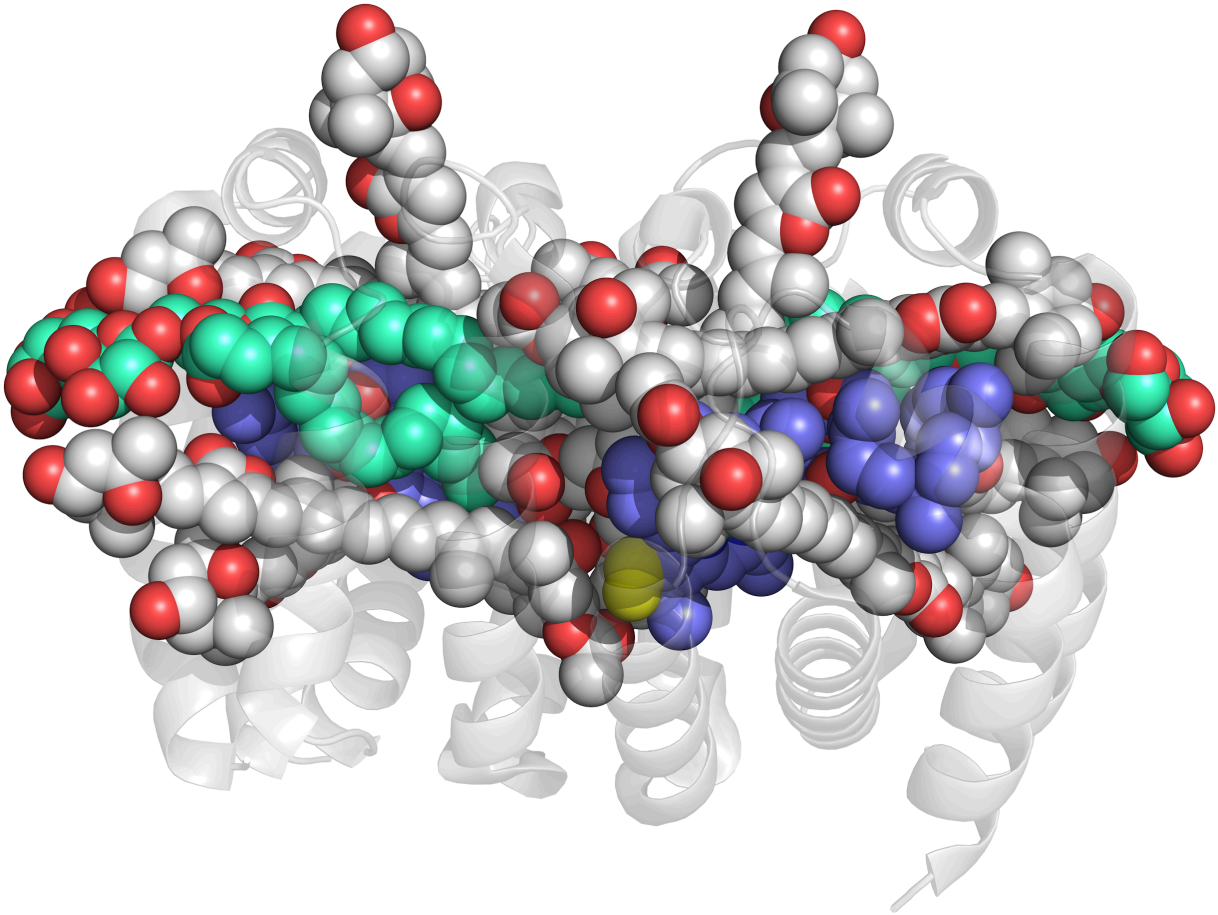

Figure A4.1. Side view of the rPCP–Chl *b* complex (PDB structure 2X20[34]) with the C_2 symmetry axis oriented vertically. Within the basket of α helices is the cluster of eight peridinins (carbon atoms, gray; oxygen atoms, red), two chlorophyll (Chl) *b* (carbon atoms, blue; oxygen atoms, red; Mg^{II} ions, green), and two digalactosyldiacylglycerol molecules (carbon atoms, light green; oxygen atoms, red). The formyl oxygen on the Chl *b* macrocycle is rendered in yellow.

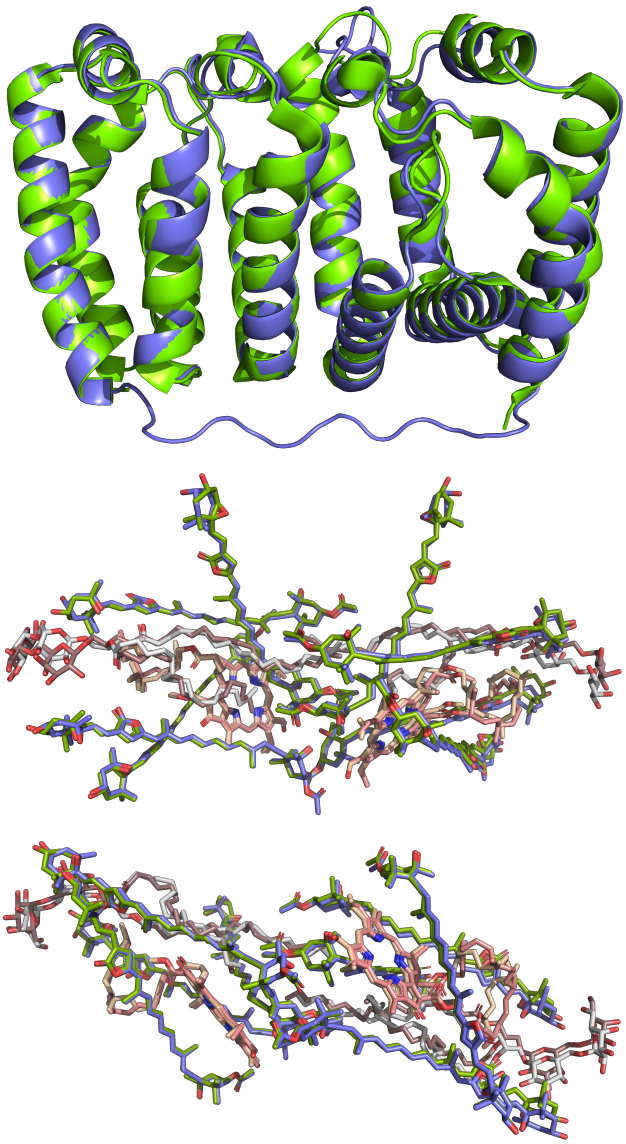

Figure A4.2. Structural alignment of the PCP residues and chromophore clusters for wtPCP–Chl *a* (PDB structure 1PPR[15]) and rPCP–Chl *b* (PDB structure 2X20[34]). *Top*: Polypeptide backbone in a ribbon representation with the C_2 symmetry axis pointing vertically, as in Figure A4.1: wtPCP–Chl *a* (blue) and rPCP–Chl *b* (green). *Middle*: Chromophore cluster with the C_2 symmetry axis pointing vertically, as in Figure A4.1. *Bottom*: Chromophore cluster viewed along the C_2 symmetry axis, as in Figure 4.1. In the bottom two panels: for the wtPCP–Chl *a* complex, the peridinins, Chl *a*, and lipids are colored blue, light red, and white, respectively; for rPCP–Chl *b*, the peridinins, Chl *b*, and lipids are colored green, light yellow, and brown, respectively.

A4.3 Site Energies and Resonance Raman-Active Vibrations

Table A4.1. Site energies used for the peridinin energy levels in the PCP cluster in Figure 4.2.

Level	Peridinin Site	Energy (cm^{-1})
1	Per614	20533
2	Per611	20661
3	Per613	21052
4	Per612	22123

The peridinin site energies were determined in an electronic structure calculation by Guberman-Pfeffer et al.[19]

Table A4.2. Site energies used for chlorophyll *a* and *b* in Figure 4.2.

State	Chl *a* Site Energy (cm^{-1})	Chl *b* Site Energy (cm^{-1})
$B_{x,y}$	22883	21763
Q_x	16077	16667
Q_y	14981	15492

The site energies for $B_{x,y}$ and Q_y were reported by Ilagan et al.[45]

Table A4.3. Resonance Raman-active vibrational frequencies used for the vibrational energy levels (solid and dashed black) in Figure 4.2.

Peridinin	Chlorophyll *a*	Chlorophyll *b*
1524 cm^{-1}	1555 cm^{-1}	1437 cm^{-1}
1181 cm^{-1}	1288 cm^{-1}	1350 cm^{-1}
1144 cm^{-1}	1187 cm^{-1}	757 cm^{-1}
--	--	745 cm^{-1}
--	--	301 cm^{-1}

The Raman frequencies for peridinin were reported by Honsell et al.[65] Only the three most intense features were included in Figure 4.2. The Raman frequencies for Chl *a* and *b* in acetone were reported by Lutz.[46] Figure 4.2 includes only the features labelled *strong*. In acetone solvent, the Mg^{II} ions in Chls are five coordinate, with a single acetone coordinated as an axial ligand;[66] in the PCP structures, the Mg^{II} ions in the Chls are five coordinate, with a single water axial ligand.[15]

A4.5 Laser Intensity and Residual Optical Phase Spectra for rPCP–Chl b 2DES

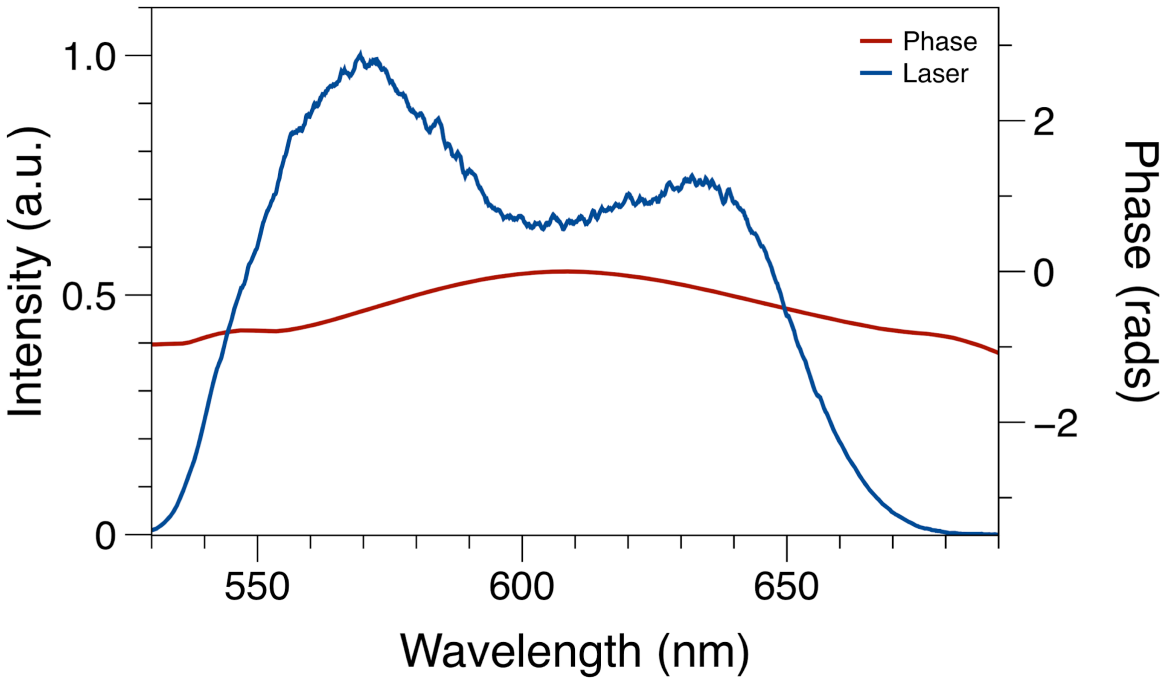

Figure A4.3. NOPA output spectrum (blue) for the probe pulses used in the 2DES experiments with rPCP–Chl *b* preparations. Superimposed is the residual optical phase, as determined by a MIIPS scan.

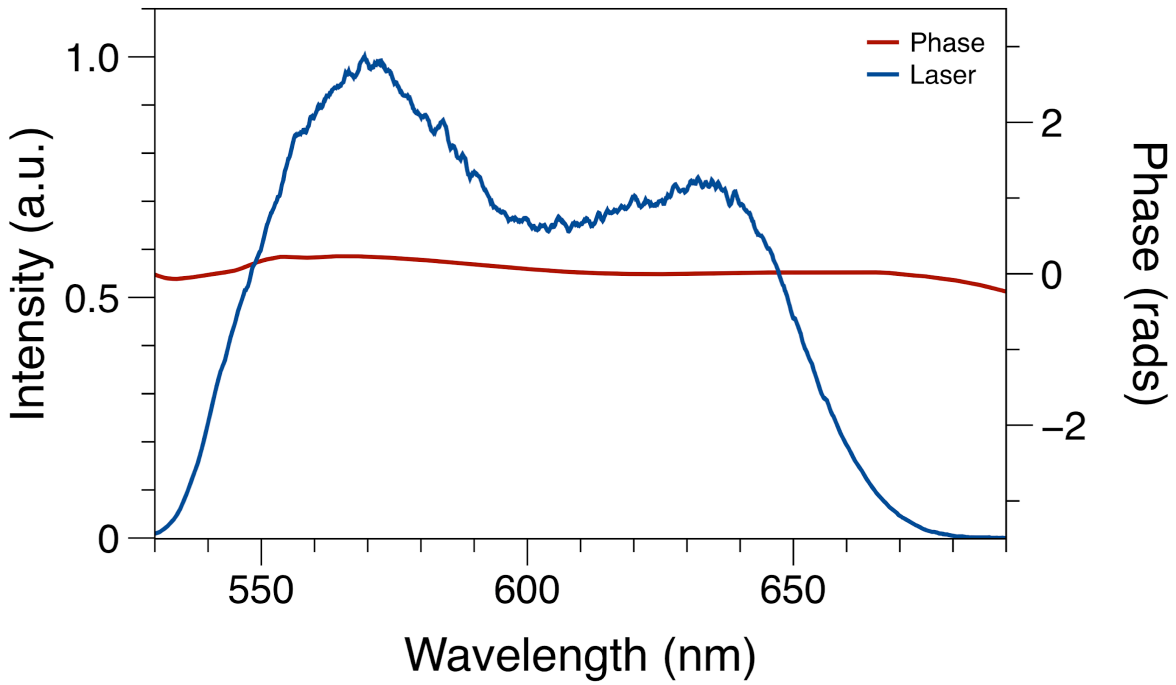

Figure A4.4. NOPA output spectrum (blue) for the pump pulses used in the 2DES experiments with rPCP–Chl *b* preparations. Superimposed is the residual optical phase, as determined by a MIIPS scan.

A4.6 Amplitude Analysis of 2DES Spectra from rPCP–Chl b

Figure 4.4 reports analysis of the quantum beating observed at the marked coordinates A and B in the 2DES spectra from the rPCP–Chl *b* complex (Figure 4.3). Tables A4.4 and A4.5 present the full models for Figure 4.4a and Figure 4.4b, respectively. Tables A4.6 through A4.9 show the full model for Figure 4.5a–d, respectively. The modulated signals were modeled using linear-prediction, singular-value decomposition (LPSVD) to obtain initial estimates for the parameters for the principal components (exponentials and cosinusoids). The model parameters for the significant principal components were then refined using nonlinear least-squares methods, which return the indicated confidence intervals.

Figures A4.5–A4.9 present amplitude profiles and models for additional coordinates in the 2DES spectra. A brief discussion is in the caption each of these figures.

Table A4.4. Model parameters for Figure 4.4, Panel A: amplitude transient at $\lambda_{ex} = 538$ nm and $\lambda_{det} = 550$ nm.

Amplitude	Frequency (cm^{-1})	Damping Time (fs)	Phase (°)
-40 ± 4	—	98 ± 20	—
182 ± 18	1160 ± 33	14 ± 1	-96 ± 6
30	(non-decaying offset)		

Table A4.5. Model parameters for Figure 4.4, Panel B: amplitude transient at $\lambda_{ex} = 602$ nm and $\lambda_{det} = 565$ nm.

Amplitude	Frequency (cm^{-1})	Damping Time (fs)	Phase (°)
-320 ± 143	—	621 ± 151	—
1261 ± 92	885 ± 41	13 ± 1	-76 ± 7
304	(non-decaying offset)		

Table A4.6. Model parameters for Figure 4.5, Panel A: relaxation of SE signals to the Chl *b* Q_y ($v = 0$) region of the detection axis at $\lambda_{ex} = 535$ nm.

Amplitude	Damping Time (fs)	Offset
-283 ± 49	14 ± 2	649 ± 3

Table A4.7. Model parameters for Figure 4.5, Panel B: relaxation of SE signals to the Chl *b* Q_y ($v = 0$) region of the detection axis at $\lambda_{ex} = 610$ nm.

Amplitude	Damping Time (fs)	Offset
-178 ± 25	12 ± 2	666 ± 4

Table A4.8. Model parameters for Figure 4.5, Panel C: the decay of the doubly excited ESA signal, as estimated from the total integral of the 2DES signal.

Amplitude	Damping Time (fs)	Offset
$(-6.5 \pm 0.7) \times 10^6$	10 ± 1	$(-5.3 \pm 3) \times 10^4$

Table A4.9. Model parameters for Figure 4.5, Panel D: decay of the ESA cross peak at $\lambda_{ex} = 595$ nm and $\lambda_{det} = 614$ nm.

Amplitude	Damping Time (ps)	Offset
-254 ± 80	2.3 ± 0.5	-53 ± 22

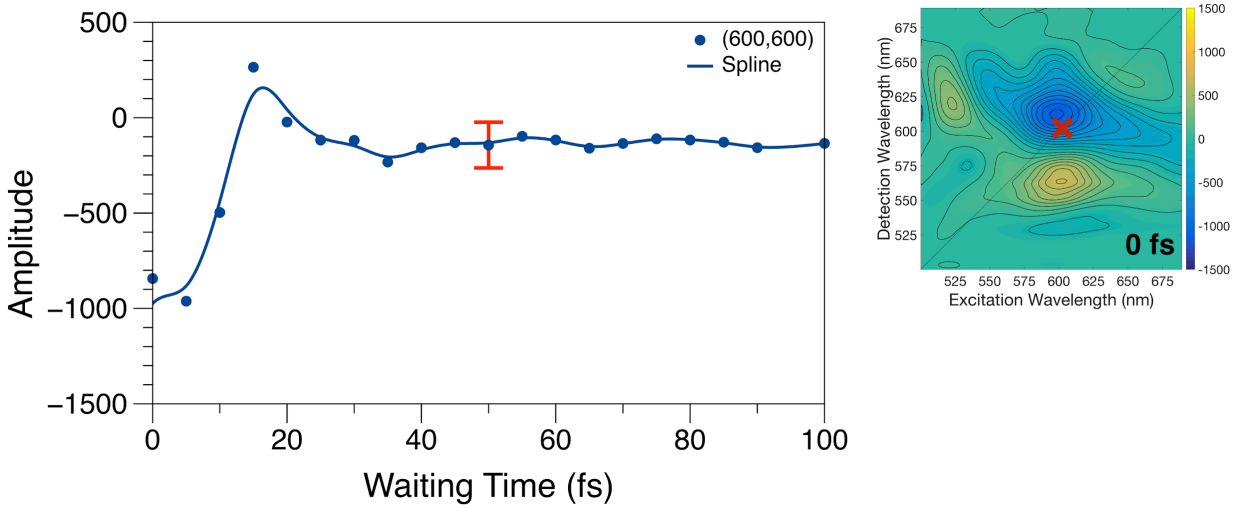

Figure A4.5. Amplitude of the on-diagonal Chl Q_x–peridinin coherence peak for $\lambda_{ex} = 600$ nm, $\lambda_{det} = 600$ nm, as marked in the $T = 0$ fs spectrum. The trend is superimposed with a cubic spline curve to connect the points. In Figure A4.5, the amplitude at $T = 0$ fs at the marked coordinate mainly reports the doubly excited excited-state absorption (ESA) character that is present instantaneously after optical preparation of peridinin excitons in the long-wavelength onset of the mid-visible absorption band. Also excited in this region are Chl excitons in the overlapping Q_x or Q_y ($v = 1$) region. The ESA transitions mark excitation principally to the Chl region of the doubly excited exciton manifold. The prompt rise in the amplitude is a result of evolution of the stimulated emission (SE) that accompanies relaxation of excitons to the Chl Q_x or Q_y ($v = 1$) state. As the excitons relax further to reach the Chl Q_y ($v = 0$) state, the signal decays. During the exciton relaxation process, the doubly excited ESA background vanishes, revealing a weaker ESA signal principally from localized peridinins that decays further over the ps timescale associated with Förster energy transfer to Chl *b*.

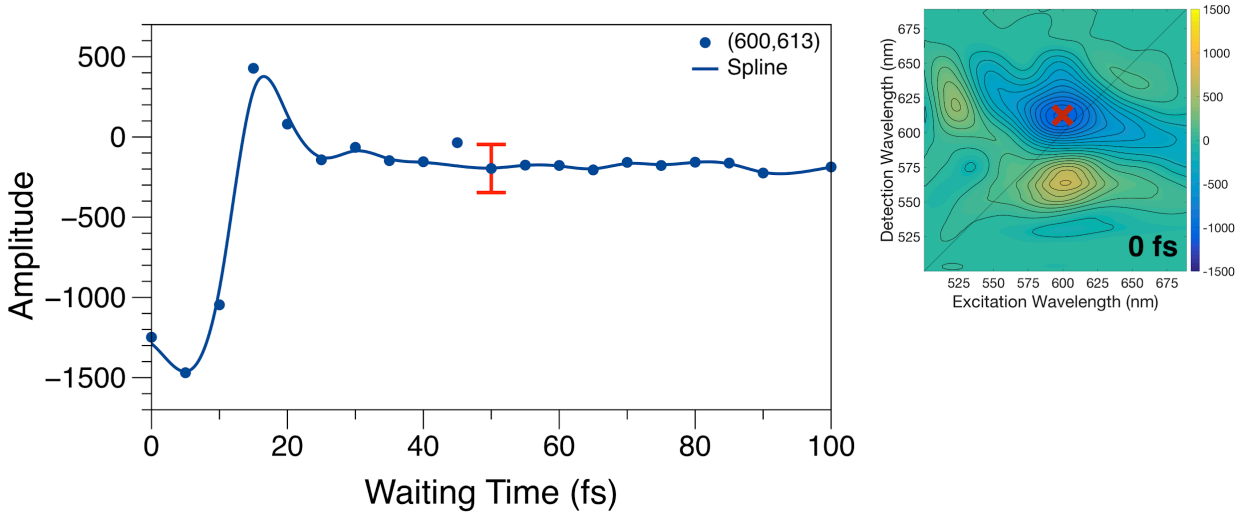

Figure A4.6. Amplitude of the off-diagonal Chl Qx-peridinin coherence peak for $\lambda_{ex} = 600$ nm, $\lambda_{det} = 613$ nm, as marked in the $T = 0$ fs spectrum. The trend is superimposed with a cubic spline curve to connect the points. The response plotted in Figure A4.6 exhibits the same signal contributions discussed above for Figure A4.5. The positive going signal at $T = 20$ fs is due to the SE emission signal relaxing vertically along the detection axis as the excitons move towards Q_y ($v = 0$).

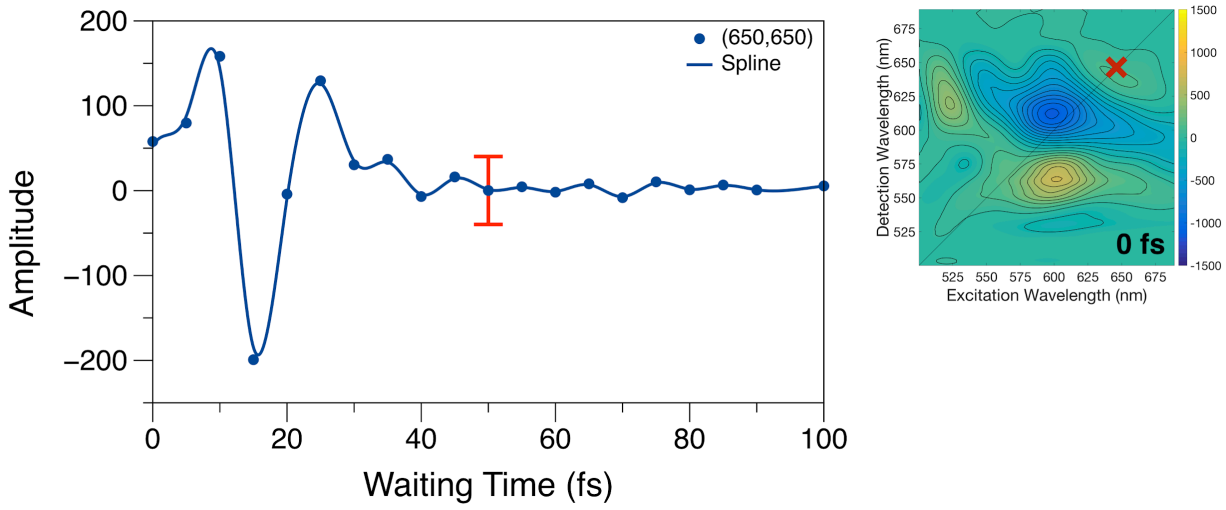

Figure A4.7. Amplitude of the on-diagonal Chl Q_y amplitude at $\lambda_{ex} = 650$ nm, $\lambda_{det} = 650$ nm, as marked in the $T = 0$ fs spectrum. The trend is superimposed with a cubic spline curve to connect the points. The signal amplitude at the marked coordinate in Figure A4.7 initially arises from the ground state bleach (GSB) and SE from the Chl Q_y state. The negative going peak that follows reports the growth of the doubly excited ESA signal discussed above. Decoherence results in loss of the doubly excited ESA signal, revealing again the net positive signal. The signal decays as the Chl Q_y exciton relaxes further to longer wavelengths and as localization occurs.

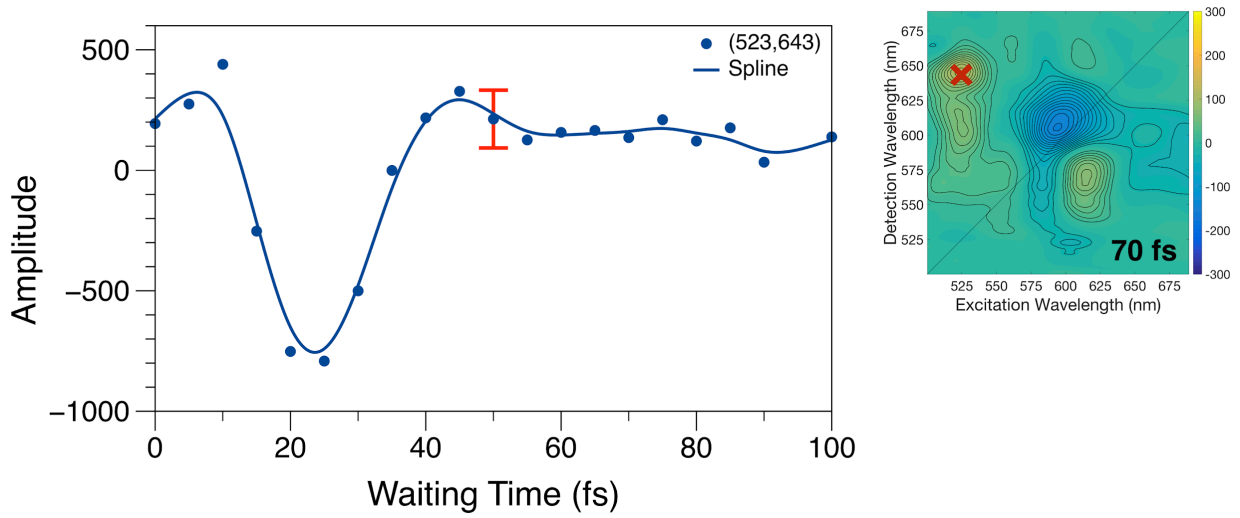

Figure A4.8. Amplitude of the off-diagonal cross peak at $\lambda_{ex} = 523$ nm, $\lambda_{det} = 643$ nm, as marked in the $T = 70$ fs spectrum. The trend is superimposed with a cubic spline curve to connect the points. The signal amplitude at this coordinate initially reports ground-state bleaching of the Chl Q_y region of the detection axis. Due to mixing of the peridinin and Chl sites, the peridinins and Chls share the same ground state, which is depleted upon optical excitation in the peridinin region of the spectrum. The doubly excited ESA signal discussed above, arising here from peridinin excitons making absorption transitions to the Chl region of the doubly excited exciton manifold, dominates over the GSB spectrum at longer waiting times T. As the peridinin excitons relax by populating Q_x and Q_y ($v = 1$) prior to reaching the Q_y ($v = 0$) region of the detection axis, the signal at the marked coordinate again increases. At the same time, decoherence contributes to disappearance of the doubly excited ESA character.

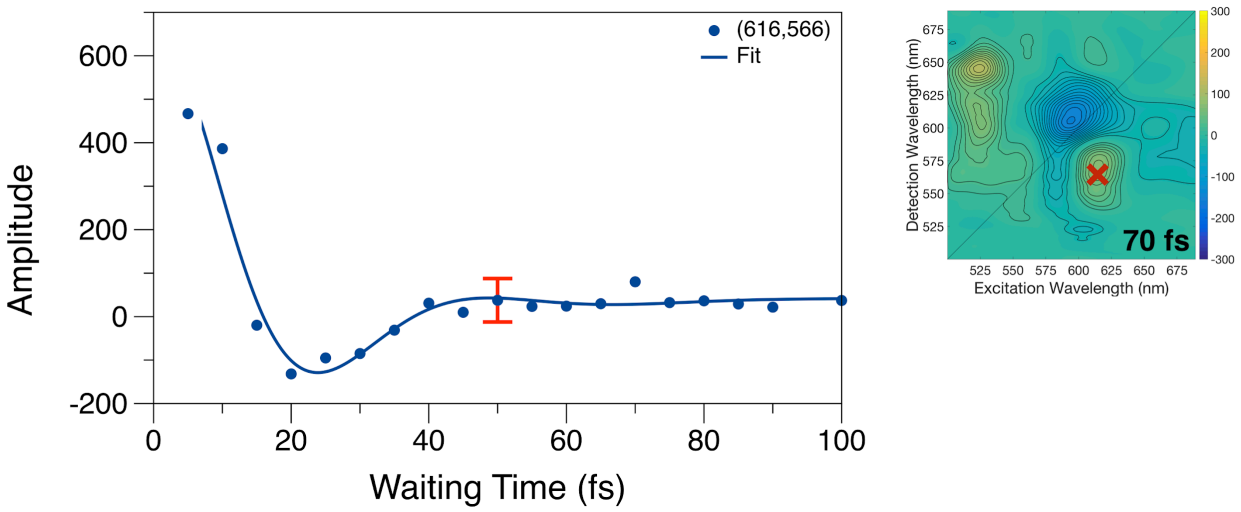

Figure A4.9. Intensity of the off-diagonal cross peak at $\lambda_{ex} = 616$ nm, $\lambda_{det} = 566$ nm, as marked in the $T = 70$ fs spectrum. The model parameters are reported in Table A4.10. The initial amplitude at the marked position includes contributions from the GSB and SE signals on the diagonal from optically prepared Chl excitons. The SE contribution decays rapidly as the excitons relax to the Q_y region on the detection axis. As the SE signal decays, it reveals an oscillatory character due to quantum beating between Chl and peridinin excitons.

Table A4.10. Fit parameters for the model plotted in Figure A4.9.

Amplitude	Frequency (cm^{-1})	Damping Time (fs)	Phase (°)
-105 ± 180	—	35 ± 129	—
836 ± 369	730 ± 83	14 ± 5	-40 ± 11
47 ± 80	(non-decaying offset)		

A4.7 Structural Comparison of wtPCP–Chl a, rPCP–Chl a, and rPCP–Chl b

A comparison of the structures of the reconstituted complexes (rPCP–Chl *a* and rPCP–Chl *b*) was reported previously,[34] but a comparison with the wild type (wtPCP–Chl *a*) complex has not appeared. The following analysis establishes that the electrostatic environment is not changed significantly and the structures of the bound chromophore clusters are not affected at all, within the resolution of the X-ray diffraction models,[15,67] by substitution of the N-terminal domain polypeptide used in the reconstituted complexes.

The structures of the rPCP complexes[34] differ from that of the wtPCP–Chl *a* complex because they incorporate two copies of a N-terminal domain apoprotein fragment, each of which associates with one of the two domains of the chromophore cluster, instead of the full length apoprotein.[36] The alignment of the amino acid sequences of the N-terminal domain apoprotein fragment and the wild-type full length apoprotein[68] is discussed in Figures A4.10–A4.13. Structural alignment of the wtPCP–Chl *a* structure with those of rPCP–Chl *a* and rCP–Chl *b* yields completely overlapping structures in 3D, and as shown above (Figure A4.2) the enclosed peridinin–Chl cluster with the two lipids is almost completely isostructural.

Figures A4.10 and S11 determine the impact of replacing the full-length PCP apoprotein (linked N-terminal and C-terminal domains) with the N-terminal domain apoprotein used in reconstituted preparations[69,37] by comparing aligned amino-acid sequences. The sequences were aligned with Jalview (http://jalview.org), which was also used to prepare the sequence graphics shown in the figures. Figures A4.12 and A4.13 show the alignments of the wtPCP–Chl *a* and rPCP–Chl *a* structures and of the rPCP–Chl *a* and rPCP–Chl *b* structures, respectively, so that changes in secondary structure of the folded polypeptide domains can be discerned. Figures

A4.12 and A4.13 also show explicit alignment of the chromophore clusters for the wtPCP–Chl *a* and rPCP–Chl *a* structures and for the rPCP–Chl *a* and rPCP–Chl *b* structures. The wtPCP–Chl *a* and rPCP–Chl *b* structures were compared in Figure A4.2, above.

The main difference between the C-terminal amino-acid sequence and that of the N-terminal domain apoprotein is the absence in the reconstituted complexes of the leading linker sequence starting at position 150, which connects the N- and C-terminal domains in the wild-type complex. After the linker sequence, there are a number of differences, but most of them are closer to the peridinins. The peridinin region of the PCP absorption spectrum in the reconstituted complexes is not shifted, however, from that of wild-type complex. It is important to note that the α helix that is closest to Chl is unchanged when the C-terminal is replaced with the N-terminal domain apoprotein (amino acids 23-36). There are, however, four point changes in the vicinity of Chl indicated in Figure A4.14. The closest change, at a distance of ~11 Å, is Ala250 to serine, which introduces a polar side chain. Next, at a distance of 14 Å away, Asn220 is replaced by lysine, removing a polar amino acid and introducing a charged side chain. About 18 Å away, Asp238 is replaced by asparagine, and here a charged side chain is replaced by a polar side chain. Lastly, at about 24 Å away, Lys194 is replaced by glutamine, again losing a charge and gaining a polar side chain. These changes in the electrostatic environment provided by the apoprotein are relatively remote from the Chls and are not expected to change the bath spectral density at the high frequencies that contribute mainly to the changes in decoherence times.

Two amino acid substitutions near the chromophore cluster might at first glance be expected to result in significant changes to the electrostatic environment. As shown in Figure A4.15, the substitution of Ser204 with Ala changes only the interaction with the end ring on

peridinin Per611, which is not in conjugation with the polyene backbone. As noted above, however, the peridinin region of the absorption spectrum is not shifted in the rPCP complexes. The substitution of Tyr248 with Trp changes the interaction with the phytol tail of Chl (Figure A4.16), which also is not in conjugation.

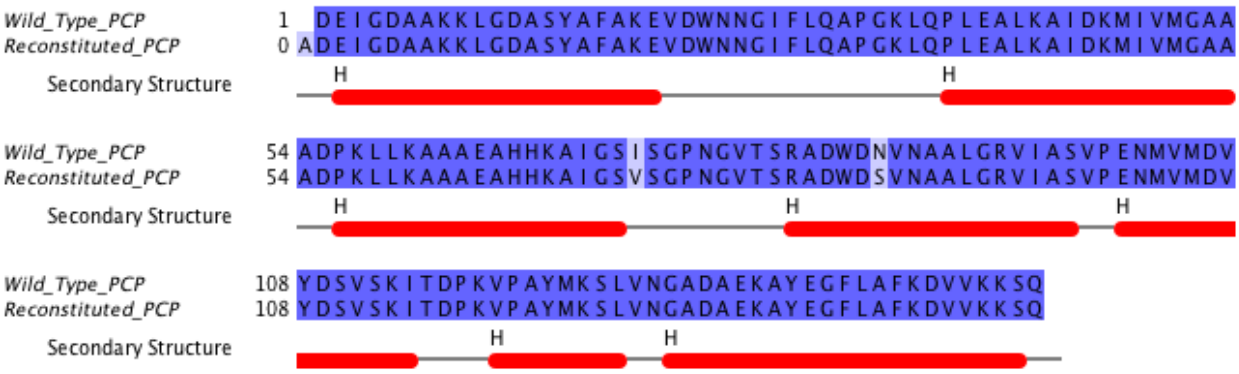

Figure A4.10. Alignment of the N-terminal amino-acid sequence of PCP apoproteins and associated secondary structure, with α helical sequences marked in red. The sequence marked Wild_Type_PCP (top row) reports the sequence of the full-length apoprotein from *Amphidinium carterae* (PDB structure 1PPR[15]). The sequence marked Reconstituted_PCP reports the sequence from the N-terminal apoprotein (PDB structure 2X20[34]). Differences in the two sequences are marked in a lighter color: at amino acid 74, valine replaces the isoleucine residue; at amino acid 88, serine replaces asparagine.

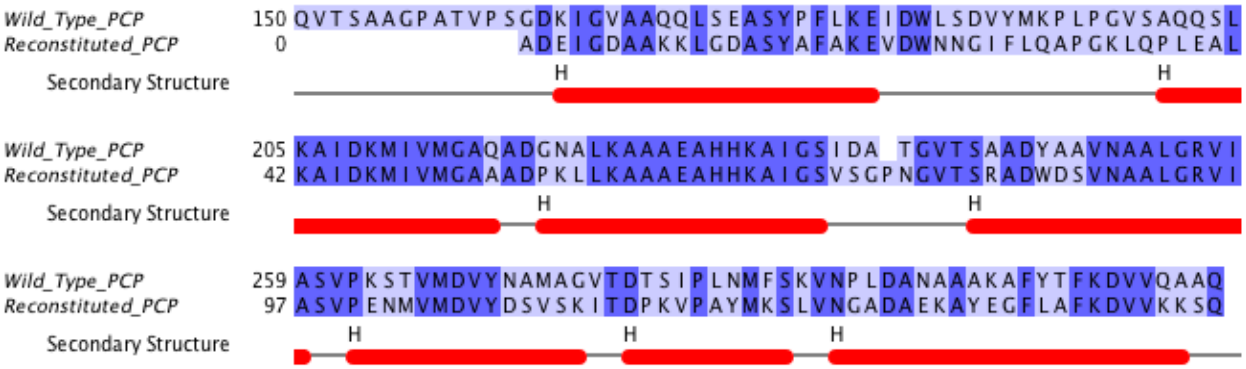

Figure A4.11. Alignment of the C-terminal amino-acid sequence of the full-length PCP apoproteins with the N-terminal domain apoprotein used in the rPCP–Chl *b* preparation and associated secondary structure. The sequence marked Wild_type_PCP (top row) reports the sequence of the full-length apoprotein from *Amphidinium carterae* (PDB structure 1PPR[15]). The sequence marked Reconstituted_PCP reports the sequence from the N-terminal apoprotein (PDB structure 2X20[34]). Differences in the two sequences are marked in a lighter color.

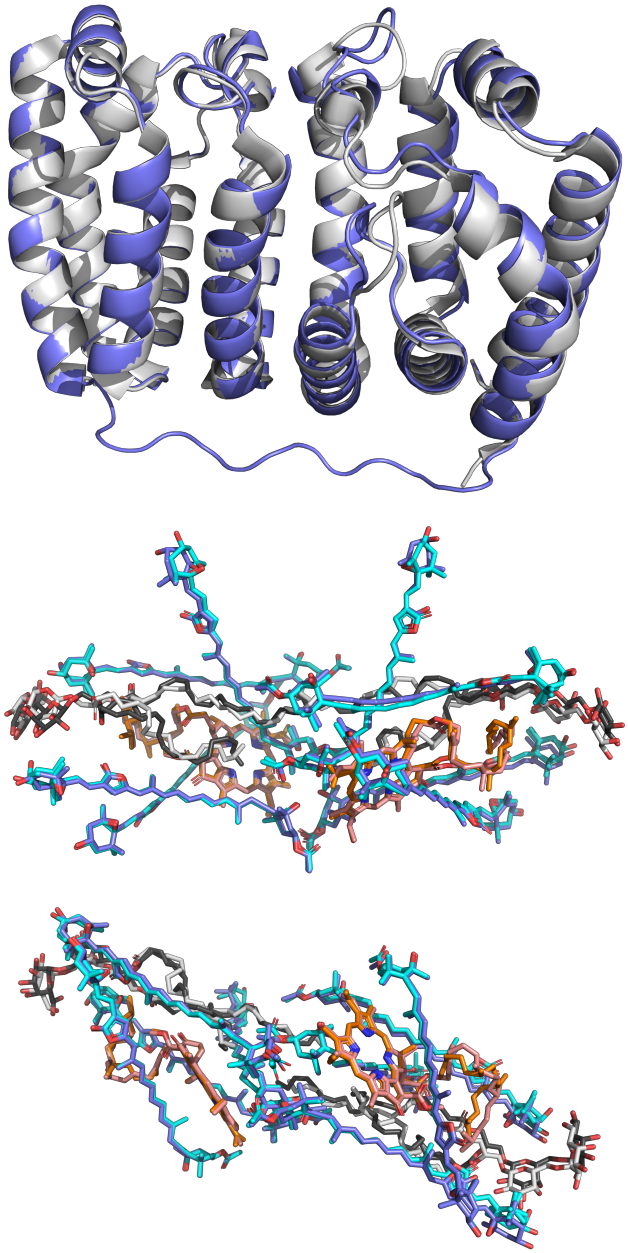

Figure A4.12. Structural alignment of the PCP residues and chromophore clusters for wtPCP–Chl *a* (PDB structure 1PPR[15]) and rPCP–Chl *a* (PDB structure 3IIS[67]). *Top*: Polypeptide backbone in a ribbon representation with the C_2 symmetry axis pointing vertically, as in Figure A4.1: wtPCP–Chl *a* (blue) and rPCP–Chl *a* (white). *Middle*: Chromophore cluster with the C_2 symmetry axis pointing vertically, as in Figure A4.1. *Bottom*: Chromophore cluster viewed along the C_2 symmetry axis, as in Figure 4.1. In the bottom two panels: for the wtPCP–Chl *a* complex, the peridinins, Chl *a*, and lipids are colored blue, light red, and white, respectively; for rPCP–Chl *a*, the peridinins, Chl *b*, and lipids are colored light blue, orange, and black, respectively.

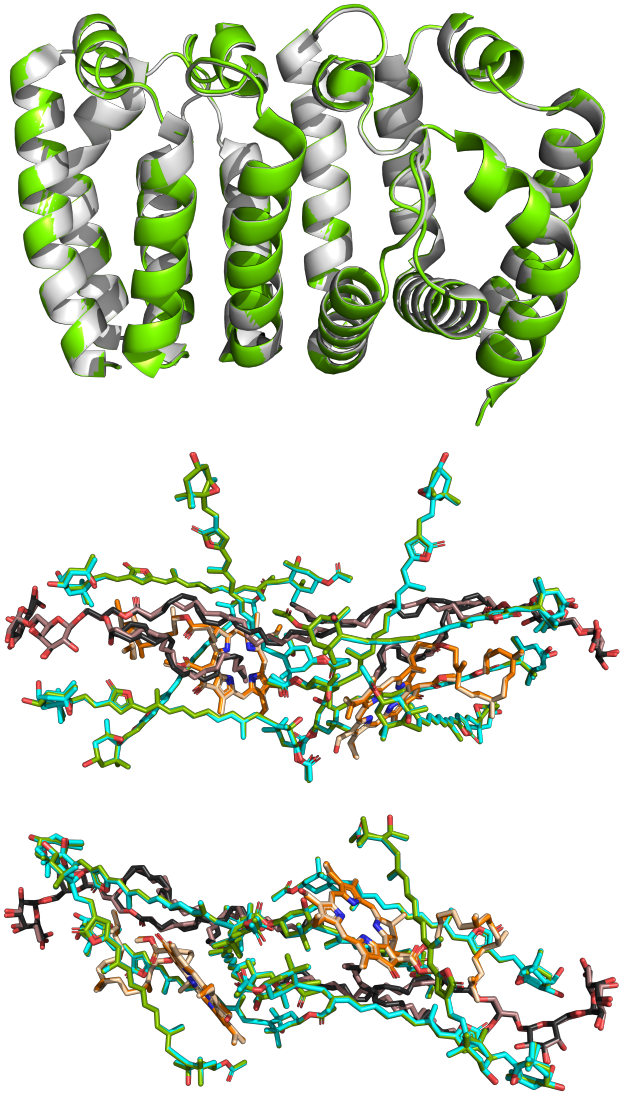

Figure A4.13. Structural alignment of the PCP residues and chromophore clusters for rPCP–Chl *a* (PDB structure 3IIS[67]) and rPCP–Chl *b* (PDB structure 2X20[34]). *Top*: Polypeptide backbone in a ribbon representation with the C_2 symmetry axis pointing vertically, as in Figure A4.1: rPCP–Chl *a* (white) and rPCP–Chl *b* (green). *Middle*: Chromophore cluster with the C_2 symmetry axis pointing vertically, as in Figure A4.1. *Bottom*: Chromophore cluster viewed along the C_2 symmetry axis, as in Figure 4.1. In the bottom two panels: for the rPCP–Chl *a* complex, the peridinins, Chl *a*, and lipids are light blue, orange, and black, respectively; for rPCP–Chl *b*, the peridinins, Chl *b*, and lipids are colored green, light yellow, and brown, respectively.

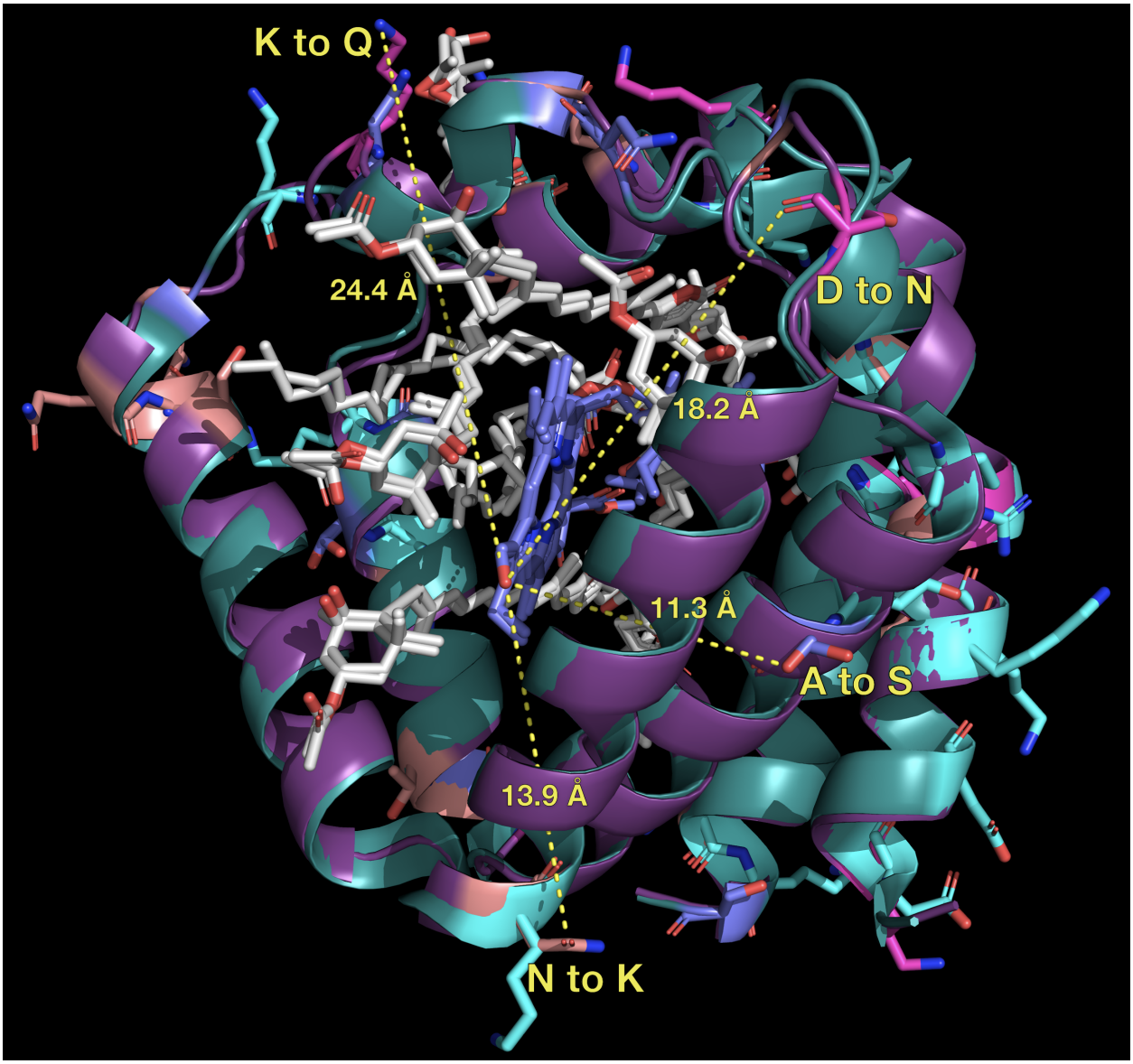

Figure A4.14. Point differences and distances from the formyl group of the Chl between the C-terminal domain apoprotein of wtPCP–Chl *a* (PDB structure 1PPR[15]) and the N-terminal domain fragment that replaces it in rPCP–Chl *b* (PDB structure 2X20[34]).

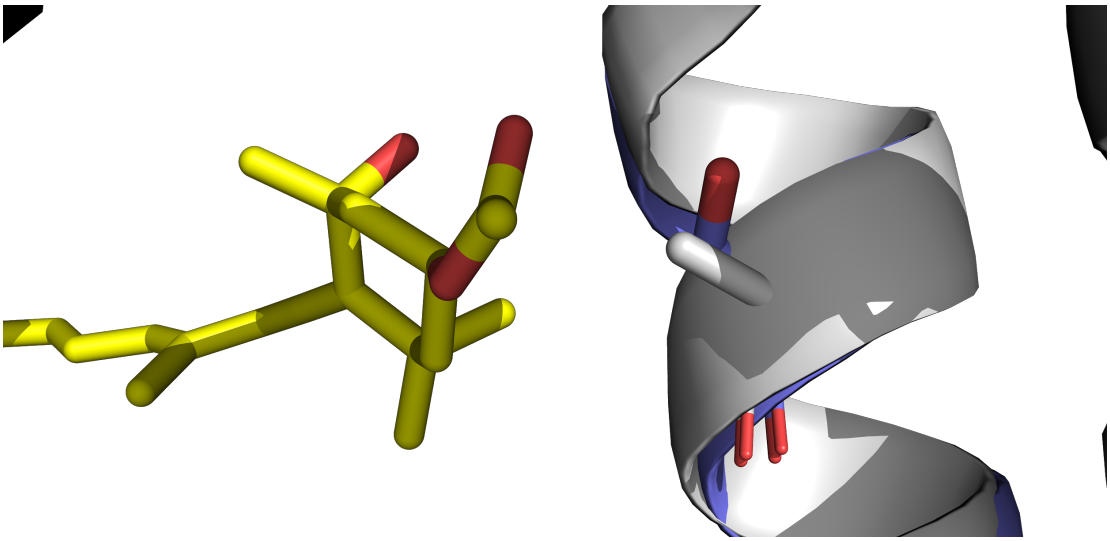

Figure A4.15. Ser204 substitution with Ala. Peridinin end ring shown in yellow. Serine shown in blue and red, and alanine shown in white.

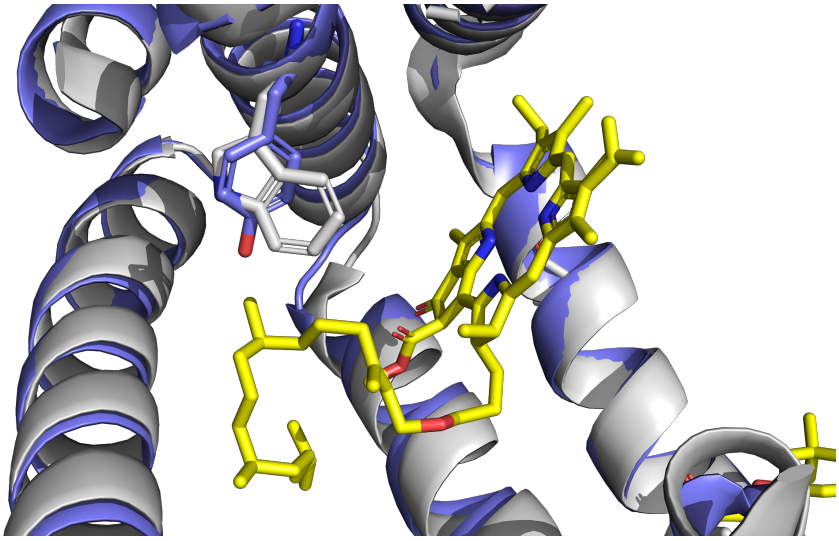

Figure A4.16. Tyr248 substitution with Trp. Chlorophyll is shown in yellow, tyrosine shown in blue and red and tryptophan shown in white.

A4.8 Phasing of PCP Chl b 2DES Spectra

The real (absorptive) and imaginary (dispersive) components of the 2DES signal were separated using a phase factor corresponding to the difference in the optical phase of the local oscillator and signal pulses (the two electric fields that generated the detected interferograms). In order to choose a proper phase factor, the projection–slice theorem[48] was applied. The absorptive component of the 2DES spectrum was projected onto the detection axis and then overlaid with the pump–probe signal measured at the same waiting time T using the same optics, as described above. The phase was then adjusted to minimize the residual difference between the pump probe spectrum and the absorptive 2DES projection. The signal/noise ratio of the reference pump–probe spectrum is not nearly as high as that of the projected 2DES spectrum, but this is judged not to affect significantly the choice of the phase factor. This process was repeated for all of the 2DES spectra at different T delays, and the phase factors were chosen to be internally continuous as T is varied. This practice improves the stability of the phases used for the 2DES time series. The following figures show the phasing of each of the 2DES spectra shown in Figure 4.3.

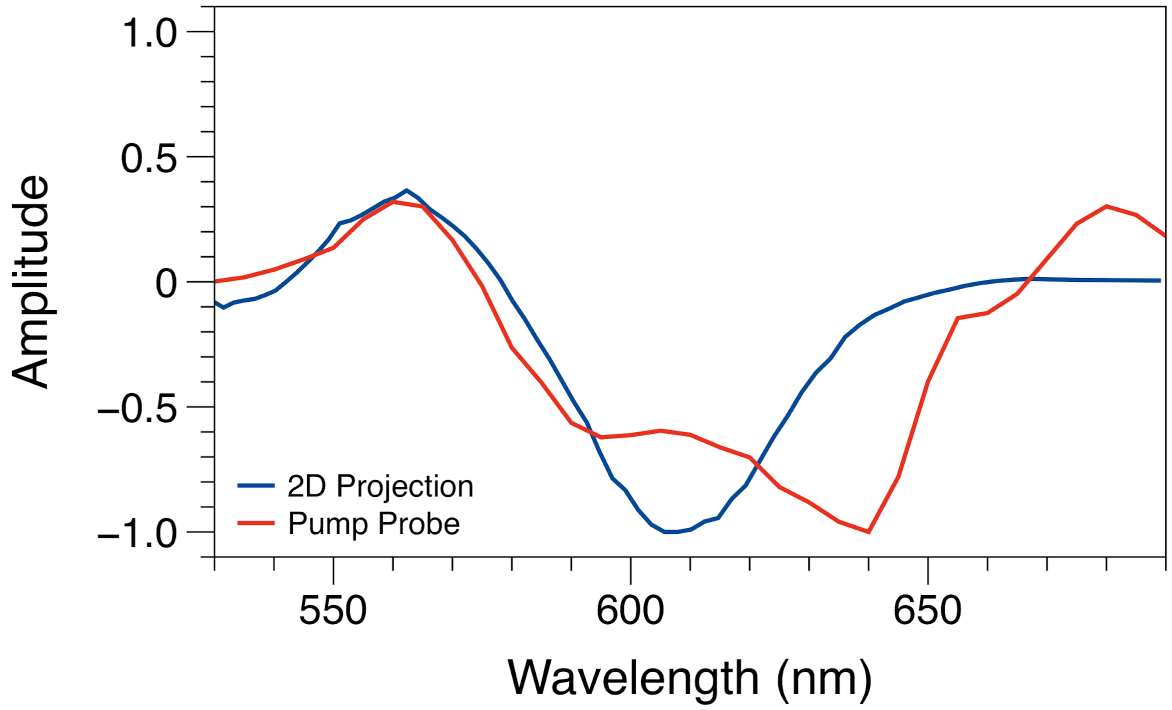

Figure A4.17. 2DES projection (blue) compared to the pump-probe spectrum (red) at waiting time $T = 5$ fs.

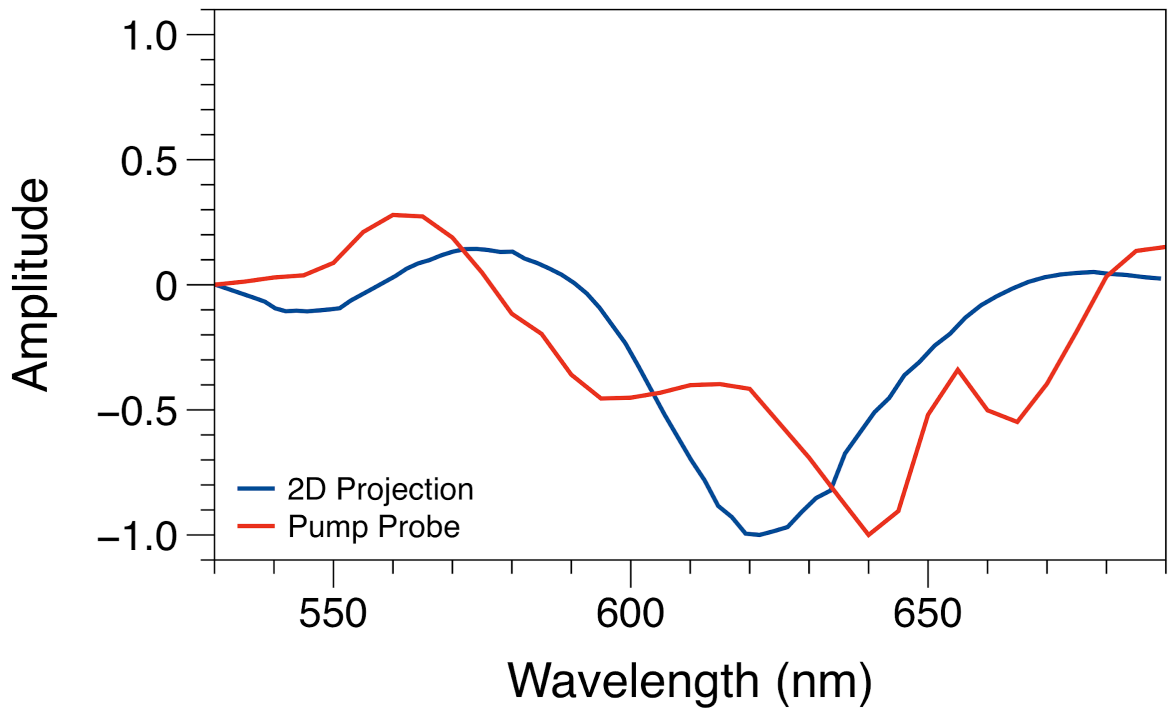

Figure A4.18. 2DES projection (blue) compared to the pump-probe spectrum (red) at waiting time $T = 15$ fs.

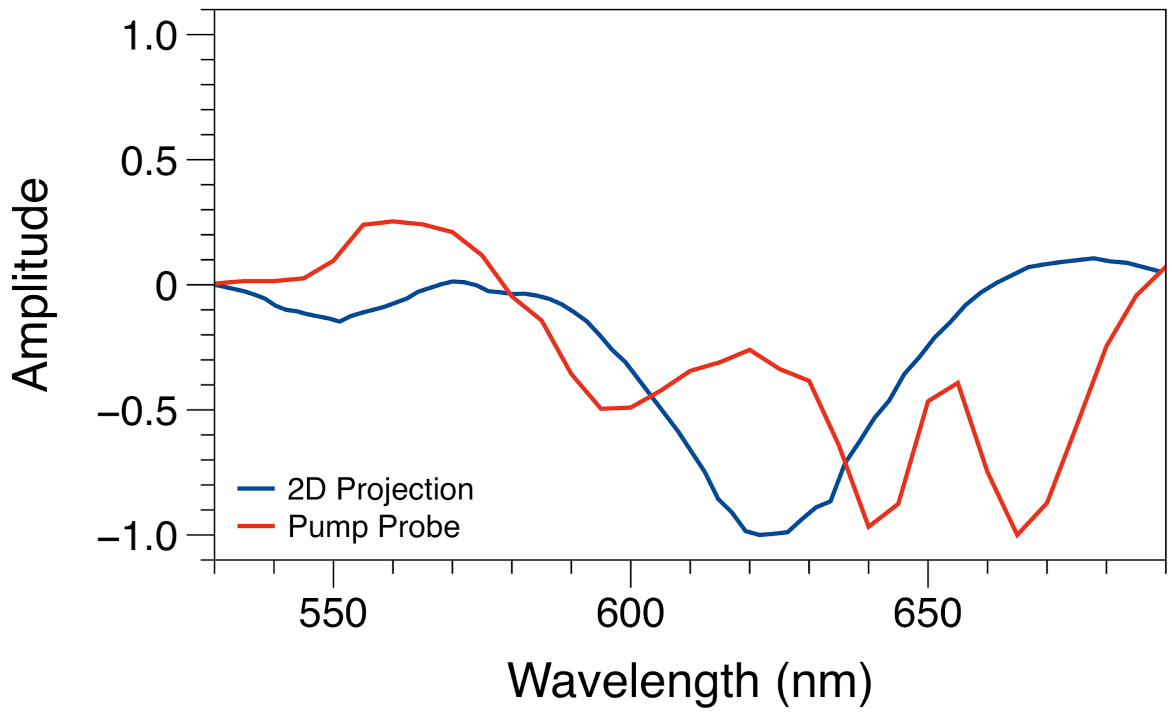

Figure A4.19. 2DES projection (blue) compared to the pump-probe spectrum (red) at waiting time $T = 25$ fs.

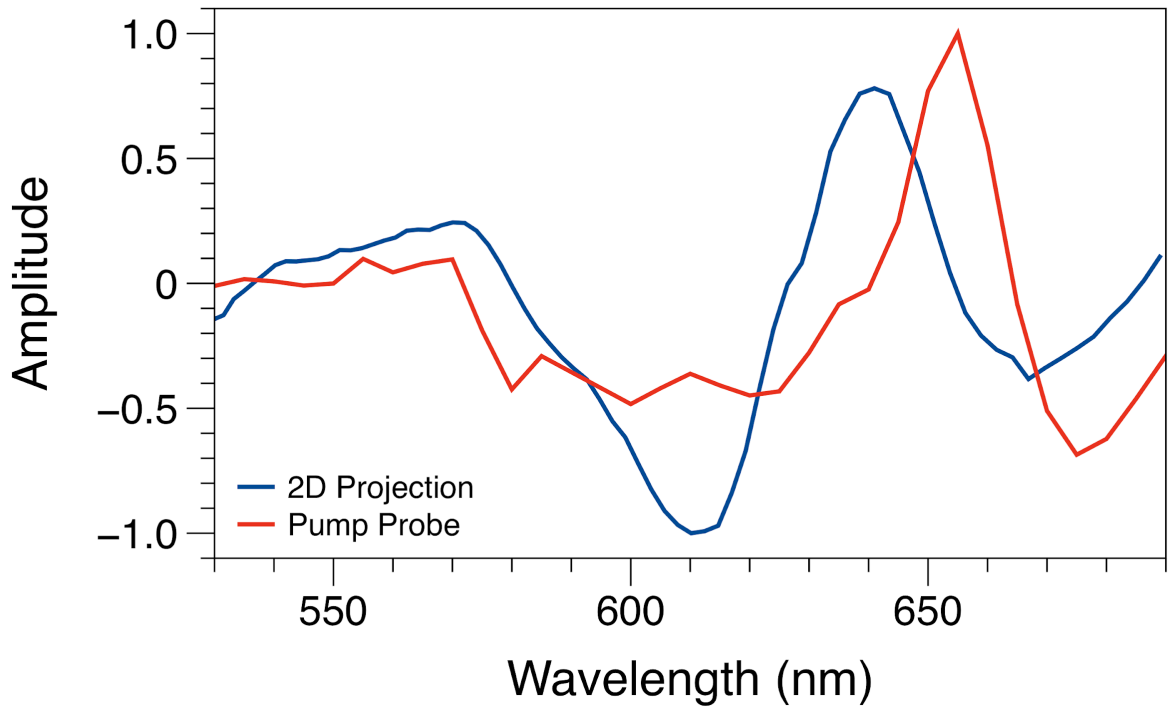

Figure A4.20. 2DES projection (blue) compared to the pump-probe spectrum (red) at waiting time $T = 50$ fs.

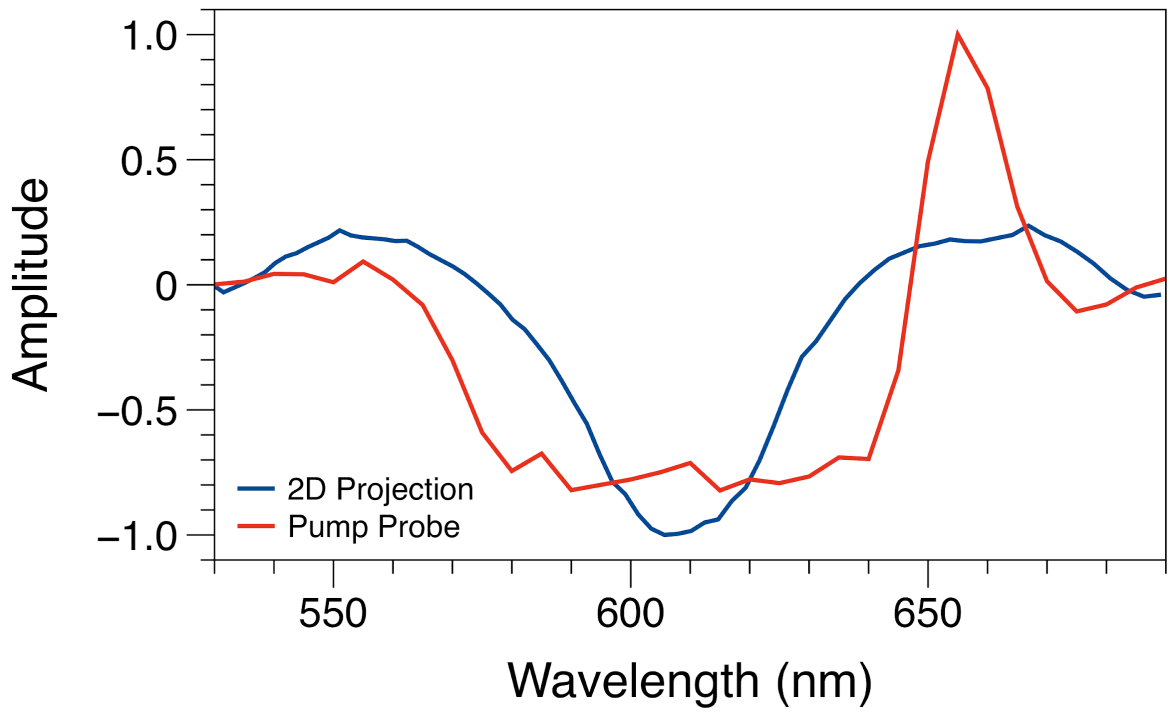

Figure A4.21. 2DES projection (blue) compared to the pump-probe spectrum (red) at waiting time $T = 1500$ fs.

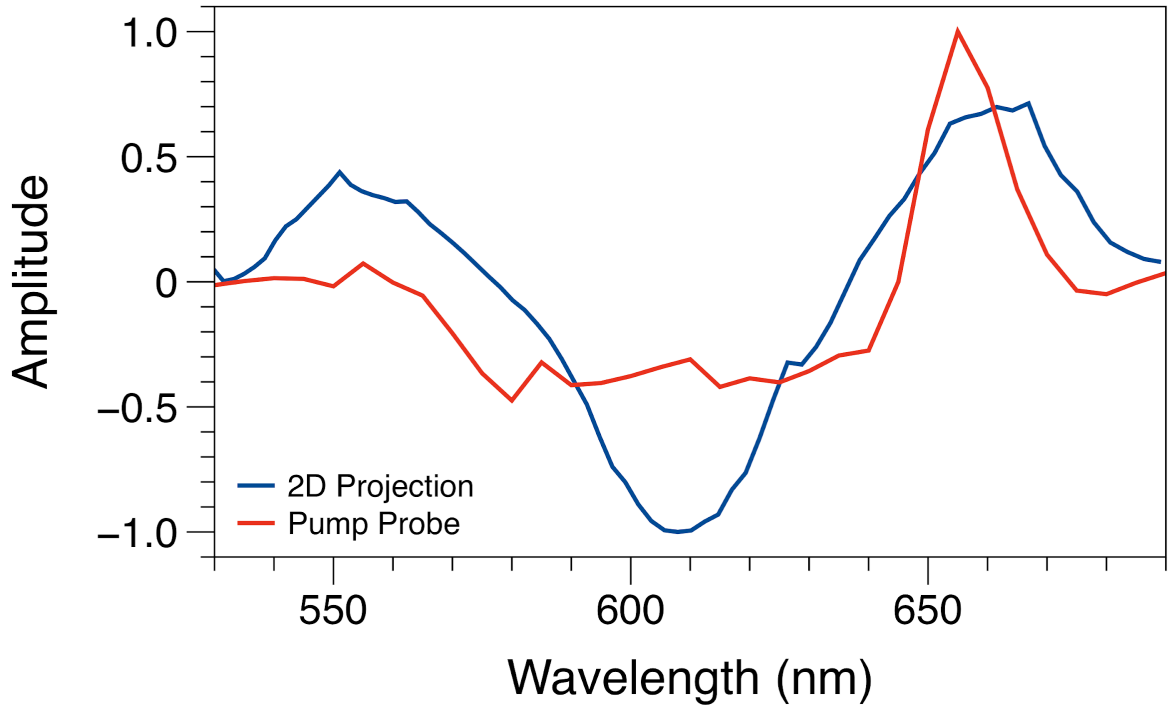

Figure A4.22. 2DES projection (blue) compared to the pump-probe spectrum (red) at waiting time $T = 7000$ fs.

REFERENCES

REFERENCES

(1) Pullerits, T.; Chachisvilis, M.; Jones, M. R.; Hunter, C. N.; Sundström, V. Exciton Dynamics in the Light-Harvesting Complexes of *Rhodobacter sphaeroides* . *Chem. Phys. Lett.* **1994**, *224* (3), 355–365.

(2) Bradforth, S. E.; Jimenez, R.; van Mourik, F.; van Grondelle, R.; Fleming, G. R. Excitation Transfer in the Core Light-Harvesting Complex (LH-1) of *Rhodobacter sphaeroides*: An Ultrafast Fluorescence Depolarization and Annihilation Study. *J. Phys. Chem.* **1995**, *99* (43), 16179–16191.

(3) Edington, M. D.; Riter, R. E.; Beck, W. F. Evidence for Coherent Energy Transfer in Allophycocyanin Trimers. *J. Phys. Chem.* **1995**, *99* (43), 15699–15704.

(4) Pullerits, T.; Chachisvilis, M.; Sundström, V. Exciton Delocalization Length in the B850 Antenna of *Rhodobacter sphaeroides*. *J. Phys. Chem.* **1996**, *100* (25), 10787–10792.

(5) Savikhin, S.; Buck, D. R.; Struve, W. S. Oscillating Anisotropies in a Bacteriochlorophyll Protein: Evidence for Quantum Beating between Exciton Levels. *Chem. Phys.* **1997**, *223* (2), 303–312.

(6) Brixner, T.; Stenger, J.; Vaswani, H. M.; Cho, M.; Blankenship, R. E.; Fleming, G. R. Two-Dimensional Spectroscopy of Electronic Couplings in Photosynthesis. *Nature* **2005**, *434* (7033), 625–628.

(7) Engel, G. S.; Calhoun, T. R.; Read, E. L.; Ahn, T. K.; Mančal, T.; Cheng, Y. C.; Blankenship, R. E.; Fleming, G. R. Evidence for Wavelike Energy Transfer through Quantum Coherence in Photosynthetic Systems. *Nature* **2007**, *446*, 782–786.

(8) Panitchayangkoon, G.; Hayes, D.; Fransted, K. A.; Caram, J. R.; Harel, E.; Wen, J.; Blankenship, R. E.; Engel, G. S. Long-Lived Quantum Coherence in Photosynthetic Complexes at Physiological Temperature. *Proc. Natl. Acad. Sci. U. S. A.* **2010**, *107* (29), 12766–12770.

(9) Collini, E.; Wong, C. Y.; Wilk, K. E.; Curmi, P. M. G.; Brumer, P.; Scholes, G. D. Coherently Wired Light-Harvesting in Photosynthetic Marine Algae at Ambient Temperature. *Nature* **2010**, *463* (7281), 644–647.

(10) Dorfman, K. E.; Voronine, D. V.; Mukamel, S.; Scully, M. O. Photosynthetic Reaction Center as a Quantum Heat Engine. *Proc. Natl. Acad. Sci. U. S. A.* **2013**, *110* (8), 2746–2751.

(11) Scholes, G. D.; Fleming, G. R.; Chen, L. X.; Aspuru-Guzik, A.; Buchleitner, A.; Coker, D. F.; Engel, G. S.; van Grondelle, R.; Ishizaki, A.; Jonas, D. M.; et al. Using Coherence to Enhance Function in Chemical and Biophysical Systems. *Nature* **2017**, *543* (7647), 647–656.

(12) Chenu, A.; Scholes, G. D. Coherence in Energy Transfer and Photosynthesis. *Annu. Rev. Phys. Chem.* **2015**, *66*, 69–96.

(13) Ishizaki, A.; Fleming, G. R. Quantum Superpositions in Photosynthetic Light Harvesting: Delocalization and Entanglement. *New J. Phys.* **2010**, *12* (5), 055004.

(14) Smyth, C.; Oblinsky, D. G.; Scholes, G. D. B800-B850 Coherence Correlates with Energy Transfer Rates in the LH2 Complex of Photosynthetic Purple Bacteria. *Phys. Chem. Chem. Phys.* **2015**, *17* (46), 30805–30816.

(15) Hofmann, E.; Wrench, P. M.; Sharples, F. P.; Hiller, R. G.; Welte, W.; Diederichs, K. Structural Basis of Light Harvesting by Carotenoids: Peridinin-Chlorophyll-Protein from *Amphidinium carterae*. *Science* **1996**, *272* (5269), 1788–1791.

(16) Ghosh, S.; Bishop, M. M.; Roscioli, J. D.; LaFountain, A. M.; Frank, H. A.; Beck, W. F. Excitation Energy Transfer by Coherent and Incoherent Mechanisms in the Peridinin–chlorophyll *a* Protein. *J. Phys. Chem. Lett.* **2017**, *8*, 463–469.

(17) Roscioli, J. D.; Ghosh, S.; LaFountain, A. M.; Frank, H. A.; Beck, W. F. Quantum Coherent Excitation Energy Transfer by Carotenoids in Photosynthetic Light Harvesting. *J. Phys. Chem. Lett.* **2017**, *8* (20), 5141–5147.

(18) Meneghin, E.; Volpato, A.; Cupellini, L.; Bolzonello, L.; Jurinovich, S.; Mascoli, V.; Carbonera, D.; Mennucci, B.; Collini, E. Coherence in Carotenoid-to-Chlorophyll Energy Transfer. *Nat. Commun.* **2018**, *9* (1), 3160.

(19) Guberman-Pfeffer, M. J.; Greco, J. A.; Birge, R. R.; Frank, H. A.; Gascón, J. A. Light Harvesting by Equally Contributing Mechanisms in a Photosynthetic Antenna Protein. *J. Phys. Chem. Lett.* **2018**, *9* (3), 563–568.

(20) Bautista, J. A.; Hiller, R. G.; Sharples, F. P.; Gosztola, D.; Wasielewski, M.; Frank, H. A. Singlet and Triplet Energy Transfer in the Peridinin−Chlorophyll *a*−Protein from Amphidinium Carterae. *J. Phys. Chem. A* **1999**, *103* (14), 2267–2273.

(21) Kleima, F. J.; Hofmann, E.; Gobets, B.; van Stokkum, I. H.; van Grondelle, R.; Diederichs, K.; van Amerongen, H. Förster Excitation Energy Transfer in Peridinin-Chlorophyll-*a*-Protein. *Biophys. J.* **2000**, *78* (1), 344–353.

(22) Krueger, B. P.; Lampoura, S. S.; van Stokkum, I. H.; Papagiannakis, E.; Salverda, J. M.; Gradinaru, C. C.; Rutkauskas, D.; Hiller, R. G.; van Grondelle, R. Energy Transfer in the Peridinin Chlorophyll-*a* Protein of *Amphidinium carterae* studied by Polarized Transient Absorption and Target Analysis. *Biophys. J.* **2001**, *80* (6), 2843–2855.

(23) Lampoura, S. S.; Krueger, B. P.; Van Stokkum, I. H. M.; Salverda, J. M.; Gradinaru, C. C.; Rutkauskas, D.; Hiller, R. G.; Van Grondelle, R. Energy Transfer in the Peridinin Chlorophyll *a* Protein of *Amphidinium carterae* Studied by Polarized Absorption Measurements. *Int. J. Mod. Phys. B* **2001**, *15*, 3849–3852.

(24) Zigmantas, D.; Hiller, R. G.; Sundstrom, V.; Polivka, T. Carotenoid to Chlorophyll Energy Transfer in the Peridinin-Chlorophyll-*a*-Protein Complex Involves an Intramolecular Charge Transfer State. *Proc. Natl. Acad. Sci. U. S. A.* **2002**, *99* (26), 16760–16765.

(25) van Stokkum, I. H. M.; Papagiannakis, E.; Vengris, M.; Salverda, J. M.; Polívka, T.; Zigmantas, D.; Larsen, D. S.; Lampoura, S. S.; Hiller, R. G.; van Grondelle, R. Inter-Pigment Interactions in the Peridinin Chlorophyll Protein Studied by Global and Target Analysis of Time Resolved Absorption Spectra. *Chem. Phys.* **2009**, *357*, 70–78.

(26) Zigmantas, D.; Hiller, R. G.; Yartsev, A.; Sundström, V.; Polívka, T. Dynamics of Excited States of the Carotenoid Peridinin in Polar Solvents: Dependence on Excitation Wavelength, Viscosity, and Temperature. *J. Phys. Chem. B* **2003**, *107* (22), 5339–5348.

(27) Shima, S.; Ilagan, R. P.; Gillespie, N.; Sommer, B. J.; Hiller, R. G.; Sharples, F. P.; Frank, H. A.; Birge, R. R. Two-Photon and Fluorescence Spectroscopy and the Effect of Environment on the Photochemical Properties of Peridinin in Solution and in the Peridinin-Chlorophyll-Protein from *Amphidinium carterae*. *J. Phys. Chem. A* **2003**, *107* (40), 8052–8066.

(28) Wagner, N. L.; Greco, J. A.; Enriquez, M. M.; Frank, H. A.; Birge, R. R. The Nature of the Intramolecular Charge Transfer State in Peridinin. *Biophys. J.* **2013**, *104*, 1314–1325.

(29) Ghosh, S.; Bishop, M. M.; Roscioli, J. D.; LaFountain, A. M.; Frank, H. A.; Beck, W. F. Femtosecond Heterodyne Transient Grating Studies of Nonradiative Deactivation of the S_2 ($1^1B_u^+$) State of Peridinin: Detection and Spectroscopic Assignment of an Intermediate in the Decay Pathway. *J. Phys. Chem. B* **2016**, *120*, 3601–3614.

(30) Ghosh, S.; Roscioli, J. D.; Bishop, M. M.; Gurchiek, J. K.; LaFountain, A. M.; Frank, H. A.; Beck, W. F. Torsional Dynamics and Intramolecular Charge Transfer in the S_2 ($1^1B_u^+$) Excited State of Peridinin: A Mechanism for Enhanced Mid-Visible Light Harvesting. *J. Phys. Chem. Lett.* **2016**, *7* (18), 3621–3626.

(31) Cerullo, G.; Polli, D.; Lanzani, G.; De Silvestri, S.; Hashimoto, H.; Cogdell, R. J. Photosynthetic Light Harvesting by Carotenoids: Detection of an Intermediate Excited State. *Science* **2002**, *298* (5602), 2395–2398.

(32) Ghosh, S.; Bishop, M. M.; Roscioli, J. D.; Mueller, J. J.; Shepherd, N. C.; LaFountain, A. M.; Frank, H. A.; Beck, W. F. Femtosecond Heterodyne Transient-Grating Studies of Nonradiative Decay of the S_2 ($1^1B_u^+$) State of β-Carotene: Contributions from Dark Intermediates and Double-Quantum Coherences. *J. Phys. Chem. B* **2015**, *119* (47), 14905–14924.

(33) Fiedor, L.; Heriyanto; Fiedor, J.; Pilch, M. Effects of Molecular Symmetry on the Electronic Transitions in Carotenoids. *J. Phys. Chem. Lett.* **2016**, *7*, 1821–1829.

(34) Schulte, T.; Hiller, R. G.; Hofmann, E. X-Ray Structures of the Peridinin-Chlorophyll-Protein Reconstituted with Different Chlorophylls. *FEBS Lett.* **2010**, *584* (5), 973–978.

(35) Kobayashi, M.; Akiyama, M.; Kano, H.; Kise, H. Spectroscopy and Structure Determination. In *Chlorophylls and Bacteriochlorophylls: Biochemistry, Biophysics, Functions and Applications*; Grimm, B., Porra, R. J., Rüdiger, W., Scheer, H., Eds.; Springer: Dordrecht, 2006; pp 79–94.

(36) Miller, D. J.; Catmull, J.; Puskeiler, R.; Tweedale, H.; Sharples, F. P.; Hiller, R. G. Reconstitution of the Peridinin-Chlorophyll *a* Protein (PCP): Evidence for Functional Flexibility in Chlorophyll Binding. *Photosynth. Res.* **2005**, *86* (1-2), 229–240.

(37) Polívka, T.; Pascher, T.; Sundström, V.; Hiller, R. G. Tuning Energy Transfer in the Peridinin-Chlorophyll Complex by Reconstitution with Different Chlorophylls. *Photosynth. Res.* **2005**, *86* (1-2), 217–227.

(38) Lutz, M. Resonance Raman Spectra of Chlorophyll in Solution. *J. Raman Spectrosc.* **1974**, *2* (5), 497–516.

(39) Di Donato, M.; Ragnoni, E.; Lapini, A.; Foggi, P.; Hiller, R. G.; Righini, R. Femtosecond Transient Infrared and Stimulated Raman Spectroscopy Shed Light on the Relaxation Mechanisms of Photo-Excited Peridinin. *J. Chem. Phys.* **2015**, *142* (21), 212409.

(40) Kleima, F. J.; Wendling, M.; Hofmann, E.; Peterman, E. J.; van Grondelle, R.; van Amerongen, H. Peridinin Chlorophyll *a* Protein: Relating Structure and Steady-State Spectroscopy. *Biochemistry* **2000**, *39* (17), 5184–5195.

(41) Womick, J. M.; Moran, A. M. Vibronic Enhancement of Exciton Sizes and Energy Transport in Photosynthetic Complexes. *J. Phys. Chem. B* **2011**, *115* (6), 1347–1356.

(42) Tiwari, V.; Peters, W. K.; Jonas, D. M. Electronic Resonance with Anticorrelated Pigment Vibrations Drives Photosynthetic Energy Transfer Outside the Adiabatic Framework. *Proc. Natl. Acad. Sci. U. S. A.* **2013**, *110* (4), 1203–1208.

(43) Monahan, D. M.; Whaley-Mayda, L.; Ishizaki, A.; Fleming, G. R. Influence of Weak Vibrational-Electronic Couplings on 2D Electronic Spectra and Inter-Site Coherence in Weakly Coupled Photosynthetic Complexes. *J. Chem. Phys.* **2015**, *143* (6), 065101.

(44) Perlík, V.; Seibt, J.; Cranston, L. J.; Cogdell, R. J.; Lincoln, C. N.; Savolainen, J.; Šanda, F.; Mančal, T.; Hauer, J. Vibronic Coupling Explains the Ultrafast Carotenoid-to-Bacteriochlorophyll Energy Transfer in Natural and Artificial Light Harvesters. *J. Chem. Phys.* **2015**, *142*, 212434.

(45) Ilagan, R. P.; Chapp, T. W.; Hiller, R. G.; Sharples, F. P.; Polívka, T.; Frank, H. A. Optical Spectroscopic Studies of Light-Harvesting by Pigment-Reconstituted Peridinin-Chlorophyll-Proteins at Cryogenic Temperatures. *Photosynth. Res.* **2006**, *90*, 5–15.

(46) Lutz, M. Resonance Raman Spectra of Chlorophyll in Solution. *J. Raman Spectrosc.* **1974**, *2* (5), 497–516.

(47) Jonas, D. M. Two-Dimensional Femtosecond Spectroscopy. *Annu. Rev. Phys. Chem.* **2003**, *54*, 425–463.

(48) Brixner, T.; Mancal, T.; Stiopkin, I. V.; Fleming, G. R. Phase-Stabilized Two-Dimensional Electronic Spectroscopy. *J. Chem. Phys.* **2004**, *121* (9), 4221–4236.

(49) Mukamel, S. Communications: Signatures of Quasiparticle Entanglement in Multidimensional Nonlinear Optical Spectroscopy of Aggregates. *J. Chem. Phys.* **2010**, *132* (24), 241105.

(50) Scholes, G. D.; Smyth, C. Perspective: Detecting and Measuring Exciton Delocalization in Photosynthetic Light Harvesting. *J. Chem. Phys.* **2014**, *140* (11), 110901.

(51) Caram, J. R.; Zheng, H.; Dahlberg, P. D.; Rolczynski, B. S.; Griffin, G. B.; Dolzhnikov, D. S.; Talapin, D. V.; Engel, G. S. Exploring Size and State Dynamics in CdSe Quantum Dots Using Two-Dimensional Electronic Spectroscopy. *J. Chem. Phys.* **2014**, *140* (8), 084701.

(52) Renge, I.; Mauring, K. Spectral Shift Mechanisms of Chlorophylls in Liquids and Proteins. *Spectrochim. Acta A Mol. Biomol. Spectrosc.* **2013**, *102*, 301–313.

(53) Jordanides, X. J.; Lang, M. J.; Song, X.; Fleming, G. R. Solvation Dynamics in Protein Environments Studied by Photon Echo Spectroscopy. *J. Phys. Chem. B* **1999**, *103* (37), 7995–8005.

(54) Lebard, D. N.; Matyushov, D. V. Protein-Water Electrostatics and Principles of Bioenergetics. *Phys. Chem. Chem. Phys.* **2010**, *12* (47), 15335–15348.

(55) Lee, H.; Cheng, Y.-C.; Fleming, G. R. Coherence Dynamics in Photosynthesis: Protein Protection of Excitonic Coherence. *Science* **2007**, *316* (5830), 1462–1465.

(56) Jumper, C. C.; Anna, J. M.; Stradomska, A.; Schins, J.; Myahkostupov, M.; Prusakova, V.; Oblinsky, D. G.; Castellano, F. N.; Knoester, J.; Scholes, G. D. Intramolecular Radiationless Transitions Dominate Exciton Relaxation Dynamics. *Chem. Phys. Lett.* **2014**, *599*, 23–33.

(57) Beenken, W. J. D.; Dahlbom, M.; Kjellberg, P.; Pullerits, T. Potential Surfaces and Delocalization of Excitons in Dimers. *J. Chem. Phys.* **2002**, *117* (12), 5810–5820.

(58) Duan, H.-G.; Prokhorenko, V. I.; Cogdell, R. J.; Ashraf, K.; Stevens, A. L.; Thorwart, M.; Miller, R. J. D. Nature Does Not Rely on Long-Lived Electronic Quantum Coherence for Photosynthetic Energy Transfer. *Proc. Natl. Acad. Sci. U. S. A.* **2017**, *114* (32), 8493–8498.

(59) Edington, M. D.; Riter, R. E.; Beck, W. F. Interexciton-State Relaxation and Exciton Localization in Allophycocyanin Trimers. *J. Phys. Chem.* **1996**, *100* (33), 14206–14217.

(60) Ishizaki, A.; Fleming, G. R. Theoretical Examination of Quantum Coherence in a Photosynthetic System at Physiological Temperature. *Proc. Natl. Acad. Sci. U. S. A.* **2009**, *106* (41), 17255–17260.

(61) Ruban, A. V.; Berera, R.; Ilioaia, C.; van Stokkum, I. H. M.; Kennis, J. T. M.; Pascal, A. A.; van Amerongen, H.; Robert, B.; Horton, P.; van Grondelle, R. Identification of a Mechanism of Photoprotective Energy Dissipation in Higher Plants. *Nature* **2007**, *450* (7169), 575–578.

(62) Lozovoy, V. V.; Pastirk, I.; Dantus, M. Multiphoton Intrapulse Interference 4: Characterization and Compensation of the Spectral Phase of Ultrashort Laser Pulses. *Opt. Lett.* **2004**, *29*, 775–777.

(63) Moran, A. M.; Maddox, J. B.; Hong, J. W.; Kim, J.; Nome, R. A.; Bazan, G. C.; Mukamel, S.; Scherer, N. F. Optical Coherence and Theoretical Study of the Excitation Dynamics of a Highly Symmetric Cyclophane-Linked Oligophenylenevinylene Dimer. *J. Chem. Phys.* **2006**, *124*, 194904.

(64) Hybl, J. D.; Albrecht, A. W.; Gallagher Faeder, S. M.; Jonas, D. M. Two-Dimensional Electronic Spectroscopy. *Chem. Phys. Lett.* **1998**, *297* (3), 307–313.

(65) Honsell, G.; Bonifacio, A.; De Bortoli, M.; Penna, A.; Battocchi, C.; Ciminiello, P.; Dell'aversano, C.; Fattorusso, E.; Sosa, S.; Yasumoto, T.; et al. New Insights on Cytological and Metabolic Features of *Ostreopsis* Cf. *ovata* Fukuyo (Dinophyceae): A Multidisciplinary Approach. *PLoS One* **2013**, *8* (2), e57291.

(66) Krawczyk, S. The Effects of Hydrogen Bonding and Coordination Interaction in Visible Absorption and Vibrational Spectra of Chlorophyll *a*. *Biochimica et Biophysica Acta (BBA) - Bioenergetics* **1989**, *976* (2), 140–149.

(67) Schulte, T.; Niedwiedzki, D. M.; Birge, R. R.; Hiller, R. G.; Polívka, T.; Hofmann, E.; Frank, H. A. Identification of a Single Peridinin Sensing Chl-*a* Excitation in Reconstituted PCP by Crystallography and Spectroscopy. *Proc. Natl. Acad. U.S.A.* **2009**, *106*, 20474–20769.

(68) Hiller, R. G.; Crossley, L. G.; Wrench, P. M.; Santucci, N.; Hofmann, E. The 15-kDa Forms of the Apo-Peridinin-Chlorophyll *a* Protein (PCP) in Dinoflagellates Show High Identity with the Apo-32 kDa PCP Forms, and Have Similar N-Terminal Leaders and Gene Arrangements. *Mol. Genet. Genomics* **2001**, *266* (2), 254–259.

(69) Miller, D. J.; Catmull, J.; Puskeiler, R.; Tweedale, H.; Sharples, F. P.; Hiller, R. G. Reconstitution of the Peridinin-Chlorophyll *a* Protein (PCP): Evidence for Functional Flexibility in Chlorophyll Binding. *Photosynth. Res.* **2005**, *86* (1-2), 229–240.

Chapter 5: Conclusions and Future Work

In this dissertation, the mechanism of excitation energy transfer (EET) between donors and acceptors in light harvesting complexes was investigated using broadband two-dimensional electronic spectroscopy (2DES). More specifically, 2DES was employed to study the role of quantum coherence in EET between peridinin and chlorophyll in the peridinin–chlorophyll protein (PCP). Previous work using femtosecond transient grating spectroscopy[1] suggested that quantum coherence may be vital the the fitness of photosynthetic organism as a means to increasing the efficiency of EET. Here, we were able to directly detect coherent, wavelike, energy transfer pathways using broadband, ultrashort laser pulses.

The 2DES studies on wild-type PCP revealed that quantum coherence in fact increased the efficiency of EET. Ultrafast exciton relaxation within the delocalized peridinin and chlorophyll cluster is effectively energy transfer from peridinin to low lying chlorophyll states. Dynamic localization of these delocalized excited states then traps the energy on localized chlorophyll. Similar process have been shown to occur in other light harvesting proteins.[2–4] It is important to note that the quantum coherence observed in this work was mainly through doubly excited ESA transitions, which occur regardless of incoherent or coherent light sources. Previous studies use quantum beating to detect quantum coherence, however, quantum beating is an interference phenomenon caused by coherent light sources, so they were unable to conclude whether the quantum coherent mechanisms occur in nature.

Following the wild-type PCP 2DES studies, 2DES studies on reconstituted PCP with chlorophyll *b* were performed. The substitution allowed for a unique opportunity to test the

nature of the energy landscape in PCP because the replacement of chlorophyll *a* with chlorophyll *b* only changed the energy gap between the donor and the accept. The structures of PCP with chlorophyll *a* and chlorophyll *b* are nearly isostructural, imparting very similar electrostatic environments for both protein complex clusters. A full analysis of the rates of decoherence and EET between the two PCP complexes was performed and it was found that PCP with chlorophyll *b* had faster decoherence times, which was consistent with longer EET time constants. Because chlorophyll *b* has a carbonyl substituent, it has stronger coupling to the surrounding. The stronger system-bath coupling in the chlorophyll *b* PCP complex results in a more rapid localization process, which decreases the efficiency of EET. Overall, this process imparts unidirectionality of EET toward lower energy chromophores assisting in a more effective EET process to the reaction center. Arguably even more importantly, the conclusions made here indicate that light harvesting complexes can control the efficiency of EET to adapt to new environmental stressors simply by varying the amount of system-bath coupling of the light harvesting cluster, which may even have implications on photosynthetic photoprotection mechanisms.[5]

In order to form a more complete picture, our laboratory plans to perform more 2DES experiments with different observation windows. For instance, 2DES experiments should be performed on a spectral region of PCP for only peridinin (between 490-560 nm) to gain a better understanding of the EET process between peridinin and chlorophyll. The experiments reported in the dissertation selected distorted peridinins in the red edge of the laser spectrum, so much could be learned by studying main band peridinins in PCP to assess whether these structural distortions of PCP play a significant role in EET. One might expect the EET process would

become less efficient because the selection of bluer peridinins increases the energy gap between peridinins and chlorophylls, decreasing the quantum mechanical coupling or mixing. Another study could be performed with a two color 2DES experiment using an ultra-broadband white light continuum as the probe for coverage out into the near IR. This could allow us to fully understand the formation of intramolecular charge transfer character which was of significant interest in the past.[6–9]

In conclusion, the work shown in the dissertation has shown for the first time that quantum coherence is indeed essential to the efficiency of energy transfer in photosynthetic organisms.[10,11] It may even be essential to the robust nature of photosynthesis, as the intricate balance between chromophore coupling and system-bath coupling could also account for a photoprotection mechanism in plants as a function of light intensity. Principles learned from this work could be used in the generation of new materials for solar energy conversion to address the current energy crisis impacting the world.

REFERENCES

REFERENCES

(1) Ghosh, S.; Bishop, M. M.; Roscioli, J. D.; LaFountain, A. M.; Frank, H. A.; Beck, W. F. Excitation Energy Transfer by Coherent and Incoherent Mechanisms in the Peridinin–chlorophyll *a* Protein. *J. Phys. Chem. Lett.* **2017**, *8*, 463–469.

(2) Edington, M. D.; Riter, R. E.; Beck, W. F. Interexciton-State Relaxation and Exciton Localization in Allophycocyanin Trimers. *J. Phys. Chem.* **1996**, *100*, 14206–14217.

(3) van Grondelle, R.; Novoderezhkin, V. Dynamics of Excitation Energy Transfer in the LH1 and LH2 Light-Harvesting Complexes of Photosynthetic Bacteria. *Biochemistry* **2001**, *40* (50), 15057–15068.

(4) Dahlberg, P. D.; Ting, P. C.; Massey, S. C.; Martin, E. C.; Hunter, C. N.; Engel, G. S. Electronic Structure and Dynamics of Higher-Lying Excited States in Light Harvesting Complex 1 from *Rhodobacter Sphaeroides*. *J. Phys. Chem. A* **2016**, *120*, 4124–4130.

(5) Ruban, A. V.; Berera, R.; Ilioaia, C.; van Stokkum, I. H. M.; Kennis, J. T. M.; Pascal, A. A.; van Amerongen, H.; Robert, B.; Horton, P.; van Grondelle, R. Identification of a Mechanism of Photoprotective Energy Dissipation in Higher Plants. *Nature* **2007**, *450* (7169), 575–578.

(6) Bautista, J. A.; Hiller, R. G.; Sharples, F. P.; Gosztola, D.; Wasielewski, M.; Frank, H. A. Singlet and Triplet Energy Transfer in the Peridinin-Chlorophyll *a*-Protein from *Amphidinium Carterae*. *J. Phys. Chem. A* **1999**, *103* (14), 2267–2273.

(7) Zigmantas, D.; Hiller, R. G.; Polívka, T.; Sundström, V. Carotenoid to Chlorophyll Energy Transfer in the Peridinin–chlorophyll-*a*–protein Complex Involves an Intramolecular Charge Transfer State. *Proc. Natl. Acad. Sci. U. S. A.* **2002**, *99*, 16760–16765.

(8) Shima, S.; Ilagan, R. P.; Gillespie, N.; Sommer, B. J.; Hiller, R. G.; Sharples, F. P.; Frank, H. A.; Birge, R. R. Two-Photon and Fluorescence Spectroscopy and the Effect of Environment on the Photochemical Properties of Peridinin in Solution and in the Peridinin-Chlorophyll-Protein from *Amphidinium Carterae*. *J. Phys. Chem. A* **2003**, *107*, 8052–8066.

(9) Wagner, N. L.; Greco, J. A.; Enriquez, M. M.; Frank, H. A.; Birge, R. R. The Nature of the Intramolecular Charge Transfer State in Peridinin. *Biophys. J.* **2013**, *104*, 1314–1325.

(10) Roscioli, J. D.; Ghosh, S.; LaFountain, A. M.; Frank, H. A.; Beck, W. F. Quantum Coherent Excitation Energy Transfer by Carotenoids in Photosynthetic Light Harvesting. *J. Phys. Chem. Lett.* **2017**, *8*, 5141−5147.

(11) Roscioli, J. D.; Ghosh, S.; LaFountain, A. M.; Frank, H. A.; Beck, W. F. Structural Tuning of Quantum Decoherence and Coherent Energy Transfer in Photosynthetic Light Harvesting. *J. Phys. Chem. Lett.* **2018**, *9* (17), 5071–5077.